# Controlled Assembly of Viral Surface Proteins into Biological Nanoparticles

Eri Nakatani-Webster

A dissertation

submitted in partial fulfillment of the

requirements for the degree of

Doctor of Philosophy

University of Washington

2013

Reading Committee:

Carlos E. Catalano, Chair

Kelly K. Lee

William M. Atkins

Program Authorized to Offer Degree:

Pharmacy- Medicinal Chemistry

University of Washington

## Abstract

Controlled Assembly of Viral Surface Proteins into Biological Nanoparticles

Eri Nakatani-Webster

Chair of the Supervisory Committee:
Professor Carlos E. Catalano
Medicinal Chemistry

In recent years, therapeutic use of engineered particles on the 1-1,000 nm scale has gained popularity; these nanoparticles have been developed for use in drug delivery, gene therapy, vaccine preparation, and diagnostics. Often, viral proteins are utilized in the design of such species, and outlined here are completed studies on the *in vitro* assembly of nanoparticles derived from two very different viral systems.

The incorporation of the human immunodeficiency virus (HIV) envelope glycoprotein precursor gp160 into phospholipid bilayer nanodiscs is discussed as a potential platform for vaccine design; efforts were successful, however yield currently limits the practical application of this approach. The utility of bacteriophage lambda (λ) procapsids and virus-like particles in therapeutic nanoparticle design is also outlined, as are efforts toward the structural and thermodynamic characterization of a urea-triggered capsid maturation event. It is demonstrated

that λ virus-like particles can be assembled from purified capsid and scaffolding proteins, and that these particles undergo urea-triggered maturation and *in vitro* decoration protein addition similar to that seen in λ procapsids. The studies on λ provided materials for the further development of nanoparticles potentially useful in a clinical setting, as well as shedding light on critical viral assembly and maturation events as they may take place *in vivo*.

# Table of Contents

* These sections appear as in Singh, et al 2013, with minor modifications.

# List of Figures

# List of Tables

# Dedication

This thesis is dedicated to my entire family,

Especially Mom, Otousan, and Evan;

Without them, none of this would have been possible.

# Acknowledgements

First and foremost, I would like to thank my lab members and classmates for all of their support, guidance, and companionship throughout this process. In particular, I wish to thank:

Elizabeth Medina, for teaching me how to purify and work on procapsids

Eva (Maggie) Medina, for teaching me to make VLP

Jenny Chang, for her guidance with cell culture and capsid assembly

Natalie (Tasha) Zolnerciks, for showing me how to assemble nanodiscs

Thaddeus Davenport for helpful advice on Western blots and ELISAs

Pragya Singh, for assistance with crosslinking experiments

Benjamin Andrews, for many helpful discussions

Natalie Garcia, for helping me to stay positive

I would also like to thank Shiu-Lok Hu and the members of the Hu Research Group at the Washington National Primate Research Center who assisted me with the gp160 nanodisc work: Baoping Tian, Taryn Urion, and Ryan Wallerstedt for providing cell cultures for gp60 purification; Maria Kahn and Brad Cleveland for overseeing my work at the primate center; and Wenjin Guo for helpful discussions.

I wish to thank Kelly Lee, Miklos Guttman, and Hiro Tsuruta for their patient assistance with SAXS experiments; Tamir Gonen, Honjing Zheng, and Scott Braswell for assistance with electron microscopy, and Breanna Vollmar for help with fitting in Chimera.

I owe a special thanks to my committee- thank you all so very much for your guidance, wisdom, helpful suggestions, and patience. In particular, I owe a great deal to my thesis advisor,

Carlos Catalano. Your unwavering support, direction, and unrelentingly positive attitude have kept me going and gotten me where I am now- thank you so much!

To my parents, Jane and Yasuhiro: I owe everything to you. Thank you for giving me all of the wonderful opportunities I've had, for all of your love and guidance, and for making me who I am today- I love you both!

To my family: You mean the world to me, and I hope I've made you all proud!

To my husband, Evan: Every single part of this entire journey would have been impossible if not for you. I can't thank you enough for everything you've done- every encouraging word you've spoken, every late night you stayed awake to pick me up from work, every single thing you did to make my life easier during the most difficult challenge I've ever undertaken. You truly are my better half. I love you.

# Chapter I. Principles of Biological Nanoparticle Design

## I.A Introduction

An intricate web is formed by the multitude of concerted chemical and physical events essential to sustaining life; it is tremendously complex, yet contains exquisite simplicity by way of modularity. Genetic material, small molecules and proteins work in harmony to form vast communication networks vital for maintenance of cellular homeostasis and intercellular crosstalk. In order to carry out nearly all of these processes, a variety of individual biological molecules and macromolecules must coalesce to create nanoscale assemblies; these may exist transiently, as do many complexes involved in cell signaling pathways, or relatively stably, as do many ion channels and pumps required to preserve electrolyte balance. The ability of these individual units to associate with one another in a controlled, specific manner ultimately gives rise to life as we know it.

### I.A.1 Nanoparticles in nature

Nanoparticles are pervasive in biological systems due to the fact that the higher order assembly of most biological molecules results in structures on the scale of $10^{-9}$ meters. Here, "nanoparticle" is used to indicate any multi-biomolecule complex of approximately 5-900 nm in diameter. The human body is rich with these complexes; they represent nodes in signaling systems, transporters, intercellular delivery vehicles, and cellular factories- not to mention the occasional unwelcome invader.

High-density lipoprotein (HDL) particles, for instance, are nanoscale assemblies of lipid and protein, and are a key component in the reverse cholesterol transport pathway. When first formed, the particles are known as pre-β HDL and consist of apolipoprotein, in particular A-I, which interacts with phospholipid to generate discoidal, cholesterol-free complexes. These pre-β HDL circulate in the serum accumulating cholesterol in the form of cholesteryl esters, ultimately developing into fully spherical, mature HDL. The HDL then bind to receptors or transfer proteins elsewhere in the body, which mediate removal of the cholesterol from circulation (Hill, 1997). Each of the components in the HDL particle is necessary for it to carry out its intricate set of duties. Binding sites on the apolipoprotein recognize cholesterol transfer enzymes and specific cellular receptors (Frank, 2000), allowing the particle to find its destination and sequester or relinquish cholesterol when appropriate. Scaffolding in the form of amphipathic apolipoprotein and phospholipid carry the cholesterol cargo safely to its destination.

Viruses- among the simplest of biological entities- are expectedly nanoscale particles as well, consisting minimally of a protein shell, or capsid, containing the virus's genetic material. These, too, are multifunctional assemblies capable of carrying out a complex, stepwise, and time-sensitive series of tasks from initial recognition of the host cell and genome delivery, to directing cellular synthesis of viral proteins, to assembly and release of new viral progeny. The mechanistic details of these events for two distinct viral systems, bacteriophage lambda (λ) and human immunodeficiency virus 1 (HIV-1), will be discussed in further detail in later chapters.

### I.A.2 Nanoparticles in the clinic

It is perhaps no surprise that in our own efforts toward multifunctional therapeutics we often mimic biological particles or make use of them for design purposes. Indeed, given the

relative lack of novel therapeutics recently discovered in comparison to rises in funding (CBO, 2006), and in particular due to the apparent decline in efficacy of newly approved drugs throughout the years (Olfson, 2013), researchers are looking increasingly to rational drug and nanoparticle design to point us in the direction of promising new therapies.

*Figure 1. Nanoparticle diversity*

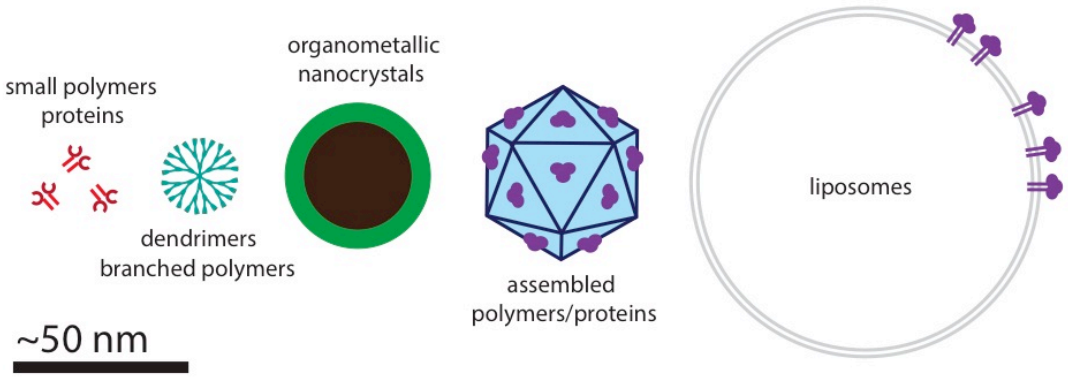


A large array of synthetic and biological nanoparticles has been engineered for use in therapy, diagnostics, or as model systems. A few common examples are shown here roughly to scale.

Nanoparticle therapy has been studied for nearly 30 years, and to date a large variety of biologically compatible nanoparticles has been engineered encompassing a vast range of functionalities, from fully synthetic polymeric nanoparticles designed for extended drug release or tissue imaging, to nanoparticle vaccines assembled entirely from native viral proteins (Figure 1). However, use of most of these particles has been restricted to research, with few true nanoparticle therapeutics having been approved by the FDA (Zhang, 2008; Davis, 2008; Petros, 2010).

In spite of much effort toward advancing nanoparticle design, relatively few studies address how the human body interacts with many of these entities. The enlarged reactive surface area of nanoparticles, coupled with their tendency to show enhanced cellular uptake, greatly complicates prediction of pharmacokinetic behaviors such as plasma clearance and patterns of organ deposition. In general, roughly spherical particles < 5-10 nm are removed from the circulation by glomerular filtration. Sinusoidal filtration in the spleen or Kupffer cells in the liver normally trap particles larger than this, which are then disposed of by the reticuloendothelial system (RES). As a result, larger nanoparticles in general see accumulation in the kidneys and liver, as well as in the bone marrow (Garnett & Kallinteri, 2006). Nevertheless, because nanoparticle sizes, shapes, and compositions are so diverse, their patterns of cellular uptake and biodistribution must be evaluated case-by-case.

Though the progress of nanoparticle therapy in a clinical sense has lagged somewhat in comparison to development of these technologies in the laboratory, data on how nanoparticle size, shape, composition and surface chemistry affect pharmacokinetic properties is becoming increasingly available (Champion, 2007; Owens, 2006; Alexis, 2008). These crucial studies will greatly enhance our ability to rationally engineer these species to exhibit both safety and multifunctional efficacy. Coupling this insight with improving methodologies for controlling nanoparticle size and homogeneity during assembly steps will hopefully serve to expand the number of such therapies approved for clinical use in the coming years. Of the limited number of highly successful nanoparticle therapeutics currently on the market, three are presented here; excellent reviews outlining other important examples are available elsewhere (Zhang, 2008; Davis, 2008; Petros, 2010).

An area of medicine that has seen particular benefit from the introduction of nanoparticle therapies is the treatment of cancer. This owes in part to the enhanced permeability effect (EPR) - nanoparticles' propensity to accumulate passively in tumors due to their leaky, poorly developed vasculature (Maeda, 2000). Traditional cancer therapies typically rely on highly toxic small molecules, many of which damage cellular DNA or otherwise prevent its replication, leading to activation of apoptotic pathways and cell death. These molecules are active against rapidly dividing cancer cells, as DNA replication occurs more frequently. They are unfortunately also quite active against healthy cells that undergo rapid division naturally, such as intestinal epithelial cells and hair follicle cells; much of the long list of highly unpleasant chemotherapy side effects results from this nonspecific action (Chidambaram, 2011). The first nanoparticle drug ever to be approved by the FDA was a result of efforts to reduce toxic side effects and target drugs more specifically to cancerous cells.

Doxorubicin is an anthracycline antibiotic, which is useful as a DNA intercalating agent in chemotherapy. However, its use is severely limited due to the occurrence of dose-dependent cardiotoxicity (Singal, 1998). Doxil®, marketed by Janssen, is a PEGylated, liposomal preparation of doxorubicin approved by the FDA in 1995 for the treatment of AIDS-related Kaposi's sarcoma (Barenholz, 2012). Liposomal incorporation appears to limit cardiotoxicity by encouraging preferential accumulation of the drug in tumor cells via the EPR effect, as well as deposition of the drug at the skin where tumors occur (Lotem, 2000). PEGylation increases the liposomal half-life and decreases immunogenicity (Barenholz, 2012). While this formulation demonstrates improvement of the more severe aspects of toxicity, this coincides with emergence of side effects localized to the skin (Lotem, 2000). More direct forms of targeting have since been applied to the surface of these liposomes and as a result, antibody-conjugated

"immunoliposomes" loaded with the drug were evaluated in phase I clinical trials with encouraging results (Matsumura, 2004).

Though antibody-based drugs are identified as nanoparticle therapeutics rather inconsistently, they warrant discussion here as the philosophy behind their construction certainly extends to that of the larger protein nanoparticles examined in later chapters. Etanercept, marketed as Enbrel®, is a benchmark for rational protein-based drug design. Developed in the early 1990s by Bruce Beutler and colleagues (Peppel, 1991), it is now marketed by Amgen as a subcutaneous injection for treatment of a number of autoimmune diseases. Its licensed indications include plaque psoriasis, rheumatoid arthritis, and ankylosing spondylitis among others (Enbrel® US Full Prescribing information, 2008).

Etanercept is a recombinant, chimeric protein comprising the 75 kDa tumor necrosis factor receptor 2 (TNFR) fused to the Fc region of human IgG1. As is the case with all nanoparticle therapeutics, the union of these two modules resulted in a particle with multiple functionalities. This protein forms stable dimers in solution and mitigates inflammatory responses by binding tightly to the proinflammatory cytokine tumor necrosis factor alpha (TNF-α), effectively reducing its serum levels (Jarvis & Faulds, 1999). The dimeric platform offers both increased affinity for TNF-α due to avidity effects, as well as increased serum half-life due to interactions of the Fc portion with endosomal receptors that salvage it from degradation (Garrison, 1999). The method of identifying active components and melding them together to form a multifunctional particle, as in the development of Enbrel®, is at the heart of rational drug design and thus of therapeutic nanoparticle design as well.

A final area in which nanoparticle therapy has enjoyed clinical success is in the design of vaccines. Virus-derived particles engineered for the purpose of inoculation are rarely included in

discussions of nanoparticle therapeutics; this seems a somewhat arbitrary distinction, as the principles underlying their design and function are fundamentally identical to those of classical nanoparticle drugs. Because of repeated exposure to nanoparticles in the form of viruses for thousands of years, our bodies are highly adept at recognizing and mounting immune responses to symmetric structures approximately 30 nm in diameter. Often, an individual needs only to encounter the outer shell of a viral particle-its capsid or envelope-in order to make antibodies capable of neutralizing the active form of the virus.

When these shells are created artificially for research or clinical use they are usually referred to as "virus-like particles" (VLP), or occasionally "virosomes" in the case of enveloped viruses. They are assembled without genetic material, thus risk of infectivity is negligible. The human papillomavirus (HPV) vaccine Gardasil® (marketed by Merck) is composed of VLP from the L1 capsid protein, which coalesce spontaneously. L1 proteins from 4 different HPV types are expressed separately in recombinant yeast, and the resulting VLP are purified and mixed at specified ratios to yield the quadrivalent vaccine. This vaccine has been shown to be effective in preventing infection with HPV types 6, 11, and most notably 16 and 18 which are responsible for approximately 70% of cervical cancers (Villa, 2007).

Taken together, these success stories make a strong case for the continued development of nanoparticle therapeutics for a variety of indications.

### I.A.3 Nanoparticles in research

Many of the most exciting nanoparticle therapies are still in development or have only recently made it to clinical trials. Great strides have been made in the creation of a diverse array of fully synthetic nanoparticles, from dendrimers to organometallic nanocrystals to carbon

nanospheres, and beyond. Work on these structures has been thoroughly reviewed (Smith, 2008; Mornet, 2004) and these studies will not be discussed here, as biological nanoparticles are the focus.

Both synthetic and biological nanoparticles have been the subject of extensive research in the field of gene therapy, the treatment of genetic disorders by introduction of corrective genes to the host cell. Viruses are often a template for the design not only of vaccines as discussed earlier, but of particles specifically intended to deliver payloads (genetic material, small molecules, or otherwise) to specific cell types. Nature has had considerable time to perfect these structures, so it seems logical to use them as a framework when creating cellular delivery vehicles of our own. The use of viruses as gene delivery devices is so common, in fact, that vectors are broadly classified as "viral" or "non-viral" (Guo & Huang, 2011).

Herpes simplex virus-1 (HSV-1) is a dsDNA virus capable of establishing latent infection in neuronal cells. This mode of infection results in long-lasting expression of certain viral (or introduced) genes without the active replication of progeny. Integration of the viral genome is not required for extended protein expression, as this cell type does not undergo division (Manservigi, 2010). As a result, HSV-1 has been engineered extensively to fashion gene delivery vehicles for treatment of neurological disorders; variants have shown promising results in treatment of animal models of epilepsy (Paradiso, 2009), multiple sclerosis (Furlan, 2007), and Alzheimer's disease (Hong, 2006), to name a few.

The development of *in vivo* imaging and diagnostic techniques has shown that nanoparticles can serve as excellent tools for research as well. These often employ a marriage between synthetic inorganic and biological media, the most common mode being targeting of inorganic nanocrystals by ligation of biomolecules such as IgG. These bio-inorganic

nanoparticles facilitate the combination of diagnostic and therapeutic functions within the same unit; this concept has given rise to the emerging field of "theragnostics". Though ambitious, feasibility is demonstrated through the success of biomolecule-targeted inorganic nanocrystals as theragnostic agents in a number of animal cancer models (Shubayev, 2009).

Coated iron and iron oxide nanocrystals are already in use clinically as contrast agents for magnetic resonance imaging (MRI). It has been discovered that in the presence of alternating magnetic fields, they can also produce heat capable of causing tumor cell death by hyperthermia; altering the properties of the fields applied can control the amount of heat produced. These nanocrystals are given a hydrophilic coating to which targeting peptides, antibodies, or other biomolecules are conjugated; this causes them to preferentially accumulate in specific tumor types which can be revealed by MRI and treated subsequently by hyperthermia (Shubayev, 2009). A fully synthetic, biocompatible precursor to these targeted nanoparticles has already shown success in controlled studies for imaging and treatment of prostate cancer in humans (Johannsen, 2005).

Nanoparticle therapeutic uses are certainly not restricted to cellular delivery and vaccine applications; in many cases they can benefit the field of medicine more indirectly as valuable research tools. Biological nanoparticles are reasonably simple and small in comparison with most fully functional *in vivo* systems, which has encouraged their use as *in vitro* models for more complex cellular events such as multiprotein complex assembly and cell membrane phase separation. Liposomes, for instance, serve as excellent model membranes (Sessa, 1968), and can be formulated to have strictly controlled dimensions and lipid compositions. Notably, a liposomal, fluorescence-based lipid mixing assay has proven quite useful in the characterization of SNARE proteins, which mediate cellular vesicle fusion (Weber, 1998; McNew, 2000). The

partitioning behavior of lipids and membrane proteins can also be studied in much larger, micron-scale versions of these model systems, which have been useful in identification of certain post-translational modifications (PTMs) necessary for membrane protein shuttling into and out of what is believed to constitute the raft phase (Levental, 2010).

### I.A.4 Assembly of protein-based nanoparticles

Methods for production of the protein and genetic components of biological nanoparticles typically consist of isolation from cell cultures or animal tissue, or in the case of shorter peptides or nucleic acids, solid or solution phase synthesis. By far the most facile way to assemble many protein-based nanoparticles is simply by coexpression of the constituent proteins in an appropriate cellular system; this is particularly true of particles that require host cell chaperones for correct protein folding and/or assembly (Figure 2, panel A). In the case of many human proteins, it is essential that this be carried out in a cell type that possesses the proper machinery to apply any necessary PTMs. Viral nanoparticles meant for vaccine (including Gardasil®) are typically produced in this manner (Govan, 2008), either from stably transfected cell lines or by infection with viral vectors; nonviral protein nanoparticles such as Enbrel® are usually expressed using this approach as well (Enbrel® US Full Prescribing information, 2008).

Nanoparticles assembled *in vivo* (i.e. for which the majority of quaternary contacts are formed within the cell), especially vaccines and gene therapy vectors, are often purified and used without much further modification. In many instances, all of the moieties required to impart functionality can be added within the context of the cell. The creation of nanoparticles with artificially implemented functionality is somewhat more difficult using this mode of assembly. Virus-derived particles serve as an exception as they can often be made pre-packaged with cargo

in the form of protein and/ or genetic material *in vivo*, but selective encapsidation of other species is non-trivial.

*Figure 2. Protein nanoparticles: formation in vivo versus in vitro*

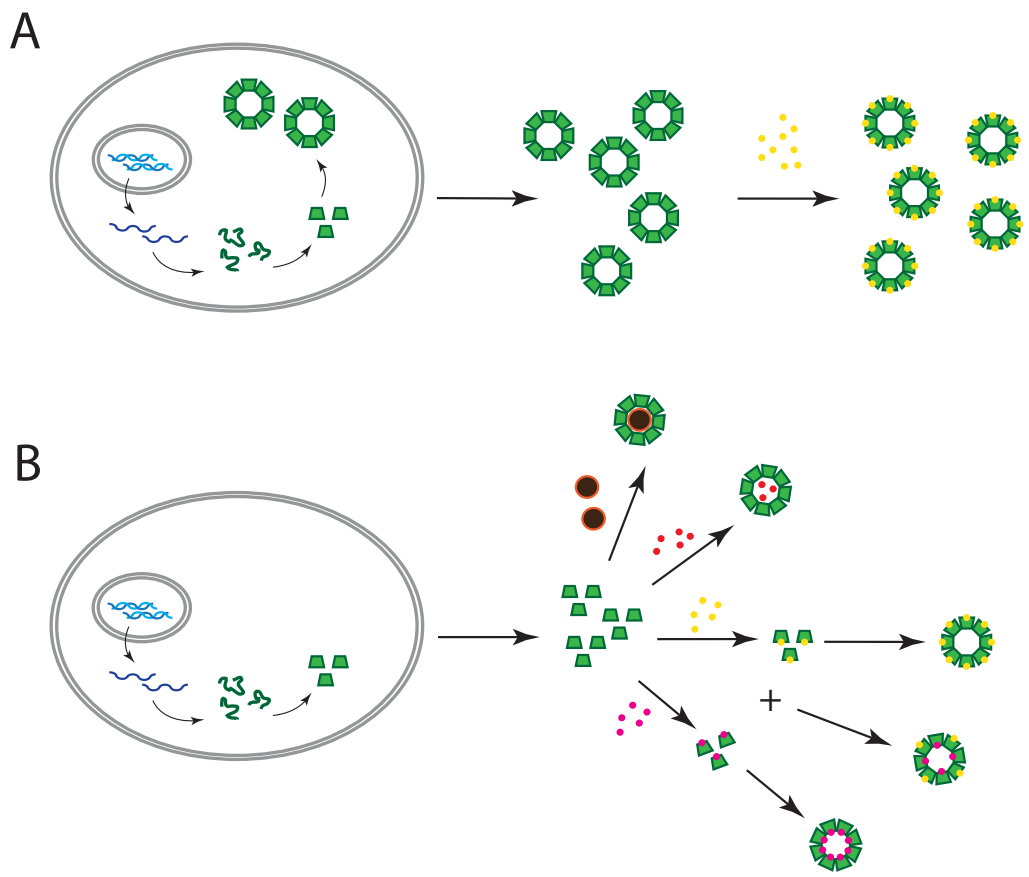


*Panel A. Full particle assembly in vivo*. Particles (green) are formed entirely within the cell expression system. This is useful in the case of budding particles or those requiring host chaperones for assembly. Any chemical modifications (yellow dots) must be made after particle formation; if an internal cavity is present it is typically inaccessible. *Panel B. Particle assembly in vitro*. Formation of particles from purified constituents is not possible in all cases, but allows for enhanced selectivity in labeling reactions (pink and yellow dots) and encapsulation of foreign species (red and brown dots).

To surmount this issue, synthetic conjugates to the nanoparticle can be made after purification either at specific sites (e.g. engineered amino acid residues and selectively reduced disulfide bonds), or by nonspecific ligation techniques. However, pre-assembly of multiprotein

complexes *in vivo* often complicates subsequent specific labeling procedures, and the use of orthogonal ligation strategies is required if more than one species is to be conjugated to the particle. The selective inclusion of small molecules, proteins, specific types of lipid (in the case of lipoprotein complexes), and other species is also decidedly challenging using *in vivo* assembly (Figure 2, panel A).

In some cases, protein-based nanoparticles can be assembled *in vitro* from separately expressed and purified constituent proteins. This ability greatly expands the possibilities for multifunctional particle engineering as it allows for selective labeling of constituent proteins prior to assembly, use of multiple labels with identical coupling chemistries, and specific inclusion of small molecules, proteins, and non-biological materials (Figure 2, panel B). Extracellular reconstitution can be advantageous for preparation of lipoprotein nanoparticles as well, as it permits greater influence over the types of lipid present in the particles and their lipid/protein ratios. The highly controlled nature of such particles has been useful in examining both biological and mechanistic aspects of HDL activity (Scanu, 2008).

The *in vitro* assembly of VLP from separately expressed, purified capsid proteins has been demonstrated in a number of viral systems, and will be outlined further in Chapter II. The assembly pathways of cowpea chlorotic mottle virus (CCMV) and brome mosaic virus (BMV) *in vivo* involves assembly of the coat proteins around the genetic material, largely mediated by nonspecific charge-charge interactions (Bancroft, 1969). *In vitro* studies have demonstrated that the purified proteins will spontaneously encapsidate anionic, inorganic nanoparticles under certain conditions (Huang, 2007; Aniagyei, 2008). This work would have been impossible without use of an *in vitro* assembly system, and underscores the ability of such systems to facilitate the design of truly unique, multifunctional nanoassemblies.

### I.A.5 Nanoparticle assembly in the coming chapters

In the series of studies presented in the next two chapters, I utilize controlled nanoparticle assembly from viral surface proteins as a strategy for rational design of agents with potential therapeutic use. Additionally, I attempt to use the information gained by studying *in vitro* assembly to shed more light on mechanistic aspects of the same pathways as they take place *in vivo*. Chapter II outlines my efforts to better characterize established *in vitro* assembly and maturation pathways for bacteriophage λ capsids; these optimized assembly conditions lay the groundwork for the development of multifunctional, targeted cellular delivery vehicles. Chapter III outlines my work toward development of soluble HIV-1 envelope protein-lipid complexes for use in biochemical studies and ultimately vaccine design. Though the nanoparticles derived from these two systems and their applications are highly dissimilar, their construction was guided by principles and processes common to all protein-based nanoparticles.

# Chapter II. Assembly & Characterization of Nanoparticles Derived from Bacteriophage λ Capsid Proteins

## II.A Introduction

Bacteriophage λ is a non-enveloped, double-stranded (ds) DNA virus which infects *Escherichia coli*. Discovered by Esther Lederberg in the1950s while conducting genetic studies on a lysogenic *E. coli* mutant known as K-12 (Lederberg, 1953), it has since become the subject of a vast compendium of genetic and biophysical work. λ is a temperate phage, transitioning between lytic (active viral reproduction) and lysogenic (latent) life cycles. The tight regulation of genes and protein expression governing the transition between these life cycles is one of the best-characterized genetic switches to date (Oppenheim, 2005).

λ has been used heavily as a model organism in other capacities as well. It has given us a great deal of insight into enzyme complexes and assembly pathways common to many dsDNA viruses, including herpesviruses (Catalano, 1995; deBeer, 2002; Steven, 2005; Baines, 2011). In λ these systems, while elegant, are conceptually manageable enough to allow us some level of control over them. The protein components and DNA required for λ assembly can be purified or purchased separately and assembled into infectious virus *in vitro*. This allows for the study of each viral component's activity and impact on overall viability of the resulting particles (Gaussier, 2006). A broad ensemble of *in vitro* assays have been developed to study various key events in λ development, and thus a wealth of biochemical information on λ is available (Tomka, 1993; Yang, 2003; Gaussier, 2006; Yang, 2008; Chang, 2012). Though these studies are

intellectually captivating, it is perhaps a logical next step to consider in what way we might apply our extensive understanding of this system to improve our own well being.

While the clinical use of a bacteriophage may not be immediately obvious, phage, in fact, have been used in medicine since the 1920s and were even commercially produced for a time by Eli Lilly (Sulakvelidze, 2001). Before the development of many small molecule antibiotics used today, they were commonly used in the treatment of bacterial infections (Sulakvelidze, 2001). This is arguably the most direct use of phage in human medicine, and may again gain importance in treating the growing number of bacterial infections resistant to antibiotic intervention.

Another potential clinical use of phage may be as a theragnostic agent. A more detailed understanding of the processes underlying λ capsid assembly and maturation would put us in a prime position to harness its surface proteins to create multifunctional nanoscale assemblies. This could open a new door for λ in clinical use, in the form of an engineered nanoparticle therapeutic. Here, I outline fundamental studies I have carried out in order to characterize, both structurally and biophysically, the *in vitro* assembly and maturation of λ capsids and virus like particles (VLP). Initial experiments are meant to address the following two major events in mature capsid formation: (*i*) initial particle assembly from constituent proteins, and (*ii*) maturation in the form of urea-triggered expansion and decoration protein binding, outlined in II.A.1 and II.A.2, respectively. As discussed in II.A.3, I have also exploited these steps in proof-of concept experiments to construct λ -based nanoparticles that may be adapted for therapeutic use in the future.

### II.A.1 Modeling λ capsid formation using a defined *in vitro* assembly protocol

Critical to the production of viable viral progeny is, of course, formation of the viral capsid. This protein shell serves to protect and deliver the virus's genetic material; without it, none of the events in the viral life cycle could occur. In some systems, such as tobacco mosaic virus (Klug 1999) and polyomaviruses (Garber, 1980), the genetic material itself nucleates capsid formation. In these cases, the genome is passively encapsidated by the growing protein lattice. In other more complex viruses (Newcomb, 2001), and as is the case for λ, the genome must be actively transported by a packaging motor into a preformed, immature "procapsid" shell (Rao, 2008; Jardine, 2006; Catalano, 1995; Casjens, 2011). The λ procapsid possesses icosahedral symmetry and is composed of 415 copies of a major capsid protein, gpE. One vertex of this icosahedron is replaced by the portal, a dodecameric ring that serves as the entry point of dsDNA during genome packaging, as well as the exit point of the DNA during infection (Catalano, 1995; Jardine, 2006; Rao, 2008). It is thought that assembly of the λ capsid *in vivo* is nucleated, at least in part, by the portal complex (Georgopoulos, 1983). The full *in vivo* λ capsid development pathway up to decoration protein binding is presented in Figure 1, panel A.

Shell assembly is the result of a compromise between granting stability to the newly growing capsid lattice, while allowing for dissociation of incorrectly bound capsid protein monomers to avoid off-pathway products. Systems such as λ and the herpesvirus groups make use of internal scaffold proteins to "chaperone" their major capsid proteins into icosahedral structures (Ziegelhoffer, 1992, Dokland, 1999). These scaffold proteins often exhibit inherent flexibility and partial intrinsic disorder (Dokland, 1999; Fane, 2003). Indeed, it seems logical that structural plasticity would be a requirement for the scaffold to chaperone the formation of

obligatory quasi-symmetric contacts between chemically identical capsid protein monomers incorporated into an icosahedral shell.

*Figure 1. λ Capsid and Viral Particle Assembly Pathways*

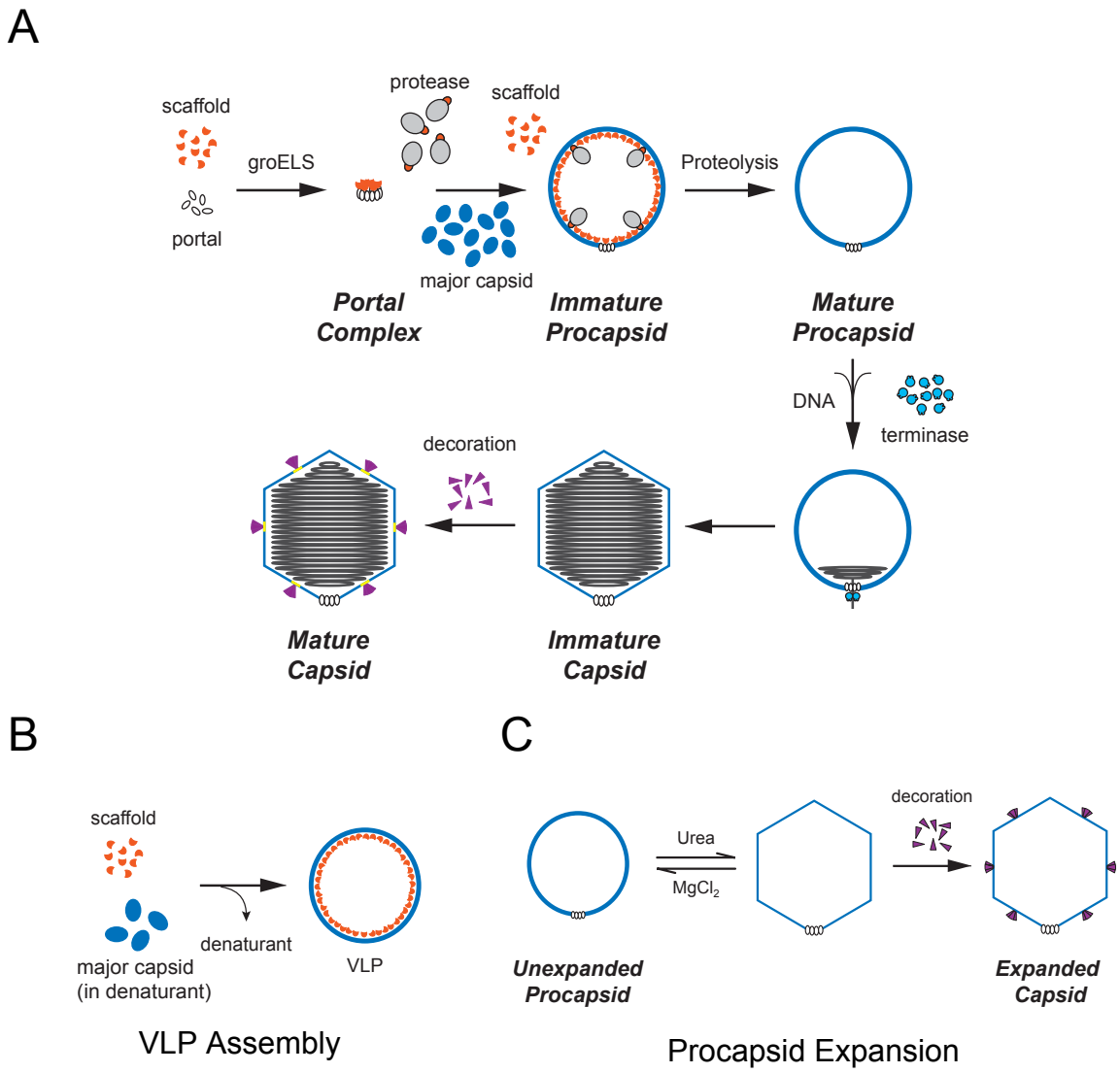


*Panel A*. Pathway for the assembly and maturation of a λ procapsid as it is thought to occur *in vivo* (courtesy J. R. Chang). *Panels B & C*. Previously determined *in vitro* assembly (*B*) and maturation (*C*) pathways (adapted from figures courtesy J. R. Chang). Details are provided in the text.

As was discussed in Chapter I, the capsid proteins in a number of systems can be purified separately and combined *in vitro* to assemble VLP. In addition to the advantages for nanoparticle therapy already outlined, these VLP assembly systems are also quite useful for modeling *in vivo* capsid assembly pathways. The thermodynamic characteristics of capsid assembly for a number of systems, including phage P22 and hepatitis B virus, have been extracted using methods based upon *in vitro* VLP assembly (Ceres, 2004; Parent, 2006; Bourne, 2008; Katen, 2009). The major capsid protein of λ can likewise be assembled *in vitro* into portal-less VLP with the assistance of its scaffold protein, known as gpNu3 (Figure 1, panel B). Studies done by Eva Medina (Medina et al, 2011) showed that the yield of λ VLP was highest when formed using a ratio of approximately 2:1 major capsid: scaffold (Figure 2). However, neither the overall morphology of the particles nor the optimal conditions for assembly were known.

In the first set of experiments summarized here, I aimed to further examine the structure of the particles obtained by the *in vitro* VLP assembly process. I then optimized the reaction parameters to produce as pure and homogeneous a preparation of λ VLP as possible. The optimized reaction conditions are useful for VLP production for further application toward nanoparticle development, as outlined in II.A.3. The results highlight the delicate balance required to maintain homogeneous capsid assembly *in vivo*.

*Figure 2. Initial formation of VLP*

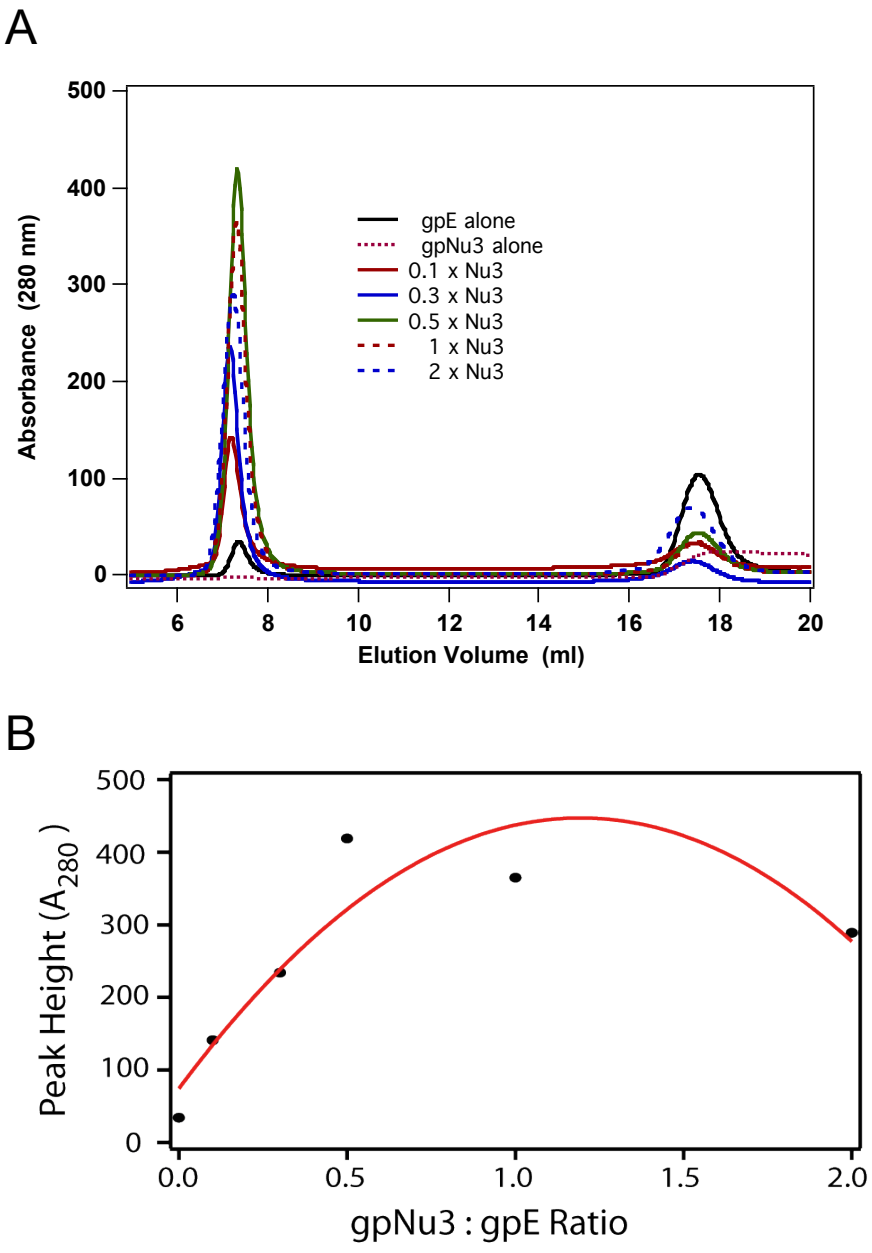


$A_{280}$ of VLP purified by gel filtration initially suggested that particle yield is optimal at a scaffold : major capsid protein ratio of 0.5:1 (adapted from figures that originally appeared in Medina et al, 2010). Experiments performed by E. M. Medina.

### II.A.2 Modeling shell expansion & decoration using *in vitro* maturation of λ capsids

*Characterization of urea-triggered capsid expansion.* In a number of viral systems, genome packaging is accompanied by a capsid rearrangement/ maturation event. This is true of HSV, phages HK97 and P22, and a host of other icosahedral viruses (Galisteo, 1993; Duda, 1995; Heymann, 2003). It was previously thought that this maturation served as an irreversible step, ensuring that particle assembly would continue along a unidirectional trajectory leading to infectious virus (Hohn, 1976). The need for capsid rearrangement may also be a consequence of the balance between establishing strong subunit contacts amongst capsid proteins in the mature shell, and avoiding off-pathway structures during shell assembly caused by formation of improper contacts too stable to be rectified. The thought is that even if optimal contacts are sacrificed during the capsid assembly step, as they must be in some subunits due to quasi-symmetry, fidelity and stability can still be imparted to the particle if these stabilizing interactions are established in a subsequent rearrangement or maturation step (Gertsman, 2009).

For λ, capsid maturation *in vivo* occurs in response to translocation of the viral genome into a preassembled procapsid (the unexpanded form of the capsid is from here on referred to as the procapsid; Figure 1, panel A) (Medina, 2010). Upon packaging of a fraction of the genome, the procapsid expands by approximately 10 nm in diameter, while its walls thin significantly (Hohn, 1976; Dokland & Murialdo 1993). A capsid decoration protein then binds in a 1:1 stoichiometry to the major capsid protein, forming trimeric spikes on the outside of the capsid at quasi three-fold axes (Lander, 2008). This helps to stabilize the mature capsid lattice against both environmental insult and the tremendous internal pressure generated by the fully packaged genome (Fuller, 2007; Yang, 2008).

In λ, procapsid expansion may be triggered artificially by urea (Kunzler & Hohn 1978), a phenomenon that has been recapitulated in similar systems (Duda, 1995). This was repeated in our lab using purified λ procapsids assembled *in vivo* from the expression vector [PT7Cap], as previously described (Yang, 2003). Expansion can be maintained even after removal of the urea if a low concentration of $Mg^{2+}$ (~1 mM) is present in the buffer. Interestingly, though, the expansion is reversible in the presence of higher concentrations (~15 mM) of $Mg^{2+}$ and other divalent metals (Figure 1, panel B). This finding was fascinating, as full reversibility of the maturation process had not been observed in other systems (Lata, 2000; Wang, 2003).

*Figure 3. Biological activity of λ capsids expanded and decorated in vitro*

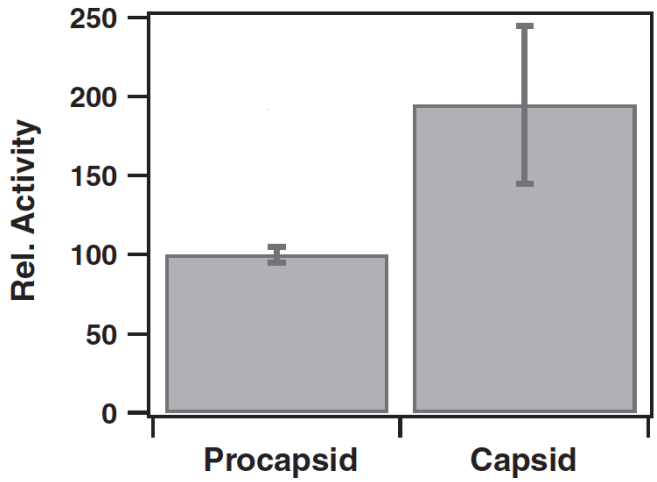


The activity of λ capsids matured *in vitro* was examined using a full genome packaging/ DNAse protection assay. Activity is shown relative to that of procapsid, and is enhanced in the pre-matured particles (originally appeared in Medina et al, 2012). Experiments performed by E. Medina.

After removal of the urea under expansion-maintaining conditions, the capsids bind decoration protein readily and at the expected ratio; only after this event is expansion rendered irreversible (Fig 1, panel B). Particles matured *in vitro* in this manner exhibit excellent biological function in the form of packaging activity, as demonstrated by DNase protection assay shown in

Figure 3 (Medina et al, 2012). Given these results, I believe that they represent the biologically active species and thus serve as an excellent model system for λ capsid maturation *in vivo*, in that that their biophysical and structural features reflect those of maturing viral particles occurring within the infected cell.

The use of chemical denaturation curves to determine the thermodynamic characteristics of two-state protein folding transitions is very well documented (Pace & Shaw, 2000; Santoro & Bolen, 1988). Given that λ urea-triggered capsid expansion also appeared to be a two-state, reversible process when monitored by native agarose gel assay, the linear extrapolation method was used to calculate the free energy of capsid expansion, $\Delta G_{H2O}$. This provided a unique opportunity to measure the energetics of viral capsid maturation in a thermodynamically rigorous manner, albeit using a somewhat low-resolution, gel-based technique. Using this approach, $\Delta G_{H2O}$ was measured to be 10 ± 3 kcal/mol in the presence of 3 mM $Mg^{2+}$(Medina et al, 2012). First and foremost in my work on *in vitro* capsid expansion, I wanted to confirm that application of a two-state model to this system was indeed appropriate, and to recapitulate the $\Delta G_{H2O}$ for capsid expansion previously determined by gel using a solution-based technique, namely small angle X-ray scattering (SAXS).

*Structural model for the λ procapsid shell.* At the time my research was initiated, there was a relative dearth of structural information on a number of the most critical proteins involved in λ assembly and maturation, including the major capsid protein. Cryo-EM reconstructions had been reported for both procapsid and expanded shell conformations, and for the decoration protein trimer spike bound to the capsid (Yang, 2000; Lander, 2008). In addition, high-resolution structures of the λ decoration protein had been solved by a number of techniques, both in-solution NMR and crystallographic approaches (Yang, 2000; Iwai, 2005).

Pseudo-atomic models based on cryo-EM capsid data, in combination with crystallographic data for the decoration protein, led to hypotheses about how the latter physically stabilizes the icosahedral shell. One postulated stabilizing interaction is the formation of a four-stranded β-sheet involving two strands donated by a loop in the major capsid protein, a third donated by the N-terminus of an adjacent capsid shell protein, and the fourth strand donated by N terminal residues in the decoration protein. The latter residues are disordered under crystallographic conditions, but were apparent in the EM density (Lander, 2008). To reveal this interaction, Lander et al. constructed a pseudo-atomic shell model using the cryoEM density and the crystal structure of the homologous HK97 major capsid protein, as data for the λ protein is nonexistent. They then incorporated the published X-ray crystal structure of λ decoration protein (Yang, 2000), into corresponding densities in the EM structure of the expanded, decorated λ capsid. Though this exercise proved highly useful in uncovering nonspecific protein backbone contacts, it was not possible to predict more specific contacts on an amino acid level without a pseudoatomic model containing the sequence of λ major capsid protein itself.

In an effort to paint a more vivid structural picture of this essential viral protein, I attempted to determine whether or not inter-subunit contacts between monomers within the capsid differ grossly between the expanded and contracted forms using chemical crosslinking and mass spectrometry (CCMS). I then combined the CCMS and cryo-EM (Lander, 2008) data, along with computational modeling by the structure prediction servers PHYRE (Kelley & Sternberg, 2009) and I-TASSER (Zhang, 2008; Roy, 2010), to elucidate stabilizing inter-residue contacts between the major capsid protein and the decoration protein.

### II.A.3 Design of multifunctional, λ-based nanoparticles

As mentioned previously, a final goal of the *in vitro* assembly and maturation work was its application toward construction of multifunctional, λ-based nanoparticles, which may be useful in therapy. With the successful preparation of homogeneous VLP in section II.A.1, I was in a position to attempt to build such particles entirely *in vitro* from expressed and purified constituent proteins.

The use of λ decoration protein in a variety of fusion constructs has been demonstrated; both in phage display and other systems it retains its ability to bind and stabilize the λ capsid even when relatively large sequences are grafted on to either terminus (Sternberg, 1995; Mikawa, 1996; Santini, 1998). Thus, it is expected to be of great use in imparting targeting and other functions to nanoparticles derived from λ. The decoration protein and thus any fusion or conjugate protein exists on the surface of the capsid in very high copy number, allowing for the possibility of multivalent interactions with a ligand. Studies have shown that when conjugated to viral proteins displayed with high symmetry and in high copy number, molecules as small as nicotine are capable of generating a robust immune response, even in humans (Cornuz, 2008; Bachmann & Jennings, 2010 ). Given these results, the high immunogenicity of λ could in fact be a desirable trait in the design of novel vaccines. λ phage itself was used in a porcine vaccine trial with no apparent adverse effects (Gamage, 2009); these combined results serve to underscore the potential for further development of phage for the purpose of vaccine applications, if not drug delivery.

As a last step in my work on phage λ, I assessed the feasibility of full *in vitro* assembly of multifunctional λ -based nanoparticles by demonstrating urea-triggered maturation and decoration protein binding to the VLP described in section II.A.1. I also assisted in the structural

characterization of full λ capsids matured and coated *in vitro* with engineered decoration protein mutants, as a stride toward bestowing the particles with multiple functions. As indicated in the previous chapter, there are a number of advantages to *in vitro* assembly, which our laboratory hopes to exploit in future experiments. Although the VLP and functionalized capsids constructed here are not yet very sophisticated, they serve as a critical proof-of concept toward the development of λ based multifunctional nanoparticle therapeutics.

## II.B Materials & Methods

### II.B.1 Protein expression & purification

*Major capsid protein, gpE.* 2 L cultures of E. coli BL21(DE3)[gpE-$His_6$] cells (Medina, 2010) were grown in 2xYT media at 37°C with constant agitation (250 RPM) until an OD of ~0.6 was reached. Cells were induced with 1 mM IPTG and maintained at 37°C with constant agitation for an additional 2 hours. Unless otherwise indicated, all subsequent steps were performed on ice or at 4°C. Cells were harvested by centrifugation and the pellet was resuspended in 50 mL of 20 mM Tris (pH 8), 1 mM EDTA, 20% sucrose. After 10 minutes of gentle agitation, the cells were harvested by centrifugation at 9,000 relative centrifugal force (RCF) for 30 minutes and resuspended in 50 mL of water. Spheroplasts were isolated with another 10 minutes of gentle mixing followed by centrifugation at 12,000 RCF for 40 minutes. The spheroplasts were resuspended in 20 mL of binding/resuspension buffer (50 mM Tris pH 8, containing 5 M guanidine hydrochloride, 100 mM NaCl, 10 mM $MgCl_2$, 10 mM imidazole), then lysed by sonication and gently stirred overnight at 4˚C. Insoluble proteins were removed by centrifugation at 12,000 RCF for 30 minutes.

A 5 mL GE HisTrap FF Ni-NTA column was equilibrated with resuspension/ binding buffer, prior to injection of the clarified supernatant at a flow rate of 1 mL/min. The column was washed with fresh resuspension / binding buffer and bound material was eluted with a linear gradient of 10-500 mM imidazole over 10 column volumes at a flow rate of 1 mL/min. Aliquots of each fraction were precipitated with 6% trichloroacetic acid (TCA) and the resuspended pellets examined for the presence of gpE by SDS-PAGE. Appropriate fractions were pooled (gpE elutes at ~ 50 mM imidazole), and the concentration of major capsid protein determined by absorbance at 280 nm using $\varepsilon_{280} = 36{,}330\ M^{-1}cm^{-1}$.

The protein concentration in the pooled sample was reduced to 20 μM or less by dilution with resuspension / binding buffer (no imidazole) to minimize precipitation and the denaturant was exchanged for urea by overnight dialysis into 40- fold excess of 50 mM Tris pH 8, containing 300 mM NaCl, 7 mM β-mercaptoethanol, and 6 M urea. The denaturant concentration was decreased by a series of step dialyses into 40-fold excess of the same buffer containing 4 M and then 2 M urea, being sure to maintain [major capsid protein] $\leq$ 15 μM to minimize aggregation. The purified protein was exchanged in to dialysis buffer containing 0.5 M guanidine HCl for storage, and kept at 4˚C until use. The purity of the preparation was > 95% as determined by SDS-PAGE.

*Scaffold protein, gpNu3*. 1 L cultures of E. coli BL21(DE3)[ pT7Init-gpC-S166A] (Medina, 2010) were prepared and harvested as for major capsid protein. Unless otherwise noted, all steps were performed on ice or at 4°C . Pellets were taken into 25 mL of resuspension buffer (20 mM Tris pH 8, containing 5 mM $MgCl_2$ and 5 mM β-mercaptoethanol). Cells were lysed by sonication, and lysozyme and 100x EDTA-free Halt Protease inhibitor (Thermo Scientific) were added to concentrations of 80 μg/mL and 1x, respectively. The mixture was incubated with

stirring for one hour. Cellular debris was removed by centrifugation at 9,000 RCF for 20 minutes, followed by addition of solid ammonium sulfate to the supernatant to 20% saturation. The sample was stirred for 45 minutes and clarified by centrifugation at 9,000 RCF for 25 minutes. Solid ammonium sulfate was added to the supernatant to 70% saturation, followed by stirring for an additional 45 minutes. The sample was clarified by centrifugation once again, and the pellet (containing scaffold) taken back into resuspension buffer.

The solution was dialyzed overnight against one liter of the resuspension buffer, then injected on to a pre-equilibrated (with resuspension buffer) 50 mL DEAE-Sepharose (GE) column at a flow rate of 1 mL/min. The column was washed with 2 column volumes (CV) of resuspension buffer containing 100 mM NaCl, and bound protein was eluted using a linear gradient of 100-500 mM NaCl over 5 CV at a flow rate of 1 mL/min. 3 mL fractions were collected and aliquots analyzed by SDS-PAGE to determine which contained scaffold. Protein signal was monitored at 230 nm, as gpNu3 is devoid of aromatic residues. Scaffold protein eluted as a broad, intense peak at 100-250 mM NaCl.

The appropriate fractions were pooled and dialyzed against the same buffer used for DEAE equilibration, and loaded onto a pre-equilibrated 6 mL Resource Q column (GE Healthcare) at a flow rate of 1 mL/min. The column was developed with a linear gradient to 350 mM NaCl. Scaffold protein eluted at 150 mM NaCl, and was located in the collected fractions by SDS-PAGE. Appropriate fractions were pooled and dialyzed in to 20 mM Tris (pH 8), containing 100 mM NaCl and 5 mM $MgCl_2$, and stored at 4ºC (or at -20ºC with the addition of 20% glycerol). Purity was > 95% as determined by SDS-PAGE. Scaffold protein concentration was determined by absorbance at 230 nm using $\varepsilon_{230} = 20{,}140\ M^{-1}cm^{-1}$.

*λ Procapsids.* Procapsids were purified according to published procedures, with slight modification (Yang, 2003). 10 mL overnight cultures derived from single colonies of *E. coli*. BL21(DE3)[pLysS][pT7Cap] were used inoculate two liters of 2X-YT media, pH 7.5, containing 25 mM potassium phosphate, 5 mM glucose, and 50 μg/ml ampicillin. The culture was maintained at 37°C with constant agitation (250 RPM) until an OD of 0.6-0.7 was reached. IPTG was added to the mixture to a final concentration of 0.5 mM, and the cells were maintained at 37°C for an additional 2 h prior to harvesting by centrifugation.

Unless otherwise indicated, all further steps were performed over ice or at 4°C. The cell pellet was resuspended in 50 ml of 50 mM Tris-HCl, pH 8.0, containing 10 mM $MgCl_2$ and 100 mM NaCl. Cells were lysed by sonication, and the crude lysate was clarified by centrifugation (8,000 RCF, 10 min). The supernatant was spun at high-speed in a Beckman L90K preparative ultracentrifuge (130,000 RCF, 3 h). The supernatants were discarded, and 1 mL overlays of buffer (the same as used for cell resuspension) were gently applied to the pellets, which were allowed to incubate undisturbed overnight. The overlays containing white, flocculent material were gently removed from the pellets and applied to 10–40% sucrose gradients prepared in the same buffer. Samples were separated under the same conditions used previously for the high-speed spin, resulting in diffuse, somewhat opaque procapsid bands near the center of the gradients. Bands were harvested by aspiration and dialyzed against 50 mM Tris-HCl, pH 8.0, containing 15 mM $MgCl_2$ and 7 mM β-mercaptoethanol. The dialyzed procapsids were loaded onto a 120 ml DEAE-Sepharose column equilibrated with the same buffer as used for dialysis, and bound material was eluted with a 0–250 mM NaCl gradient. The procapsid-containing fractions (eluting at ~50 mM NaCl) were pooled and dialyzed once again against the same buffer. The final procapsid stock was concentrated in 100 kDa MWCO Amicon centrifugal filter

units and stored at 4°C. Procapsid concentration was calculated from absorbance at 280 nm in the presence of 6 M guanidinium chloride using the previously determined extinction coefficient, $\varepsilon_{280}$ =16.65 $\mu M^{-1}$ $cm^{-1}$.

*Capsid decoration protein.* Decoration protein purified according to published protocols (Yang, 2003) was a kind gift from Elizabeth Medina.

**II.B.2 *in vitro* assembly of λ VLP**

Major capsid protein (15 μM) was combined with scaffold protein in indicated molar ratios on ice, typically in 2 mL reaction volumes. The guanidinium concentration was maintained at 0.5 M to minimize aggregation, and unless otherwise indicated, the mixtures were dialyzed at 4ºC against VLP formation buffer (50 mM Tris (pH 8), initially containing 300 mM NaCl, 15 mM $MgCl_2$, and 7 mM β-mercaptoethanol; once effect of salt concentration on VLP assembly had been determined, [NaCl] was adjusted to 150 mM for subsequent reactions). The assembly mixtures were then concentrated to 500 μL and any precipitate removed by centrifugation at 12,000 RCF for 15 minutes. Gel filtration purification was achieved using a Superose 6 HR10/300 GL gel filtration column (GE Healthcare) pre-equilibrated with VLP formation buffer containing 150 mM NaCl in all cases. Samples were injected in 250 μL aliquots using an isocratic flow of the above buffer at 0.5 mL/min over 1 column volume. 0.5 mL fractions were collected and stored at 4ºC for future use. VLP appeared to remain intact for months at 4ºC by EM, however freezing was strictly avoided as it causes damage to capsids and VLP.

### II.B.3 Urea-triggered expansion of λ procapsids/VLP

For expansion and gpD addition experiments, protocols followed those previously established for *in vitro* maturation of procapsids, with the exception of gpD addition to VLP, which was carried out at a gpD:gpE ratio of 10:1 instead of 1.5:1 (Medina, 2012). VLP assembled under the optimized conditions above were concentrated to approximately 20 nM and incubated in the presence of gpD at room temperature for 1 hour either untreated or after urea-triggered expansion followed by buffer exchange into 1 mM $Mg^{2+}$ containing buffer. 20 μL aliquots at all steps were analyzed by 0.8% agarose gel and stained with Coomassie Brilliant Blue. VLP were then purified by SEC as indicated in II.B.2, and void volume peak fractions were analyzed by SDS-PAGE performed on 15% gels and quantitated by video densitometry as described below.

### II.B.4 Polyacrylamide & native agarose gel electrophoresis; densitometry

*Electrophoresis.* Samples intended for SDS-PAGE were treated with 0.25 equivalents of 5 x reducing SDS-PAGE loading buffer and boiled for no more than 45 seconds to minimize heat-induced degradation of the major capsid protein. 10-20 μL of samples were loaded on to 15% polyacrylamide gels, and electrophoresis was performed at 150 V, until the dye front was approximately 1 cm from the bottom of the gel. Samples intended for native gel electrophoresis were treated with 0.17 equivalents of 6 x DNA loading buffer and 10-20 μL loaded on to 40 mL 0.8% agarose gels. Electrophoresis was performed at 100 V, until the bromophenol blue band had completely exited the gel. In either case, protein bands were visualized by staining with Coomassie Brilliant Blue R-250.

*Gel densitometry*. Protein and DNA gels were imaged using an EpiChemi$^3$ darkroom system (UVP Bioimaging Systems) equipped with a Hamamatsu camera. Video densitometry of the bands was performed using the Image Quant software package (Molecular Dynamics). Protein molar ratio was calculated assuming Coomassie staining of major capsid and decoration proteins was quantitative and proportional to mass.

**II.B.5 Chemical Crosslinking & Mass Spectrometry**

*Chemical crosslinking & sample digestion*. Bacteriophage λ procapsids were purified as described above. The samples (86 μg) were incubated at room temperature in a reaction mixture (43 ul) that contained 50 mM sodium phosphate buffer, pH 7.2, plus either EDC (10 mM) or $BS^2G$-$d_0$ (2 mM) for two hours or one hour, respectively. The reactions were then quenched by buffer exchange into 25 mM $NH_4HCO_3$ buffer using 100 kDa MWCO Amicon® centrifugal filter units. A mock-treated control sample was prepared analogously except that cross-linker was omitted from the reaction mixture. SDA (1 mM) cross-linking reactions were initiated identically but were first incubated in the dark for 30 minutes. Excess SDA was then removed by exchange into 50 mM sodium phosphate buffer and the cross-linking reactions were initiated by irradiation of the samples with long-wave (366 nm) UV light for 10 minutes. The samples were then exchanged into 25 mM $NH_4HCO_3$ as described above.

In all cases, urea and 1,4-dithioerythritol were added to the quenched cross-linking reaction mixtures to final concentrations of 6 M and 4 mM, respectively, and the solutions were incubated at 37°C for one hour. Iodoacetamide was then added to 40 mM and the mixture was maintained at room temperature for an additional hour in the dark. The urea was diluted to 2

molar using 25 mM $NH_4HCO_3$ buffer containing 10% acetonitrile for trypsin digestion of the protein.

The cross-linked, reduced, and carboxymethylated protein samples were digested with trypsin (1:30 mass ratio) for one hour at 37°C. An additional aliquot of trypsin was then added and the mixture was kept at 37˚C overnight. The fully digested samples were desalted with Vydac C18 Silica macrospin columns (The Nest Group, Southboro, MA, USA), dried *in vacuo*, and stored at −80°C until mass spectrometry analysis.

The trypsin-digested samples were resuspended in 0.1% formic acid in water and analyzed by electrospray ionization in the positive ion mode. For each injection, 500 ng of peptide mixture was loaded onto the pre-column and the column was washed with 5% acetonitrile in water containing 0.1% (v/v) formic acid at flow rate of 4 μL/min. Peptides were then eluted at a flow rate of 250 nL/min using the following linear gradients of acetonitrile in 0.1% (v/v) formic acid in water: 5% to 35% over 55 minutes; 35% to 90% over 10 minutes; and 90% (isocratic) for 9 minutes.

*Mass spectrometry, data analysis and cross-link identification (performed by P. Singh).* All MS survey scans were performed in the Orbitrap from *m*/*z* 400−2000, at resolution of 60,000 (*m*/*z* 400) and ion populations of $5 \times 10^5$. For tandem mass spectrometry with ion detection in the Orbitrap, the ion population was set to $2 \times 10^5$, resolution to 7,500, and the precursor isolation width to 4 *m*/*z* units. Collision energy was set to 40% for collision-induced dissociation (CID) in the LTQ. All data-dependent analyses were performed using MS survey scans followed by data-dependent selection of the five most abundant precursors for tandem mass spectrometry. In order to increase the probability of conducting CID on cross-linked peptides, typically present at higher charge states (Singh, 2008), singly, doubly, and triply charged precursors were rejected

from data-dependent ion selection. The dynamic exclusion feature of the mass spectrometer was utilized to increase the likelihood of detecting novel peptides by preventing re-selection of precursor ions (−0.1/+1.1 Da) for 45 sec after CID after which they were allowed to be selected again for CID.

Post acquisition, tandem mass spectral data files were processed through our chemical cross-linking and mass spectrometry (CCMS) pipeline as described previously (Singh, 2008). Briefly, tandem mass spectral data files were deconvoluted and searched with the Phenyx search engine (GeneBio SA, Geneva, Switzerland). The output of this process is peptide sequence identification and removal of tandem mass spectra matching non-cross-linked, linear peptides from the data set. The remaining spectra were searched using Popitam (http://www.expasy.ch/tools/popitam/) in an "open-search mode". Any mass modification between −50 and +3000 Da at any amino acid was searched using trypsin specificity and one missed cleavage, against a database containing protein sequences of interest. The smallest possible tolerance (0.01 Da) was used for fragment ion matching. A list of cross-linked peptide candidates was obtained by querying the modification masses generated from Popitam against masses of tryptic peptides from known proteins in the procapsid. In all data sets measured mass accuracy of cross-linked precursor ions and fragment ions (±5 ppm) were used to confirm the presence of cross-linked peptides.

### II.B.6 Computational modeling

Structural homology models were generated using the Protein Homology/analogY Recognition Engine (PHYRE) search engine (http://www.sbg.bio.ic.ac.uk/phyre2) and the I-TASSER search engine (http://zhanglab.ccmb.med.umich.edu/I-TASSER/) using gpE as the

query sequence. Chemical cross-links identified by mass spectrometry (Table 1) were visualized in the context of the I-TASSER model and those deemed appropriate were used as intramolecular distance constraints in a second I-TASSER query to afford a refined structural model. Identified $BS^2G$ cross-linked atoms were constrained to a distance of 7.7 Å and identified EDC cross-linked atoms were constrained to a distance of 1.4 Å.

The refined gpE structural homology model constructed above was manually fit into the 13.3 Å electron density map of unexpanded bacteriophage λ procapsid (EMDB reference number EMD-1507) using the UCSF Chimera package (Resource for Biocomputing, Visualization, and Informatics, University of California, San Francisco; Pettersen, 2004). Briefly, density maps for gpE penton and hexon capsomers, and for the three-fold axis were extracted from the full capsid cryo-EM structure. Individual gpE subunits were manually fit into the density maps to within approximately 5-10 Å of their desired location. Iterative rounds of shifting and rotational displacement were performed using the Chimera "Fit in Map" tool until no further improvement in fit could be achieved. Multiple fits from different starting positions were carried out to ensure convergence to the same final position.

**II.B.7 Electron microscopy & particle measurements**

2 μL of samples (approximately 10 nM capsid or VLP) were applied to negatively glow-discharged, 300 mesh carbon-coated copper grids (Ted Pella or EMS) for 20-30 seconds. Excess sample was blotted, and the grids were washed thrice with water and stained either with 2% uranyl acetate or Nano-W (Nanoprobes), a commercial preparation of methylamine tungstate. Bright field electron microscopy was performed either in the Tamir Gonen Laboratory on an FEI Morgagni 268 100-kV electron microscope or at the NanoTech User Facility at the University of

Washington on an FEI Tecnai G2 F20 S-Twin TEM, both equipped with Gatan CCD imaging systems. Images were collected at 14,000 and 38,000 x magnification. Particle measurements were carried out using the Adobe Photoshop software package; each was the average of three separate measurements distributed radially.

### II.B.8 Small angle X-ray scattering

SAXS was performed with the kind assistance of Prof. Kelly Lee on beamline 4-2 at the Stanford Synchotron Radiation Lightsource (SLAC National Accelerator Laboratory, Menlo Park, CA), based on published procedures (Lee, 2004). Procapsid samples contained approximately 1 mg/mL material, with measurements made on serial dilutions to check for concentration effects. Procapsids were dialyzed into buffer containing 20 mM Tris pH 8 at 4°C, 15 mM $MgCl_2$ for unexpanded samples or an identical buffer containing 2.5 M urea and 1 mM $MgCl_2$ for fully expanded samples. Aliquots were exchanged by dialysis into buffer containing 20 mM Tris and 1 mM $MgCl_2$ only for expanded/ buffer exchanged samples, or back into 20 mM Tris and 15 mM $MgCl_2$ to re-contract the shells. Measurements were taken at 8°C, as low as the dew point allowed.

Urea concentrations used for preliminary titration experiments were determined based on those used when monitoring expansion by agarose gel (Medina, 2012). Titration of urea into reaction mixtures for SAXS measurements was carried out such that the $Mg^{2+}$ concentration was maintained at 3 mM. Manual sample mixing minimally results in 90 seconds of dead time before the beginning of data acquisition. Data was adjusted using the Primus software package (EMBL; Konarev, 2003).

## II.C Results & Discussion

### II.C.1 Effect of scaffold : major capsid protein ratio on λ VLP assembly

Previous studies in our lab demonstrated that in the presence of scaffold protein, major capsid protein spontaneously assembles into VLP with similar morphology to λ capsids, upon removal of the denaturant by dialysis. These preliminary experiments indicate that optimal particle formation occurs at a ratio of 0.5:1 scaffold : major capsid, as evidenced by gel filtration (Figure 2).

When I examined these particles by transmission electron microscopy (TEM, using 2% uranyl acetate as a stain), it was revealed that while particle yield seemed most efficient at this ratio, the fraction of misshapen particles was higher than those formed at lower ratios. Thus, particle *fidelity* is more highly preserved at a ratio of 0.3:1 (Figure 4). I conducted a finer titration (0.05-0.5:1 scaffold : major capsid in 0.05-fold increments) and again examined particle yield and morphology as a function of scaffold : major capsid ratio. In the absence of scaffold, the bulk of the material forms a flocculent precipitate in solution with sparse, abnormal soluble particles observed. Particle yield increases with increasing scaffold protein concentration, again up to ratios of 0.5:1 (Figure 5, panel A); particle uniformity is highest at ~0.1-0.3:1 scaffold : major capsid protein, as was observed previously (Table 1). Increase in ratios beyond 0.5:1 cause a steady reduction in yield and homogeneity, and eventually precipitation is observed. A ratio of 0.3:1 gives the optimal balance of particle yield and homogeneity and was used for all further studies.

*Figure 4. Electron microscopy of VLP*

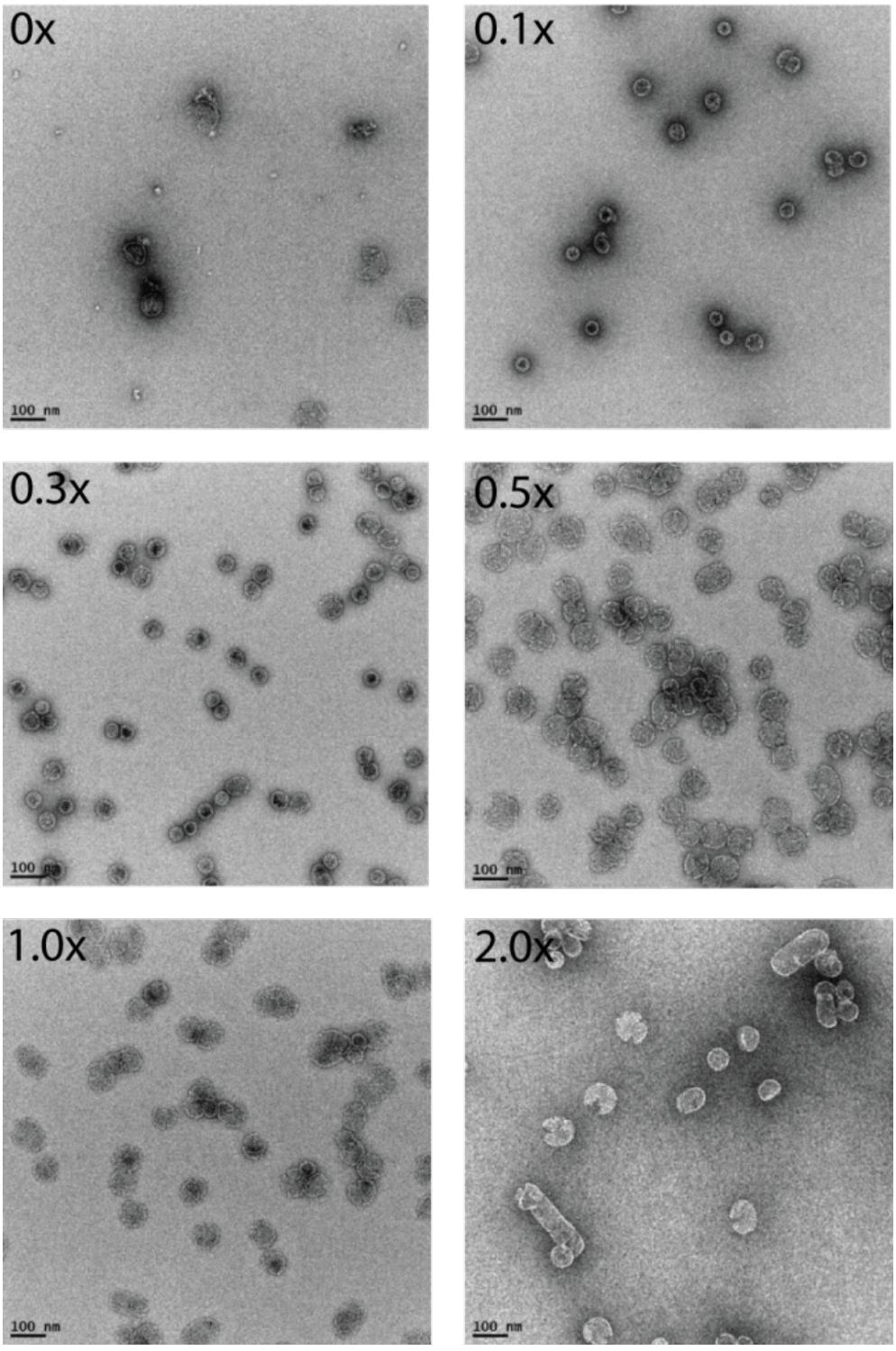


VLP formed at various scaffold : major capsid ratios were examined by transmission electron microscopy. Extremely low ratios result in partially formed shells and low particle yield, while high ratios result in the formation of tube-like structures. Figure originally appeared in Medina et al, 2010.

*Table 1. Fidelity of VLP formation in vitro*

| gpNu3 : gpE ratio | Particles Counted | Normal VLP[a] (%) | Damaged VLP[b] (%) | Aberrant VLP[c] (%) |
|---|---|---|---|---|
| 0:1 | 12 | 8 | ND[d] | 92 |
| 0.1:1 | 100 | 69 | 20 | 11 |
| 0.3:1 | 312 | 72 | 17 | 11 |
| 0.5:1 | 288 | 48 | 35 | 17 |
| 1:1 | 103 | 22 | 58 | 20 |
| 2:1 | 59 | 44 | 31 | 25 |

[a]Normal VLP were between 45 and 55 nm in diameter, and possessed a morphology similar to that of intact procapsids
[b]Damaged VLPs appeared flattened by the staining process, but had no other obvious morphological defects
[c]Aberrant VLPs were elongated or partially formed structures
[d]ND, none detected
Table originally appeared in Medina et al, 2010.

It is interesting to note that the optimal concentration of scaffold protein determined here is similar to that found in λ -infected cells. AUC studies carried out in our lab demonstrate weak self-association of the scaffold protein at these concentrations (Medina, 2010), suggesting that while a majority of monomer is required for capsid growth, a small amount of dimer must be maintained as well. It is thought that the dimeric and monomeric forms of many viral scaffold proteins mediate nucleation of capsid formation and capsid growth, respectively (Tuma, 2008). A sub-optimal concentration of scaffold protein, and thus dimer, would preclude this particular nucleation event, resulting in low particle yield; on the other hand, an excess would exclusively promote nucleation events at the expense of monomer addition, resulting in the formation of incomplete shells. While the former is observed in this system, high levels of scaffold protein in this case appear to promote an elongation phase in capsid formation, resulting in tube-like structures. This may be a result of the λ scaffold protein's ability to self-associate into structures even higher order than dimer, which could sterically impede formation of the special inter-subunit contacts required for vertex assembly.

*Figure 5. Scaffold ratio, salt effects on VLP yield*

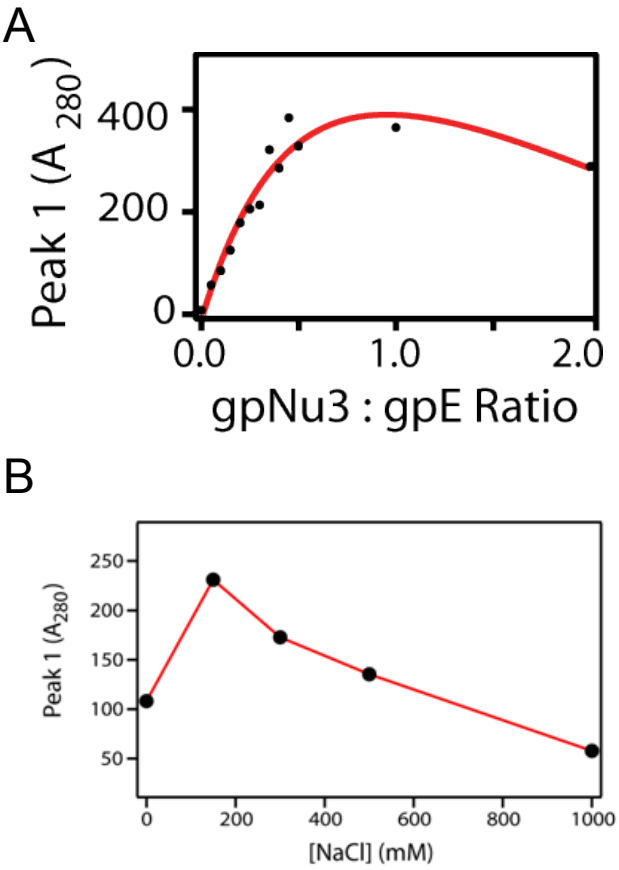


Maximum absorbance of the VLP-containing gel filtration peak at 280 nm was used as a measure of yield of particle assembly and is shown as a function of scaffold : major capsid protein ratio (*Panel A*) and salt concentration (*Panel B*). Adapted from figures that originally appeared in Medina et al, 2010.

**II.C.2 Effect of salt on λ VLP assembly**

Next, the effect of salt concentration on the VLP assembly reaction was examined. Concentrations of NaCl ranging from 0-1 M were included in the reaction mixture, and it was found that concentrations of salt above approximately 150 mM attenuate VLP assembly (Figure 5, panel B). This has similarly been observed in other bacteriophage assembly systems (Parent, 2005; Fu, 2007) and all further VLP assembly reactions were carried out at a salt concentration of 150 mM NaCl. At this point, optimization of the assembly reaction was deemed efficient enough to proceed with further VLP studies, discussed later. With the conclusion of my studies

on the initial assembly step in λ particle formation, I turned to the structural and thermodynamic characterization of subsequent events in the *in vitro* λ development pathway; namely, capsid expansion and decoration protein binding.

### II.C.3 Is λ procapsid expansion truly a two state transition?

To further probe structural and thermodynamic aspects of urea-triggered expansion, a series of SAXS measurements were collected after expansion of mature λ procapsids in various concentrations of urea, as well as procapsids and expanded capsids in the absence of urea. Prior titration data performed in the lab had indicated that urea-triggered expansion is a relatively fast process, with equilibrium reached after about 3 minutes (Medina, 2012). Kinetic SAXS measurements on freshly mixed samples yielded similar results; for most of the population, expansion occurrs within less than the experimental dead time (90 s) at 8°C.

*Thermodynamic analysis of urea-triggered expansion.* In good agreement with the gel-based method, any transitions that take place during the titration appear to be entirely two-state in the presence of urea, as evidenced by the occurrence of iso-scattering points in the titration data (Lee, 2005) (Figure 7, Panel A). Dialysis of the urea into buffer containing 15 mM $Mg^{2+}$ affords re-contracted procapsids that are grossly indistinguishable from expansion-naïve particles by SAXS. Since the expansion process is confirmed to be two-state in the presence of urea, the data were fit as linear combinations of fully unexpanded and fully expanded signals to determine the fraction of each species present, based on published procedures for HK97 (Lee, 2004). The presence of a fraction of pre-expanded capsid material that often contaminates our procapsid preparations should in theory not complicate this type of analysis, assuming that the population

remains constant throughout the titration. Quantitation of the fraction expanded can be used to calculate an equilibrium constant, and thus a ΔG for the transition at each urea concentration.

*Figure 6. Urea titrations: 15 minute equilibration vs. overnight dialysis*

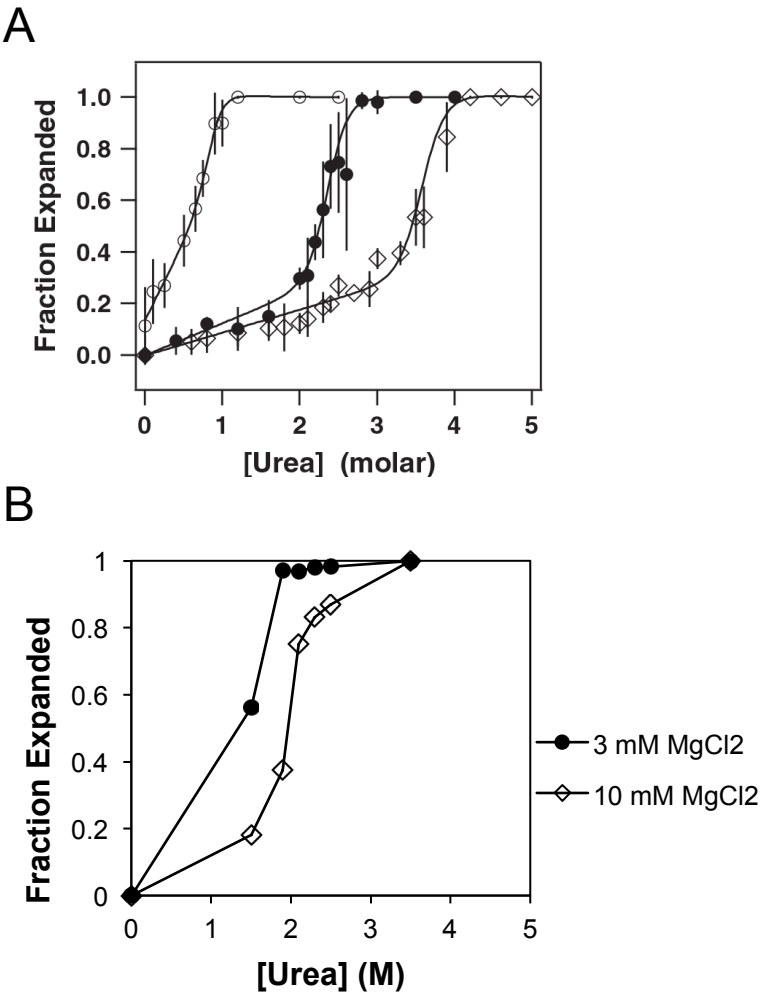


*Panel A.* Urea expansion titration data measured in-gel with a 15 minute equilibration period (from Medina et al, 2012). Titration curves and resulting fits are shown at <1 mM (open circles), 3 mM (filled circles) and 10 mM (diamonds) $Mg^{2+}$. Experiments performed by E. Medina and S. Kruse. *Panel B.* Result of calculation of fraction expanded particles from SAXS signals of procapsids dialyzed overnight into urea. Lines do not represent fitting here, and are only meant to aid the eye.

*Figure 7. SAXS analysis of capsid expansion*

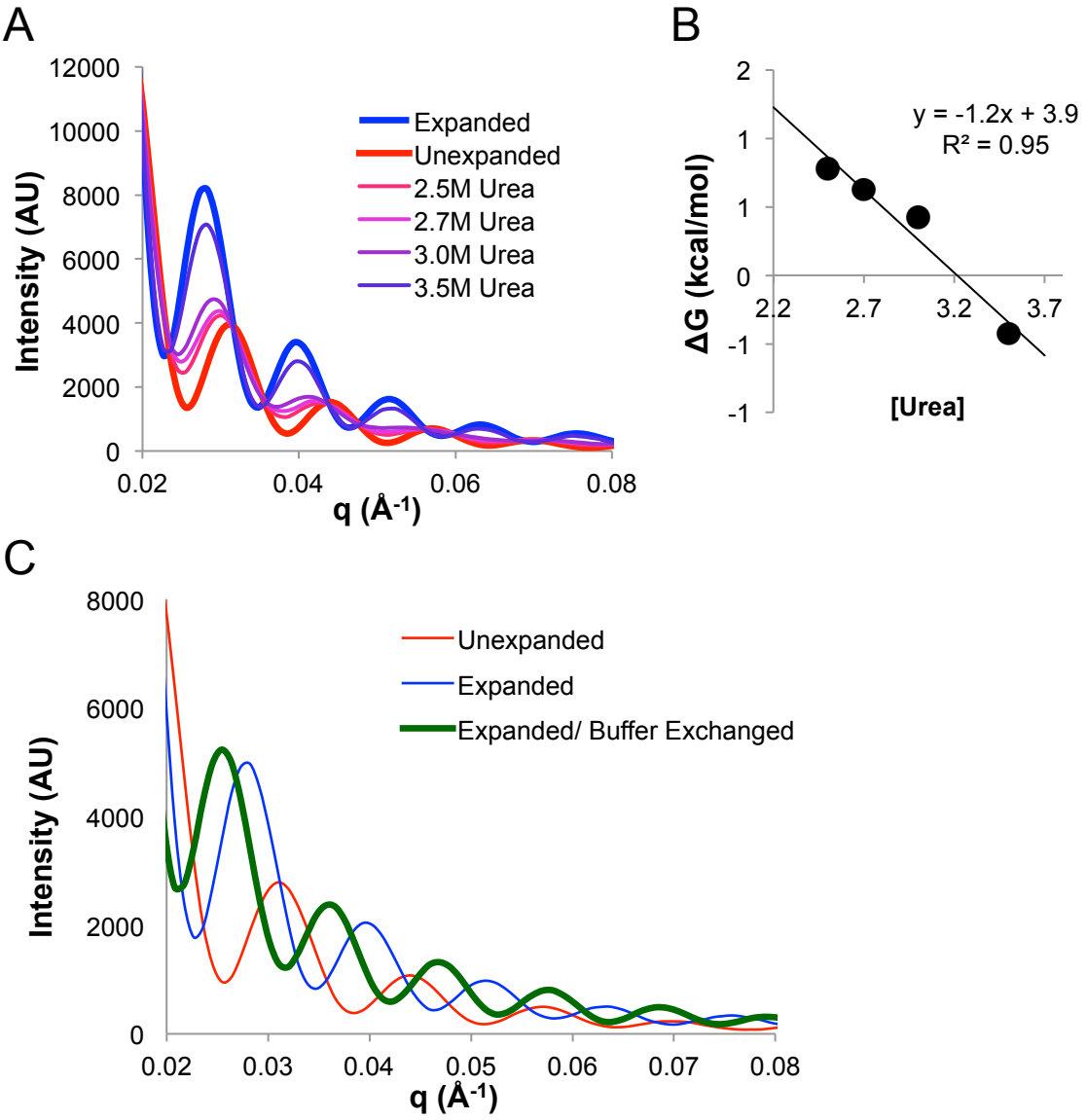


*Panel A*. SAXS scattering data collected for procapsids (red), fully expanded capsids (blue), and capsids at intermediate levels of expansion in the presence of varying concentrations of urea and 3 mM $Mg^{2+}$ (magenta and purple). Scattering intensity is shown as a function of scattering vector q. Note the presence of iso-scattering points, indicative of a 2-state transition. *Panel B*. Treatment of the titration data by linear extrapolation. Note that $\Delta G_{H2O}$ = 4 ± 2 kcal/mol calculated here is slightly lower than, but in overall agreement with, that measured by gel-based methods. *Panel C.* Dialysis of the urea into buffer containing 1 mM $MgCl_2$ afforded a third, distinct species (green), which appears slightly larger than the species in urea and no longer shares iso-scattering points with urea titration data.

Figure 7, Panel B shows the results of this analysis and a linear fit of the data. Based on the well-accepted linear extrapolation approach, a $\Delta G_{H2O}$ can be derived (4 ± 2 kcal/mol), which

agrees reasonably well with that calculated using the agarose gel-based method (Medina, 2012). Though the two values are close to within experimental error, it is possible that the modestly lower $\Delta G_{H2O}$ measured using SAXS as compared to the gel-based technique reflects a tendency of the gel matrix to strip urea from the capsids as they are subjected to electrophoresis. This may cause some to re-contract, artificially elevating $\Delta G_{H2O}$ values determined by this method.

In contrast to what is observed for brief (~15 minute) incubation in the presence of urea, studies performed on material dialyzed into urea overnight shows elevated fractions of expanded material compared with freshly mixed samples examined by agarose gel (Figure 6) and SAXS. This was highly surprising, and is suggestive either of a fraction of slowly expanding species or of a very slow, secondary equilibration step.

Observation of the scattering for up to one hour after manual mixing of urea at an intermediate concentration (with a decrease in sampling rate to reduce sample damage) did not reveal appreciable change in signal; sample deterioration prevented observation for more extended intervals. Nonetheless, the discrepancy between relatively brief, benchtop incubation and extended dialysis suggests a need to investigate very long equilibration times, and may indicate the presence of an extremely slowly expanding population.

*Discovery of an intermediate species.* Another surprising finding was that dialysis of the urea in the presence of only 1 mM $Mg^{2+}$ affords an apparently distinct species, which no longer shares iso-scattering points with the urea titration curves (Figure 7, Panel C). This presents the first evidence of intermediate (in urea) and more fully mature (buffer exchanged) *in vitro* expansion states. Unfortunately, more detailed structural analysis of the SAXS data was complicated by the presence of the aforementioned pre-expanded population of capsids. This has

proven exceedingly difficult to purify away from the stock, and ongoing work in our lab is being carried out to address this issue.

### II.C.4 Creation of a structural homology model of the λ major capsid protein*.

The lack of high-resolution information for the λ major capsid protein gives little structural context for the biochemical studies on capsid maturation that have been carried out in our lab. As a first step towards structural characterization, I generated a structural homology model of the λ major capsid protein using two independent programs, the PHYRE[2] Protein Homology/Analogy Recognition program and the I-TASSER Protein Structure and Function Prediction program. Both programs returned the prophage CFT073 protein (RCSB PDB 3BQW) as the top structural homology candidate. This putative capsid protein, which shows greater than 43% sequence identity to the λ capsid protein, crystallizes as a monomer (Zhang, unpublished). The PHYRE and I-TASSER structural homology models are quite similar (not shown) and both are of high quality (Table 2). For simplicity, the I-TASSER model was utilized for further interrogation.

While the λ major capsid protein structural model is based on the crystal structure of the CFT073 capsid protein monomer, the essential structural features show a striking similarity to those observed with the HK97 major capsid protein assembled into a procapsid shell (Huang, 2011). These include the apical (A) domain, the procapsid (P) domain, and the spine helix (Figure 8). A major difference between the two structures is the position of the "E-loop" (yellow). This loop, which was identified in the crystal structure of the HK97 procapsid shell, extends from the spine helix and contributes two strands of a three-stranded β-sheet; the third β-strand is donated by N-terminal residues of a neighboring subunit in the capsid shell (Gertsman,

2009;Veesler, 2012). The putative E-loop in the λ homology structure is folded back upon itself in the model presented here, likely a result of energy minimization procedures used in structure prediction only reflecting the protein as a monomer; potentially stabilizing inter-subunit contacts are not taken into consideration using these methods. Expansion of the HK97 procapsid shell is accompanied by disruption of spine-helix/E-loop interactions and extension of the E-loop to its final position in the mature shell (Gertsman, 2009;Veesler, 2012). It is my expectation that the E-loop in the λ major capsid protein monomer similarly adopts an extended conformation during assembly into the procapsid shell to form the stabilizing contacts described in the HK97 shell structure.

*Table 2. Quality of structural models for major capsid protein*

| **PHYRE**[2] | | **I-TASSER** | |
|---|---|---|---|
| E-value | $3.4x10^{-28}$ | C-score | 2.221 |
| Estimated Precision | 100% | TM-score | 0.99±0.04 |

Originally appeared in Singh et al, 2013.

*Figure 8. Comparison of HK97 and λ major capsid proteins*

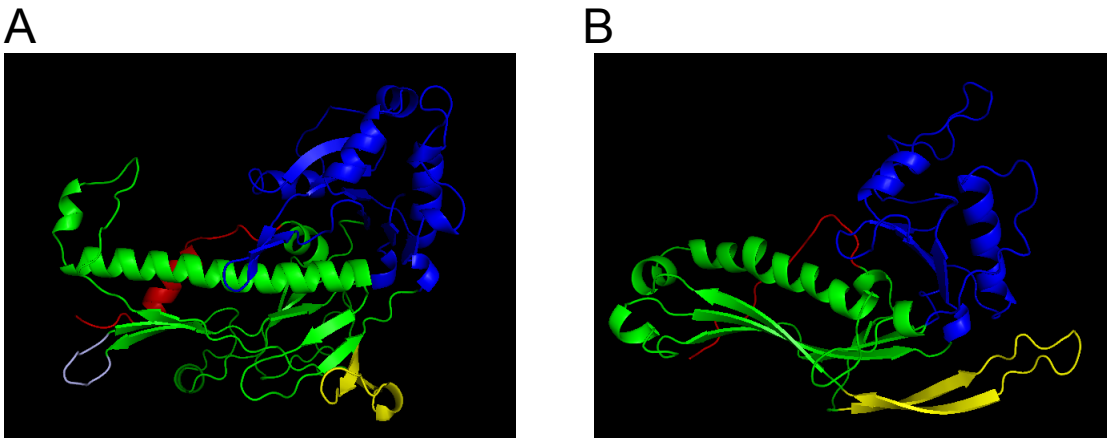


*Panel A*. Structural Homology Model for gpE, the λ major capsid protein. The apical (A) and procapsid (P) domains are colored in blue and green, respectively, and the E-loop is colored yellow. *Panel B*. Crystal Structure for gp5, the HK97 major capsid protein (RCSB PDB 1FH6). From Singh et al, 2013.

*Validation of the major capsid protein structural model, and evaluation of structural differences between procapsid and expanded capsid using CCMS*[*]. A rigorous protocol for the identification of neighboring residues within a protein using a CCMS process had been reported previously (Singh, 2008). This method allows characterization of chemical and native cross-links without the necessity for specialized or heavy-labeled cross-linking reagents or software. Selective enrichment of high charge-state peptides and high mass accuracy of parent and fragment ions increase database selectivity and significantly decrease false positives in (Singh, 2008). With the kind assistance of Pragya Singh, I extended this method to identify cross-linked residues in a complex biological structure, the λ procapsid shell.

Purified procapsids and expanded capsids exchanged out of urea were cross-linked with the indicated reagent and chemical cross-links identified by mass spectrometry as described in II.B.5. The $BS^2G$ and EDC cross-linking experiments were repeated three times with three separate procapsid preparations to identify reproducible cross-links in the major capsid protein assembled into the procapsid shell. The SDA cross-linking experiment was conducted only once, but the results are included for completion. Though no differences in cross-links are observable between the procapsid and capsid samples, interpretation is again complicated by the presence of a contaminating pre-expanded species present in both cases. The lack of additional cross-links identified in the procapsid sample suggests that at the very least, no cross-linkable protein-protein contacts are *broken* upon capsid expansion. The extent to which the contaminating species masks additional contacts *formed* upon expansion is unknown.

I next mapped the identified cross-links onto the structural homology model as shown in Figure 9. Most of the cross-linked residues are disposed on the protein surface and the intra-molecular Cα-Cα distances between these residues are within the acceptable range for the

respective cross-linking reagent (Table 3). These distances were used as constraints in a second round of model building using I-TASSER, which refined but did not significantly alter the results (not shown). This provides confidence that the model accurately reflects the essential features of the major capsid protein monomer.

*Figure 9. Pseudoatomic model of major capsid protein monomer*

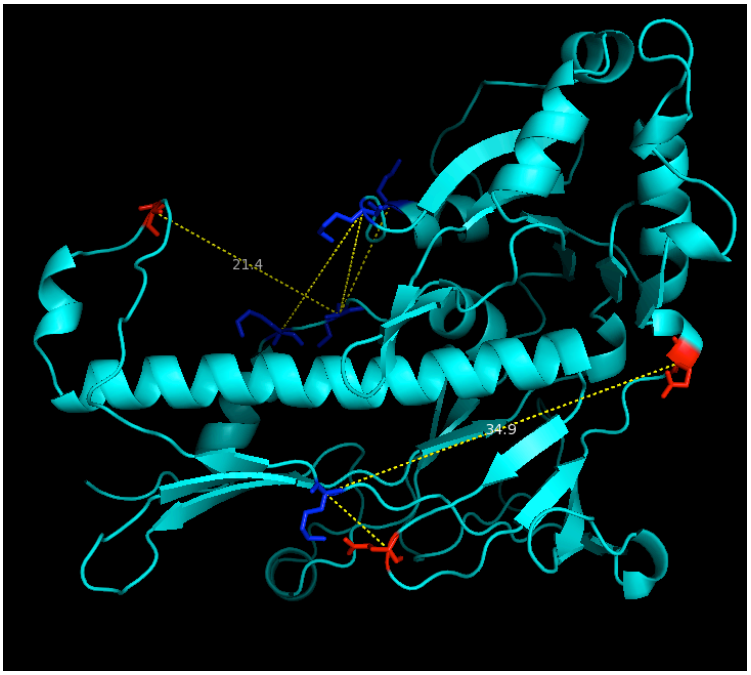


Chemical cross-links identified in the major capsid protein assembled into the λ procapsid shell. Refined I-TASSER structural homology model with identified intra-molecular cross-links shown in the monomer. Relevant glutamic acid and lysine residues are shown as sticks in red and blue, respectively. The measured Cα-Cα distances between residues in the identified cross-links are presented in Table 3. From Singh et al, 2013.

The inter-residue distances dictated by most of the cross-links identified are in agreement with the monomeric model; however, several cannot be accounted for. For instance, $BS^2G$ cross-links between K212-K212 and K233-K233 are inexplicable in the context of a monomeric protein. Further, K18 and D95 are reproducibly cross-linked with EDC, but they are too far apart

in the monomeric structural model to be cross-linked with this reagent. A similar issue is observed with residues K79 and E158. I reasoned that these represent an *inter*-molecular interaction between major capsid protein subunits assembled into the capsid shell. To test this hypothesis, I went on to construct a pseudo-atomic model of the λ procapsid shell.

*Table 3. Distances between identified cross-linked residues in the gpE monomer structural model*

| **EDC (10 Å)**[a] | | **$BS^2G$ (21 Å)**[a] | | **SDA (16 Å)**[a] | |
|---|---|---|---|---|---|
| *Cross-link* | *Distance*[b] | *Cross-link* | *Distance*[b] | *Cross-link* | *Distance*[b] |
| K18---(D95/E96/D97)[c] | 22.2 Å | K16---K237 | 17.9 Å | E229---K233 | 6.8 Å |
| K79---E145 | 8.0 Å | K18---K233 | 12.3 Å | K18---(G223-E227)[d] | 15.9 Å |
| K79---E158 | 34.6 Å | K18---K237 | 14.9 Å | - | - |
| | | K212-K212 | - | - | - |
| | | K233-K233 | - | - | - |

[a]Reasonable Cα-Cα distance for chemically cross-linked residues. These values represent the length of each cross-linked side chain plus the length of the linker; conservatively ~21 Å for a Lys-Lys $BS^2G$ cross-link, ~11 Å for Lys-Glu EDC cross-link, ~10 Å for Lys-Asp EDC cross-link; ~16 Å for Lys-Glu SDA cross-link.
[b]Closest intra-molecular Cα-Cα distance between the identified residues in the initial gpE structural homology model. These distance constraints were used in a second round of model building.
[c]The residue cross-linked to K18 could not be unambiguously identified in this peptide. Glu95 was used for the distance calculation.
[d]The residue cross-linked to K18 could not be unambiguously identified in this peptide. Glu227 was used for the distance calculation.
Table from Singh et al, 2013.

*Pseudo-atomic model for the λ procapsid shell*[*]. 415 copies of the λ major capsid protein assemble into hexamers that form the 20 faces of the icosahedron, as well as pentamers that reside at 11 of the icosahedral vertices. I constructed pseudo-atomic models for these "hexon" and "penton" capsomers using the cryo-EM structure obtained by Johnson and co-workers (Lander, 2008) and the major capsid protein homology model described above. The model

[*] These sections adapted from Singh et al, 2013.

structure was fit into the penton and hexon cryoEM densities of the λ procapsid shell as described in II.B.6; this yields a reasonable fit as shown in Figure 10.

I then re-evaluated the identified cross-links, in particular those not explained by the monomer model alone. K212, which cross-links to "itself" lies at the crest of each subunit assembled into the capsomers (Figure 10). These residues form a ring at the top of a central groove, and the Cα-Cα inter-molecular distance between these residues is well within the range required for a $BS^2G$ chemical cross-link (Table 4). K233 residues form a similar pattern, but at the base of the capsomer groove; the Cα-Cα distance between them is consistent with the identified K233-K233 chemical cross-link. Finally, residues K18 and D95, which are separated by over 22 Å in the major capsid protein monomer model, are within 5 Å and 10 Å in adjacent subunits in the penton and hexon capsomers, respectively. This distance is consistent with that predicted by a $BS^2G$ cross-link (Table 4, Figure 10).

*Table 4. Distances between identified cross-linked residues in the capsomer models*

| **EDC (10 Å)[a]** | | **$BS^2G$ (21 Å)[a]** | |
|---|---|---|---|
| *Cross-link* | *Distance[b]* | *Cross-link* | *Distance[b]* |
| K18---(D95/E96/D97)[c] | 5.2 Å (penton)<br>9.9 Å (hexon) | K212---K212 | 19.5 (penton)<br>15.9 (hexon) |
| K79---E158 | 44.9 Å (penton)<br>38.3 Å (hexon) | K233---K233 | 17.0 (penton)<br>19.4 (hexon) |

[a]Reasonable Cα-Cα distance for chemically cross-linked residues. These values represent the length of each cross-linked side chain plus the length of the linker; conservatively ~21 Å for a Lys-Lys $BS^2G$ cross-link, ~11 Å for Lys-Glu EDC cross-link, ~10 Å for Lys-Asp EDC cross-link.
[b]Closest inter-molecular Cα-Cα distance between the identified residues in adjacent gpE subunits within the petamer and hexamer capsomers, as indicated.
[c]The residue cross-linked to K18 could not be unambiguously identified in this peptide. Glu95 was used for the distance calculation.
Table from Singh et al, 2013.

The only cross-link not accounted for in the structural homology models is that of K79-E158. These residues are separated by over 30 Å in the monomer model, over 38Å in adjacent subunits in the capsomers. It is notable that K79 lies within the predicted "E-loop" of the major capsid protein; movement of the loop toward the position it likely assumes in the assembled capsid shell (discussed above) could situate K79 to interact with E158. Whatever the case, the ensemble of models presented here are consistent with virtually all of the CCMS data presented in Tables 3 and 4, which provides confidence in the proposed structures.

*Figure 10. Pseudoatomic models of capsomers*

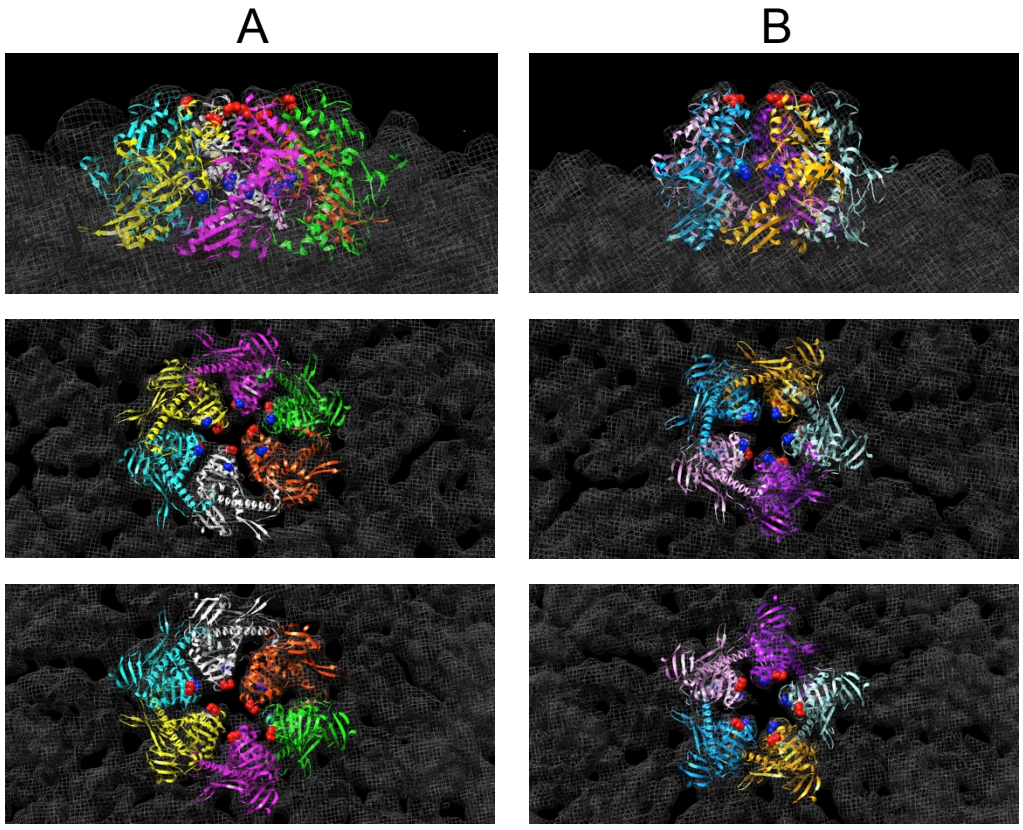


*Panel A*. Hexon capsomer structure shown in side, bottom (relative to capsid shell) and top views. *Panel B*. Penton capsomer structure shown in side, bottom (relative to capsid shell) and top views. Individual gpE monomers within the capsomers are uniquely colored. Note that residues K212 (red spheres) and K233 (blue spheres), lay in a ring pattern at the top and bottom, respectively, of a central channel. Originally appeared in Singh et al, 2013.

*Biological implications of the λ procapsid structural model - procapsid expansion and gpD binding*[*] Genome packaging in the dsDNA viruses triggers a striking re-organization of the proteins assembled into procapsid, which typically results in thinning, angularization, and expansion of the capsid shell (Hohn, 1976; Dokland & Murialdo, 1993). The λ system is remarkable in that the procapsid expansion reaction is fully reversible *in vitro* and we have characterized the thermodynamic parameters of the transition (Medina, 2012). The data indicate that capsid expansion is accompanied by significant exposure of hydrophobic surface area. The viral decoration protein does not interact with the procapsid, but adds as a trimer spike at the three-fold axes of the expanded capsid shell (Lander, 2008; Medina, 2012).

Structural studies show that the base of the decoration protein spike is highly hydrophobic (Yang, 2000). We have hypothesized that expansion of the procapsid shell exposes hydrophobic patches at the three-fold axis of the shell, which serves to nucleate the assembly of the spike (Medina, 2012). To investigate this further, I constructed a pseudo atomic model for the major capsid protein assembled at the three-fold axes of the procapsid shell (Figure 11, panel A). The model reveals that a number of hydrophobic residues displayed at the shell exterior and in particular within hydrophobic grooves extending radially from the center of the three-fold axes. It is noteworthy that these radially disposed grooves match hydrophobic spines observed at the base of the decoration protein spike (Figure 11, panel B). It is tempting to speculate that rotation of the A domains toward the shell surface, as observed during expansion of the HK97 procapsid, exposes these hydrophobic grooves to provide a nucleation site for decoration protein trimer assembly at the three-fold axes of the expanded capsid lattice. Indeed, current studies in our lab indicate that hydrophobic interactions, at least in part, mediate binding to the expanded capsid shell (Kruse and Catalano, in progress).

*Figure 11. Pseudoatomic model of quasi-three fold axis with decoration protein binding surface*

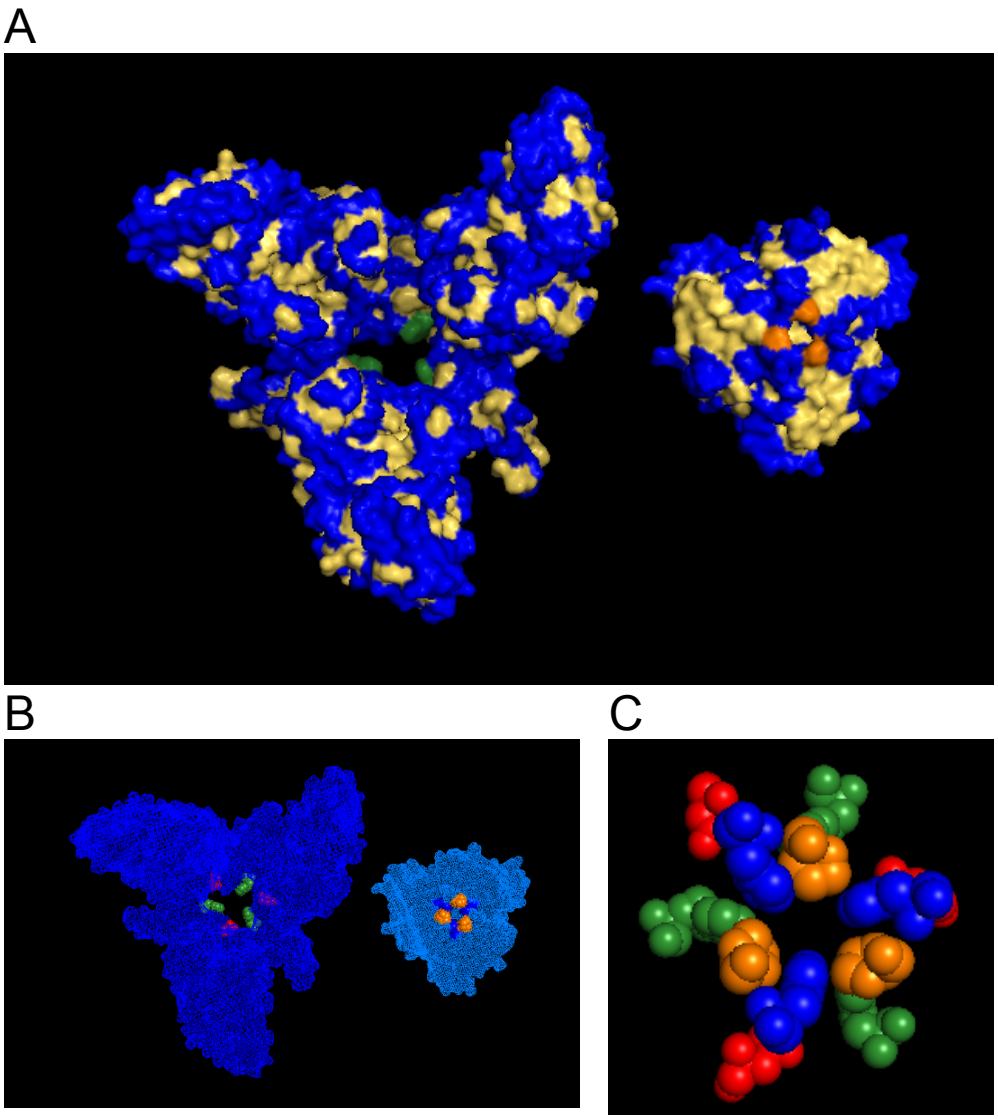


*Panel A Left*: pseudo-atomic model for gpE assembled at the icosahedral 3-fold axes of a λ procapsid shell, viewed from the exterior. The proteins are displayed in surface representation with hydrophobic residues colored yellow. Hydrophobic grooves are observed within each gpE monomer extending outwards from the central channel. Shown in yellow are Val78, Pro80, Ala122, Ile123, Val126, Met129, Val132, Leu136, Ala146, Phe147, Phe266, Pro268, Ala291, Trp308, Phe318 and Met320. *Panel A Right*: crystal structure of the gpD trimer spike (PDB ID shown from the base of the structure in surface representation. Hydrophobic residues are colored yellow. *Panel B* A mesh surface representation is displayed; gpE is shown in dark blue with Trp308 and Asp292 as green and red spheres, respectively. gpD is shown in light blue with Pro17 and His19 as orange and dark blue spheres, respectively. *Panel C* Superposition of residues in the gpD trimer spike with those in the gpE trimer, in the same orientation and colored as in *B*. Originally appeared in Singh et al, 2013.

Close inspection of the trimeric decoration protein crystal structure reveals a ring of three histidines (His19), alternating with a ring of three prolines (Pro17) radially displayed on the spike base (Figure 11, Panels B and C); it has been proposed that these residues play an important role in assembly at the capsid surface (Yang, 2000). Close inspection of the procapsid structural model reveals similarly disposed alternating trimers of aspartic acid (Asp292) and tryptophan (Trp308) at the center of the three-fold axes on the procapsid shell surface (Figure 11, Panels B and C). Thus, the Asp292 trimer ring in the procapsid is poised to provide three salt bridges to the three His19 residues in a trimer spike. Further, the three radially disposed Trp308 residues at the procapsid surface are poised to interact with the Pro17 residues in the decoration protein. This array could provide over 40 kcal/mol binding energy towards trimer spike assembly at each of the 140 three-fold axes at the expanded capsid surface.

### II.C.5 Expansion and decoration protein binding of λ VLP assembled *in vitro*.

Now that the *in vitro* VLP assembly and procapsid maturation pathways had been elucidated and optimized to a sufficient degree, I hoped to combine these techniques in the construction of fully mature, decorated λ -based nanoparticles assembled entirely in solution. VLP were assembled under the previously determined optimum conditions, expanded in the presence of 2.5 M urea, exchanged into buffer containing under expansion-maintaining conditions, and incubated in the presence of saturating concentrations of decoration protein (Figure 12) prior to purification by gel filtration.

*Figure 12. Full in-vitro VLP assembly and maturation*

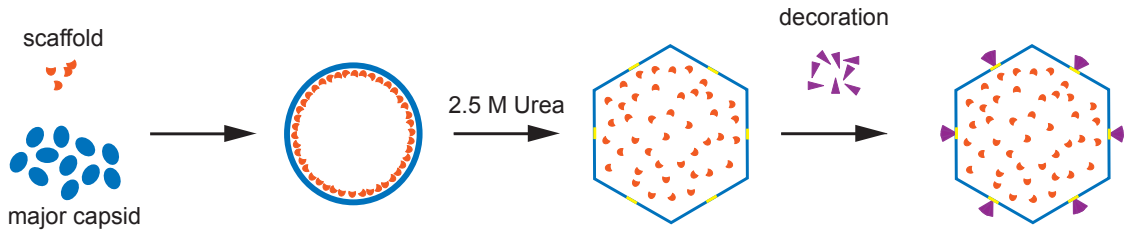


Major capsid protein and scaffold are combined in a 0.3:1 molar ratio. VLP form upon removal of denaturant which is required to solubilize the major capsid protein in the absence of scaffold. The resulting VLP are expanded using the same protocol for full procapsids, and the buffer-exchanged particles are coated with decoration protein. The fate of the scaffold protein upon VLP expansion is unknown; in the case of fully closed particles it is expected to remain within the interior of the shell.

Procapsids and VLP at various stages of maturation show striking similarities when monitored by native agarose gel (Figure 13, Panels A & B). Slight differences in migration may be attributable to the absence of portal proteins in the VLP; it is also notable that on the percentage gel used here the decorated (and therefore more massive) species has a higher mobility than the un-decorated, likely due to increased negative charge of the particle upon decoration protein binding. Though the model constructed in the previous section predicts the opposite change in surface charge at on a residue level at the decoration protein binding site, the decoration protein itself carries an overall negative charge at neutral pH and is likely the cause of this phenomenon.

Micrographs of the VLP also bear a strong resemblance to those taken of procapsids at corresponding stages (Figure 13, Panels C & D). Both expanded and unexpanded VLPs appear to interact with decoration protein under the experimental conditions, as evidenced by their co-elution when decorated particles are purified by gel filtration (decoration protein does not elute in the void volume when run alone under identical conditions).

*Figure 13. Comparison of VLP and procapsid in vitro maturation*

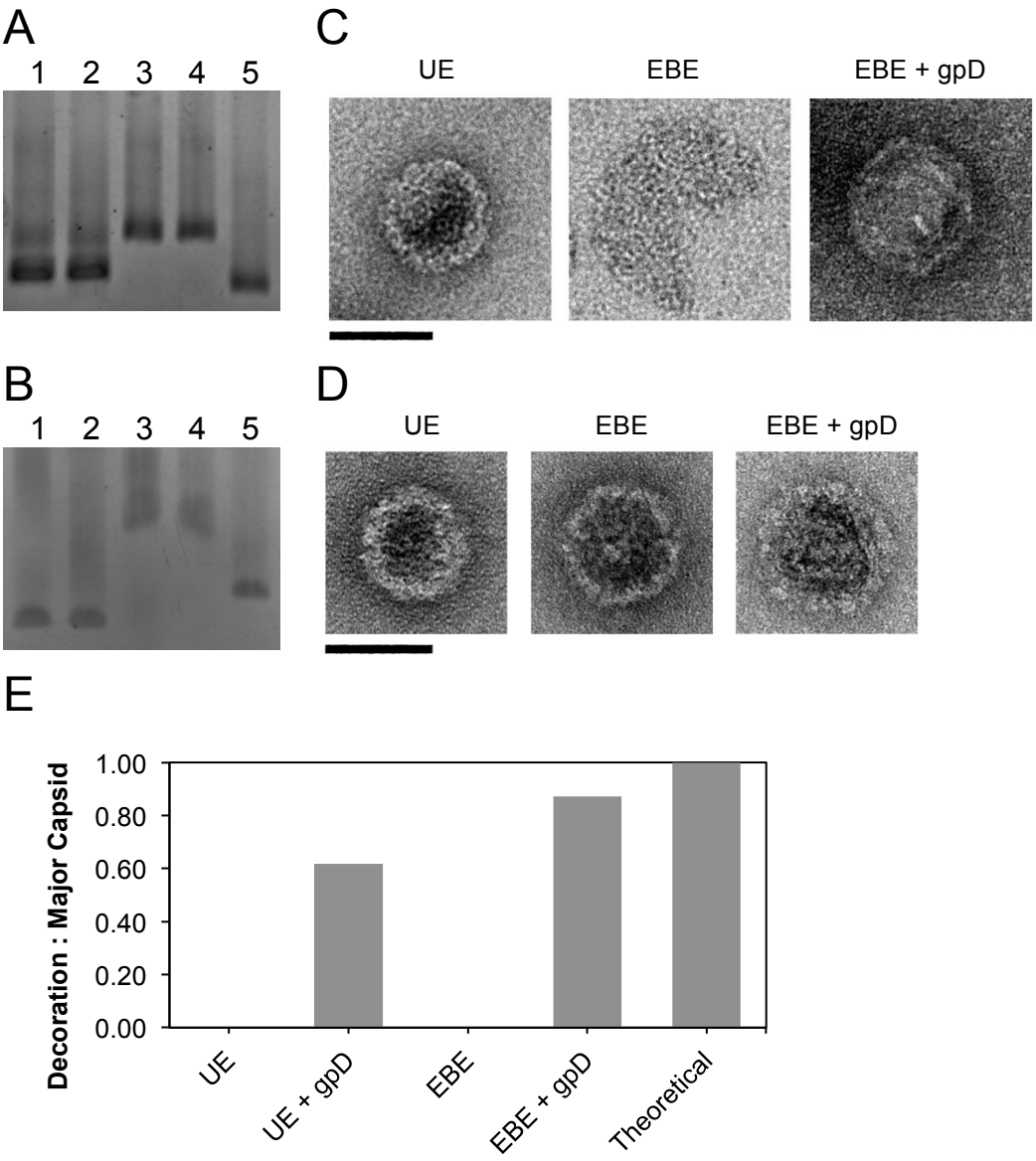


*Panels A & B*. Procapsids (*A*) and VLP (*B*) at varying stages of urea-triggered maturation and decoration as visualized by agarose gel. Lanes labeled 1 and 2 contain the unexpanded particles in the absence (UE) and presence of decoration protein (UE + gpD), respectively. Lanes 3 and 4 contain expanded particles in the presence (E) and absence (EBE) of urea, respectively. Lane 5 contains the expanded particles in the absence of urea after incubation with decoration protein (EBE + gpD). *Panels C & D*. Electron micrographs collected of the capsids (*C*) and VLP (*D*), using 2% uranyl acetate for negative staining. Note that in both cases the expanded, undecorated species appears less stable to staining than unexpanded or decorated particles. *Panel E*. Decorated and undecorated VLP were purified by SEC, and resulting fractions analyzed by SDS-PAGE. Decoration protein was found to co-elute with VLP when incubated either with unexpanded or expanded, buffer exchanged particles. The expected 1:1 ratio was only achieved with the expanded, buffer exchanged species.

When quantitated by video densitometry, it was found that decoration protein interaction with major capsid protein in expanded VLPs occurs at very close to the expected 1:1 ratio, assuming equal staining of proteins and adjusting for differences in mass. Binding to unexpanded VLP occurs to a somewhat lesser but appreciable extent (Figure 13, panel E). This is hypothesized to result from assembly of some fraction of pre-expanded VLP that are still homogeneous in appearance, as these are also observed in the case of procapsid preparations (discussed above). In the contaminating capsid material and possibly also in VLP, these pre-expanded particles do appear capable of binding to decoration protein. It has been shown, however, that the unexpanded procapsid species assembled *in vivo* do not interact with the decoration protein prior to expansion (Medina, 2012). This is an interesting discrepancy between the assembly systems, though for the strict purposes of nanoparticle design interaction of decoration protein with both expanded and unexpanded forms is acceptable, so long as those interactions are equally stable in both cases.

Taken together, all of these data allow the construction of a complete model of λ assembly and maturation *in vitro* (Figure 12). Under the optimized conditions, a scaffold protein monomer-dimer equilibrium is established, which is critical to chaperone the major scaffold protein into regular, icosahedral lattices. The optimal balance between particle yield and fidelity is found at a ratio of 0.3:1 scaffold : major capsid protein. Similar concentrations of scaffold protein likely chaperone assembly of the viral capsids prior to packaging of DNA and expansion (Figure 14, Panel A).

*Figure 14. Revised in vivo and in vitro assembly and maturation pathways*

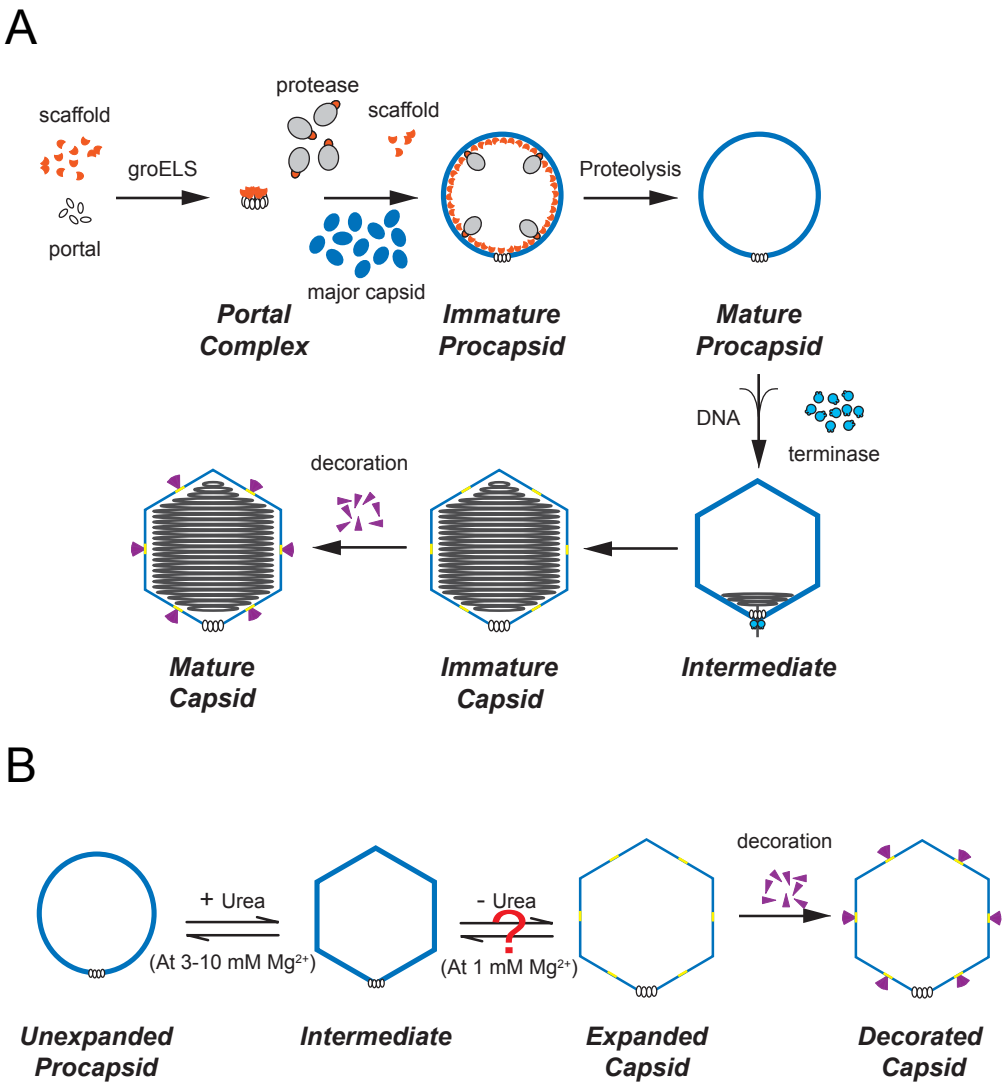


*Panel A.* The *in vivo* assembly pathway for λ, with revisions based on the work presented here. Capsid assembly likely takes place at a scaffold : major capsid protein ratio of approximately 0.3 : 1, and may require low levels of scaffold protein dimer. Early stages of DNA packaging may promote the formation of a pre-expanded intermediate, followed by full expansion, which exposes decoration protein binding sites, shown in yellow. Decoration protein then binds at these sites, stabilized by a combination of stacking/ hydrophobic interactions and salt bridges. *Panel B*. Urea-triggered capsid expansion pathway, with intermediates filled in. Microscopic reversibility of expansion to the intermediate has been demonstrated indirectly in the range of [$Mg^{2+}$] indicated; reversibility of the expanded capsid and the intermediate at the [$Mg^{2+}$] indicated is expected but has not yet been explored.

Urea-triggered procapsid maturation to an intermediate state is a reversible, two-state process in the presence of ~3-10 mM $Mg^{2+}$, however dropping the concentration of $Mg^{2+}$ to 1

mM causes the process to be irreversible, instead promoting the formation of a fully expanded state capable of binding to decoration protein (Figure 14, Panel B). Limitations in material precluded the recapitulation of these studies on VLP, however it is expected that the results obtained would be highly similar if a preparation of fully unexpanded particles were used (see above).

In the future, comparison between VLP and mature procapsids could be useful in uncovering any role of the portal complex in the energetics of expansion. It is unknown whether the intermediate seen in the presence of urea is biologically relevant; it is possible that the partially expanded species represents the conformation adopted by the capsid at an intermediate level of genome packaging while the more fully expanded species likely represents the form of the capsid which binds decoration protein (Figure 14, Panel A).

Decoration protein binding, both *in vitro* and *in vivo*, is likely mediated by a combination of nonspecific hydrophobic interactions and more specific stacking and salt contacts between residues on the major capsid protein and those located at the base of the decoration protein trimer. These residues are buried in the context of the procapsid but become exposed upon expansion. This binding event stabilizes the structure and prevents contraction, even in the presence of elevated $Mg^{2+}$ concentrations.

### II.C.6 Binding of functionalized decoration protein to λ capsids

In the spirit of nanoparticle design, I wish to make note of a number of recent studies carried out in our lab by Dr. Jenny Chang, who used the basis described here to create a set of engineered decoration proteins amenable to use in multifunctional λ nanoparticle assembly (Fig 15, Panel A).

*Figure 15. Further work toward multifunctional nanoparticles*

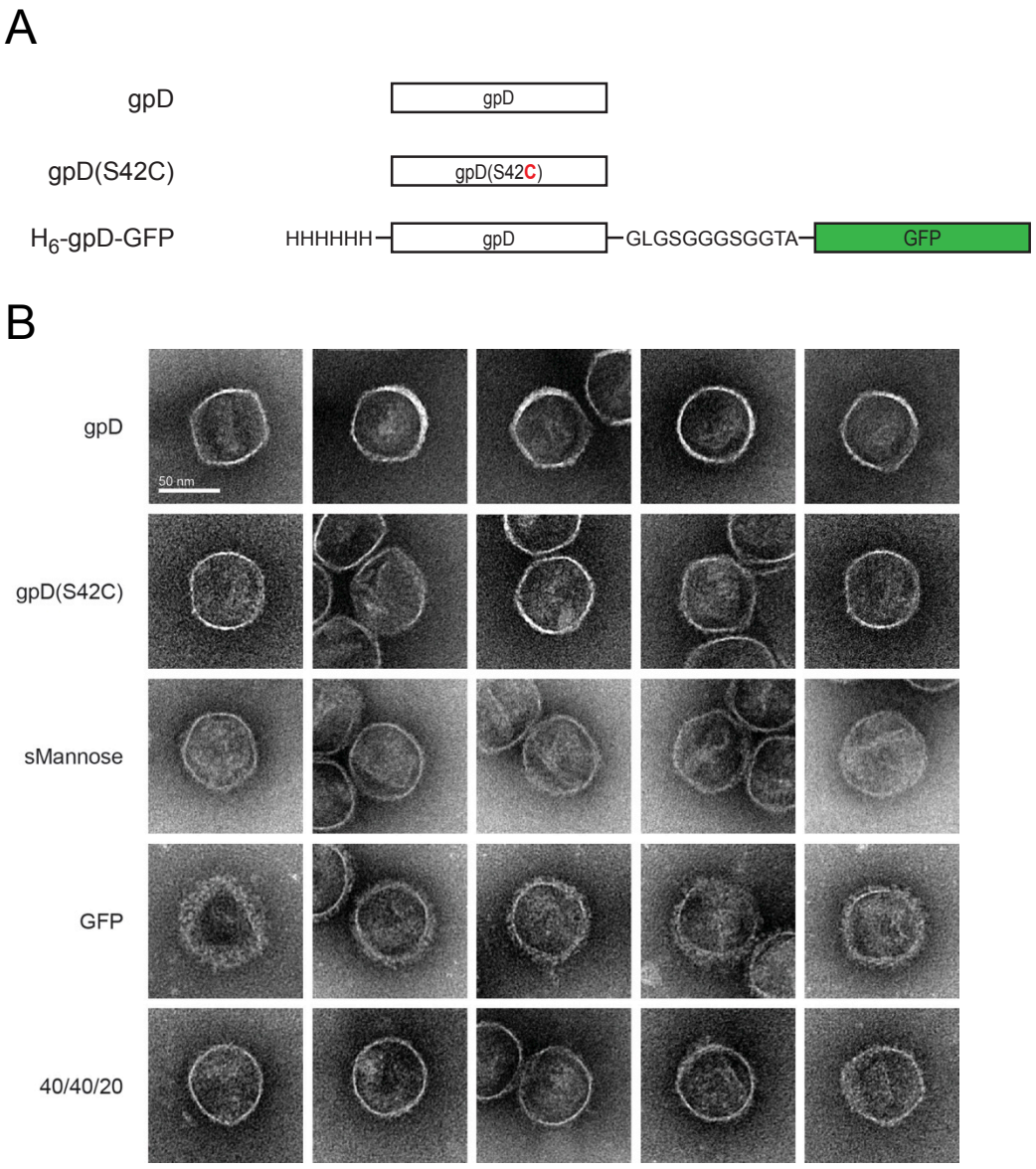


*Panel A*. Decoration protein clones prepared by J. R. Chang (figure courtesy J. R. Chang). *Panel B*. Electron microscopy of capsids decorated with the mutants indicated stable binding of all, as well as the ability to create multifunctional nanoparticles coated with a 40/40/20 mixture of gpD, gpD S42C, and gpD-GFP.

Notably, a construct with a gpD-S42C mutation introduced was created for the purpose of chemical ligation, as well as a fusion to green fluorescent protein (GFP) to demonstrate the decoration protein's ability to assemble and properly stabilize the capsid even in the presence of

relatively large, artificially introduced domains. She was able to demonstrate conjugation of a single mannose moiety to the S42C mutant prior to full particle assembly, as well as subsequent binding of gpD-S42C, gpD-S42C-mannose, and gpD-GFP to capsids expanded *in vitro*. She also demonstrated the assembly of multifunctional particles using various ratios of the three decoration protein variants (J. R. Chang, manuscript in preparation).

Upon examination of these particles by electron microscopy, I found that they are indistinguishable in morphology from those assembled using wild-type decoration protein, with the exception of those displaying the GFP fusion which have extended, diffuse shells owing to the presence of GFP at the surface of the capsids (Figure 15, Panel B). These encouraging results serve as further evidence that construction of multifunctional λ nanoparticles is in fact possible, and combined with promising data regarding the assembly of VLP containing scaffold fusion proteins, it seems as though it will be possible to assemble modular, customizable nanoparticles such as these entirely *in vitro* in the very near future.

# Chapter III. Assembly of Nanoparticles Derived from HIV-1 Envelope Protein and Human Apolipoprotein A-I

## III.A Introduction

At the end of 2012, an estimated 35.3 million individuals in the world were living with HIV, the infectious agent causing acquired immune deficiency syndrome (AIDS), while approximately 1.6 million died that year from AIDS-related complications (UNAIDS). It is agreed that containment of the pandemic is contingent upon prevention of infection (Fauci, 2008), and though commendable efforts have been made toward the development of a vaccine, no attempts so far have proven successful in humans (Hu & Stamatatos, 2007; Walker & Burton, 2008).

HIV infection is initiated by viral attachment to the host cell upon binding to CD4, a receptor found on T helper, dendritic, and other immune cells. Binding to chemokine receptors CCR5 or CXCR4 is also necessary for subsequent fusion of the host cell membrane and viral envelope (Alkhatib, 2009). The genetic material contained within the newly discharged viral capsid is uncoated (Forshey, 2002), and reverse transcription of the viral ssRNA to dsDNA proceeds. This process is decidedly error-prone, giving rise to HIV's exceedingly high mutation rate (Preston, 1988). Translocation of viral cDNA into the nucleus is followed by stable integration of the newly synthesized viral DNA into the host genome by virally encoded integrase enzyme; after this step infection is effectively permanent. The host cell transcribes mRNA from the integrated DNA, which is translated into viral proteins and also serves as viral

genetic material; these assemble into new viral particles, which bud from the cell surface and go on to begin the cycle in a new host.

*Figure 1-The HIV-1 Envelope Protein*

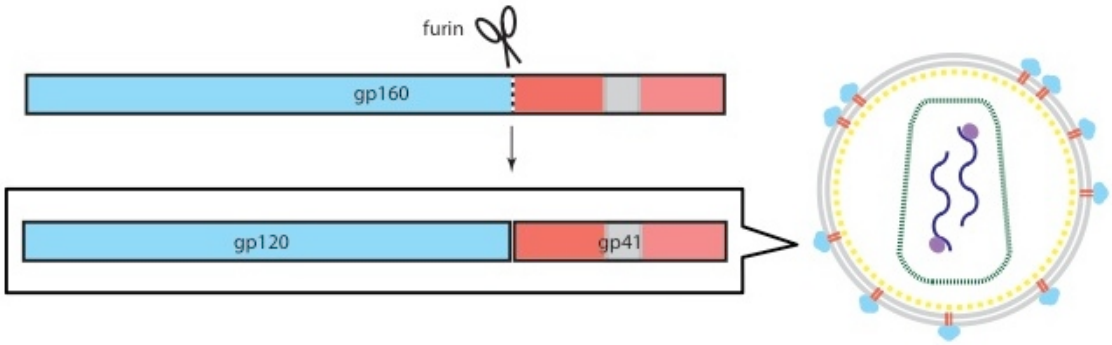


The HIV-1 envelope glycoprotein Env is expressed as a 160 kDa precursor which is cleaved in the trans-golgi network by furin. The resulting surface (gp120) and transmembrane (gp41) subunits remain noncovalently associated. The transmembrane domain of gp41 is shown in gray, and the ectodomain and cytoplasmic domain are shown in dark and light orange, respectively.

HIV particles display only a single envelope protein that comprises the target for all known broadly neutralizing antibodies (bNAbs) directed at the virus (Schief, 2009, Hoxie 2010). This surface protein, Env (Figure 1), is expressed as a 160 kDa precursor (gp160) which is heavily glycosylated and forms trimeric spikes anchored in the lipid bilayer of the Golgi. Proteolytic maturation of the precursor to a 41 kDa transmembrane subunit (gp41) and a 120 kDa surface subunit (gp120) is likely mediated by cellular furin, and possibly other proprotein convertases, in the *trans* Golgi network (Moulard & Decroly, 2000). This yields the mature envelope spike, which is incorporated into the viral envelope during budding and mediates all initial attachment events, including CD4/coreceptor binding and fusion. It is noted that gp120 and gp41 remain noncovalently associated after proteolytic maturation of the precursor; although this event is not

strictly required for CD4 binding, the immature viral spike cannot support fusion (Gu, 1995; Moulard & Decroly 2000).

Earlier antibody-based vaccination trials focused upon generating an immune response toward recombinant, monomeric gp120 and have been uniformly unsuccessful in generating bNAbs (Hoxie, 2010). This type of preparation may have been unsuccessful against whole virus due in part to the fact that immunogenic regions of gp120 not normally accessible on the native spike are exposed when it is in monomeric form. Efforts have also been made toward use of oligomeric forms of Env in an attempt to present the spike in a more native quaternary configuration, in particular solubilized "gp140" mutants containing gp120 and the ectodomain of gp41. Although results are in general more promising when oligomeric envelope constructs are used (Hoxie, 2010; Phogat & Wyatt, 2007), it has been concluded that the failure of most rationally designed immunogens to elicit bNAbs to primary isolates of HIV results in large part from their inability to mimic the natural presentation of epitopes in the HIV particle (Hu, 2007; Walker & Burton, 2008; Hedestam, 2008).

One obstacle in engineering of a native-like, oligomeric gp120/gp41 antigen appears to be maintaining protein-protein contacts within each gp120-gp41 protomer, as gp120 monomers have been known to shed from the envelope spike leaving behind gp41 stubs (Moore, 1990). This occurs in spite of the fact that the intact complex is required for infectivity, and is especially problematic in vaccine preparations that typically undergo numerous purification steps and repeated freeze-thaw cycles. A number of mutations have been introduced to some of the gp140s in order to stabilize these contacts or remove the natural furin cleavage site altogether (Sanders, 2002; Beddows, 2007; Dey, 2009). A recent study has shown that instead of the trimer form that was previously assumed, several of these uncleaved mutants actually comprise dimer and

monomer, with only the latter species appearing to adopt a native conformation (Guttman, 2013). This is in agreement with another very recent report, which also demonstrated that retention of the native cleavage site in these species is critical for native quaternary structure of the spike (Ringe, 2013).

It has been suggested that Env which maintains its wild-type sequence but remains unprocessed by furin (referred to here as gp160 for clarity) may actually represent a significant, "non-native" species that is, in fact, present on the surface of infectious viral particles, and could be a target of recognition by certain bNAbs (Poignard, 2003; Moore 2006, Leaman, 2010). The role it may play in eliciting these bNAbs is poorly understood, and further investigation into the oligomeric states it may adopt and its antigenicity seems warranted.

As is highlighted by the rigorous study of gp140 oligomeric state, maintaining protein-protein contacts within the context of the trimer or any other active oligomeric species presents its own challenges. Electron tomography studies have indicated that Env may exist on viral particles in a number of conformations and oligomeric states, with trimer being most predominant as expected (Zhu, 2003; Liu, 2008). Although envelope proteins likely adopt their most native conformations on the surface of inactivated virus or HIV virosomes, gp120/gp41 is generally present in exceedingly low copy number, only about 8-10 per virion (Zhu, 2003). Shedding of gp120, as mentioned previously, presents a significant issue in these systems as well, and immunization using a virosome strategy yielded neutralizing antibodies with a narrow range and limited potency (Doan, 2005).

An alternative method for harnessing membrane proteins for further study and use in nanoparticle therapy is their incorporation into phospholipid bilayer nanodiscs (ND). ND (Figure 2) consist of discoidal portions of phospholipid bilayer encompassed by a "belt" composed of

two copies of a membrane scaffold protein (MSP). The MSP is an amphipathic helical protein derived from human apolipoprotein A-I; ND thus closely resemble the nascent, pre-β HDL mentioned in Chapter I. Nanodiscs can be reconstituted *in vitro* by combination of detergent-solubilized lipid and MSP; the particles self-assemble upon removal of the detergent. If a detergent-solubilized membrane protein is present in the ND reconstitution mixture, it can be incorporated into the discs during self-assembly (Bayburt & Sligar, 2010).

ND have gained popularity for solubilization of membrane proteins as they more closely resemble the lipid bilayer of a cell or viral envelope than do detergents. Incorporation of proteins into ND eliminates the need for truncation or deletion of transmembrane domains, which can negatively impact folding and/or protein function. Specific binding of certain detergents to sites on proteins is also a considerable issue in some cases (Li-Blatter, 2009), complicating biochemical and biophysical analysis of protein-protein and protein-substrate interactions in detergent solubilized systems.

Another advantage of ND is that the lipid composition can be varied easily to simulate different types of biological membrane; ND have been assembled using a diverse range of lipids including but not limited to: *E. coli* cell membrane lipid; 1-palmitoyl-2-oleoyl-*sn*-glycerophosphatidylcholine (POPC); 1,2-dimyristoylphosphatidylcholine; and mixtures of phosphatidylcholine, phosphatidylethanolamine, and phosphatidylserine (Bayburt & Sligar, 2010). Genetic engineering has yielded MSPs of various lengths, which assemble monodisperse preparations of ND ranging from 9.5-12.8 nm; longer MSPs yield larger discs (Denisov, 2004).

*Figure 2. Lipid Nanodiscs*

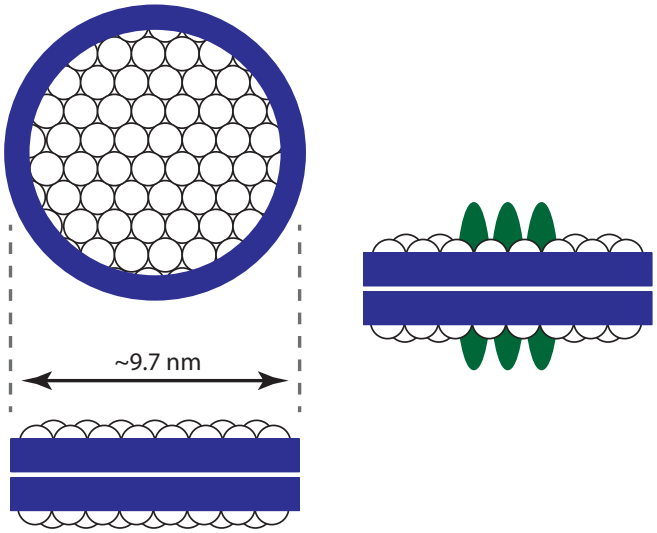


Lipid nanodiscs are composed of lipid membranes surrounded by an amphipathic helical scaffold protein. Shown here are nanodiscs comprised of MSP1D1 (blue) which yield ND of approximately 10 nm in diameter. Membrane proteins (green) can be incorporated into the discs, solubilizing them in a native-like bilayer.

Lipid ND are more stable, monodisperse, and facilely prepared than are other lipid bilayer systems such as liposomes (Bayburt & Sligar, 2010). When successfully purified, they contain a defined ratio of one functional target protein unit (monomer or mulitmer) per disc, as opposed to highly variable liposomal preparations. This lends an obvious advantage for use with techniques in which sample homogeneity is a strict requirement. To date, a large number of membrane proteins have been incorporated into lipid ND including monomeric and trimeric bacteriorhodopsin (Bayburt & Sligar, 2003; Bayburt, 2006), Tar bacterial chemoreceptor (Boldog, 2006), and cytochrome P450 3A4 (Baas, 2004).

NDs' potential as a nanoparticle therapeutic was recently demonstrated in a mouse vaccine trial against influenza. Influenza hemagglutinin is a trimeric envelope glycoprotein similar to

HIV Env; when incorporated into ND and administered either by inhalation or intramuscular injection, it offered protective immunity against viral challenge comparable to that provided by two commercially available, hemagglutinin-based vaccine preparations. The study found no evidence of toxicity in the mice related to the ND (Bhattacharya, 2010), and it is anticipated that few adverse effects would be seen in humans owing to NDs' resemblance to human HDL particles (Ryan, 2010).

Given that ND incorporation has been shown to be a valuable tool both in the aforementioned vaccine study and for the study of proteins with a variety of oligomeric states (Boldog, 2006), I conjectured that full length, recombinant gp160 may be solubilized and stabilized as trimers, and possibly dimers and monomers, by incorporation into ND (gp160 ND). Here, uncleaved gp160 was selected both because it circumvents the shedding issue, and also because I hoped to investigate the importance of this form of Env as outlined above.

The experiments presented here demonstrate that incorporation of gp160 into ND is possible and appears to capture two reasonably distinct oligomeric states, albeit in limited amounts. These particles possess bNAb-binding activities comparable to the detergent-solubilized form, while seeming to allow for more complete segregation of oligomeric forms and a more defined preparation. The successful completion of this research lays the groundwork for use of gp160 ND in more detailed biophysical studies. Future adaptation into a vaccine candidate may be possible, though considerable improvement to gp160 ND yield will be required for this to come to fruition.

## III.B Materials & Methods

### III.B.1 Purification of recombinant gp160, MSP1D1, other reagents

Recombinant gp160 (1084i) was purified from BSC40 cells using vaccinia as the expression vector (Hu, 1986). Unless otherwise specified, all steps were carried out on ice or at 4°C. Lysis was performed in Buffer A (20 mM Tris pH 8, 500 mM NaCl) containing 1% Triton X-100. The clarified lysate was purified by lentil lectin affinity chromatography at which point the detergent was changed to 1% β-octyl glucopyranoside plus 1% sodium deoxycholate, which was included along with 500 mM methyl α-D-mannopyranoside (Sigma) in the elution buffer. The eluted material containing gp160 was then concentrated to approximately 10 μM on a 2 mL GE Healthcare HiTrap Q HP column using a step gradient of Buffer A containing octyl glucoside and deoxycholate as specified above, plus 50 mM NaCl for protein binding and washing steps, and 500 mM NaCl for elution. The gp160 intended for ND assembly was used without further purification; material for use as standards in binding activity assays was further purified by gel filtration on a Superdex 200 10/300 GL column (GE Healthcare) using Buffer A, as for Q column elution. MSP1D1 was purified according to established protocols (Ritchie, 2009). Absorbance spectra of protein stocks were collected using a NanoDrop 2000c UV-Vis spectrophotometer (Thermo Scientific). 1-palmitoyl-2-oleoyl-*sn*-glycero-3-phosphocholine (POPC) and cholesterol powder were purchased from Avanti Polar Lipids. All other materials were of the highest quality available.

### III.B.2 Assembly of ND (Figure 3)

The ND assembly protocol was based upon previously described methods (Ritchie, 2009). Unless otherwise specified, all steps were carried out on ice or at 4°C. Briefly, POPC

stock solution (20 mM, solubilized in 200 mM sodium cholate) was combined with recombinant gp160 and MSP1D1 to give final concentrations of 2 mM POPC, 20 mM sodium cholate, 4.5 μM gp160, and 32 μM MSP1D1 (a 125:0.28:2 molar ratio, which would yield 10-fold excess empty ND assuming complete incorporation of gp160 in trimeric form). Where indicated, cholesterol was added to lipid films at a 4:6 molar ratio to POPC. Octyl glucoside and deoxycholate were maintained at 1% each until the self-assembly step. For empty ND reactions, gp160 was replaced with an equal volume of identical buffer. Reaction mixtures were incubated 1 hour with gentle agitation. Detergent was removed by incubation with 0.8 g Bio Beads SM-2 (BioRad) for each mL solution with gentle agitation for 4 hours. The supernatant was aspirated through a 25 g needle and residual detergent removed by overnight dialysis into at least 100 volumes of binding buffer (20 mM sodium phosphate pH 7.4, 500 mM NaCl) containing 50 mM imidazole, with a minimum of one buffer change. Dialyzed solutions were then applied to 0.5 mL of Ni Sepharose 6 FF medium (GE Healthcare) per 1.5 mL solution equilibrated with binding buffer containing 50 mM imidazole and purified with a step gradient of binding buffer for binding and washing, followed by elution in Buffer A (20 mM Tris pH 8, 500 mM NaCl) containing 500 mM imidazole. Finally, eluted material was separated on a Superose 6 10/300 GL gel filtration column (GE Healthcare) using Buffer A for equilibration and as the mobile phase prior to further analysis.

### III.B.3 SDS- and blue native (BN-) PAGE

SDS-PAGE and BN-PAGE were performed using 4-12% NuPAGE and 3-12% NativePAGE Novex Bis-Tris polyacrylamide gradient gels (Invitrogen), respectively, according to manufacturer instructions. BN-PAGE was carried out on ice or at 4°C. For SDS-PAGE, ND

samples were first disassembled by treatment with 0.15% sodium cholate followed by precipitation in 6% trichloroacetic acid. The pelleted protein was resuspended in 200 mM Tris pH 8, 4% SDS, 150 mM NaOH prior to electrophoresis. Protein was visualized by staining with Coomassie R-250.

*Figure 3. Assembly of gp160 nanodiscs*

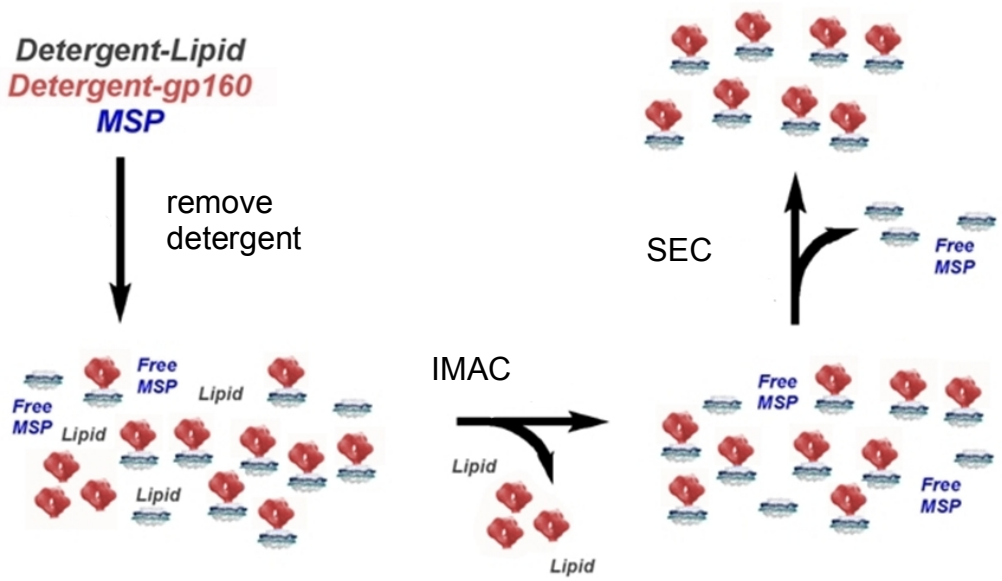


*Assembly of gp160 ND*. Detergent-solubilized lipid, detergent solubilized gp160, and MSP are mixed as specified in Materials & Methods. ND self-assembly is initiated by removal of detergent. Free lipid and gp160 are eliminated by nickel affinity chromatography, and the resulting mixture of products is fractionated by size exclusion chromatography. Adapted from an image courtesy C. E. Catalano.

**III.B.4 Western blot**

SDS- and BN-PAGE were performed as above and transfer of protein to PVDF membranes was performed according to gel manufacturer instructions. Tris-buffered saline containing 0.05% Tween-20 (TBST) + 4% nonfat dry milk was used for blocking and all dilutions. Membranes were blotted using 1:2,000 dilution of HIV-IG (obtained through the NIH AIDS Reagent Program, Division of AIDS, NIAID, NIH: Catalog #3957, HIV-IG from NABI

and NHLBI) and 1:500 dilution of Rabbit Anti-$His_6$ IgG (Bethyl) to visualize gp160 and MSP1D1, respectively. Recombinant HRP-Protein G (Invitrogen) was used as a secondary conjugate at a 1:10,000 dilution. Bands were developed using Pierce ECL Plus Western Blotting Substrate (Thermo Pierce) according to manufacturer instructions.

### III.B.5 Gel densitometry

SDS-PAGE was performed as indicated above. After staining, gels were imaged using an EpiChemi$^3$ darkroom system (UVP Bioimaging Systems) equipped with a Hamamatsu camera. Video densitometry of the bands was performed using the Image Quant software package (Molecular Dynamics). Samples to be quantitated were run along with a standard curve comprised of molar ratios of 1:2, 2:2, and 3:2 gp160:MSP1D1 corresponding to one monomer, dimer, and trimer per ND (all samples and standards run in quadruplicate). Construction of a standard curve using detergent-solubilized protein was complicated by heavy amounts of protein deposited at the gel wells (figure 6). In these lanes, the average volume contributed by the edge of an empty well was subtracted from the measured band volume.

### III.B.6 Quantitation of phospholipid

Total phospholipid in chloroform lipid stock solutions and ND samples was quantitated by phosphomolybdate assay as previously reported (Chen, 1956). ND samples were dialyzed in to 10 mM Tris pH 8, 20 mM NaCl and the solvent evaporated by heating at 200°C prior to analysis.

### III.B.7 Electron Microscopy

300 mesh carbon coated copper grids (Electron Microscopy Sciences) were treated by negative glow discharge prior to sample application. Staining was achieved using Nano-W (Nanoprobes) according to manufacturer protocols. Transmission electron microscopy was performed at the NanoTech User Facility at the University of Washington on a FEI Tecnai G2 F20 S-Twin TEM.

### III.B.8 ELISAs

*sCD4 direct binding and competition ELISAs.* sCD4 was obtained through the NIH AIDS Reagent Program, Division of AIDS, NIAID, NIH: Soluble Human CD4 from Progenics. All ELISAs were carried out at room temperature and in order to preserve the integrity of the ND, phosphate-buffered saline containing only 0.005% Tween-20 (PBST) was used. gp160 ND material was exceedingly limiting, so sCD4 titration data presented is the average of duplicate wells in a single experiment. Competition and saturation binding data is the average of quadruplicate wells between at least three separate experiments, performed on three separate preparations of ND. For Env capture experiments, sheep anti-gp120 mAb D7324 (Aalto Bioreagents) was rehydrated according to manufacturer instructions, diluted 1:100 in PBS and immobilized 50 µL/well in Costar high binding EIA/RIA flat bottom 96-well plates (Corning). Alternatively, the same dilution of rabbit anti-$His_6$ IgG (Bethyl) was used in order to capture MSP1D1. Wells were blocked with 100 µL/well of 5% nonfat dry milk in PBST. gp160 and gp160 ND samples containing 3µg/mL gp160 in PBST + 2% nonfat dry milk (also used for all subsequent dilutions) were added at 50 µL/well and allowed to incubate for 2 hours. Wells were then treated with 50 µL/well of 5µg/mL 4-domain human sCD4 (and subsequent dilutions, where

indicated) and allowed to incubate 1 hour. sCD4 binding was detected by labeling first with mouse anti-CD4 antibody OKT4 (a 1:100 dilution of OKT4 cell supernatant, a kind gift from the Hu laboratory), followed by goat anti-mouse HRP conjugate (Thermo Pierce) in a 1:1,000 dilution, 50 μL/well each. Wells were developed using 50 μL/well TMB substrate solution (Thermo Pierce) and quenched after signal had reached sufficient levels (5-30 minutes, depending on assay) using 25 μL/well 2 M $H_2SO_4$. Absorbance at 450 nm was measured on an Infinite plate reader (Tecan).

VRC01 and VRC03 were obtained through the NIH AIDS Reagent Program, Division of AIDS, NIAID, NIH: HIV-1 gp120 MAb VRC01 and VRC03, from Dr. John Mascola. Competition binding assays followed the gp120 capture procedure except that at the sCD4 binding step, 25 μL/well of either VRC01 or VRC03 at twice the desired final concentration was added to each well prior to application of 25 μL/well of sCD4 at twice the desired final concentration. Extent of inhibition was examined by setting the signal at [VRC01] = 0 to a relative signal of 0. $IC_{50}$s for VRC01 for each peak were determined using a hyperbolic fit.

*Broadly Neutralizing Antibody Binding ELISA*. Monoclonal antibodies b12, 4E10, and pg9 were obtained through the NIH AIDS Reagent Program, Division of AIDS, NIAID, NIH: HIV-1 gp120 Monoclonal Antibody (IgG1 b12) from Dr. Dennis Burton and Carlos Barbas; HIV-1 gp41 Monoclonal Antibody 4E10 from Dr. Hermann Katinger. gp160 and gp160ND samples were diluted to 2 μg/mL gp160 in PBS and immobilized in 96-well plates either directly or using D7324 as the capture antibody. Wells were blocked as described above. The bNAbs were added at indicated concentrations, 50 μL/well, and allowed to incubate 1 hour. Detection of bound antibody was achieved using 50 μL/well of goat anti-human HRP conjugate (Invitrogen), 1:1,000 to 1:10,000 dilution, followed by development of wells and measurement of $A_{450}$ as

described above. gp160 ND material was exceedingly limiting, so bNAb titration data presented is the average of duplicate wells in a single experiment. All ELISA titration data were fit using the Matlab software package.

### III.C Results & Discussion

#### III.C.1 Purification of detergent-solubilized gp160

One of the goals of this study was to evaluate different oligomeric states of gp160 and determine what effect, if any, the oligomeric state had on bNAB binding. In order to evaluate the oligomeric nature of species present in detergent-solubilized forms of Env, I purified full length, uncleaved gp160 from the 1084i isolate, a clade C virus (Rasmussen, 2006).

*Figure 4. SEC of uncleaved gp160 solubilized in detergent*

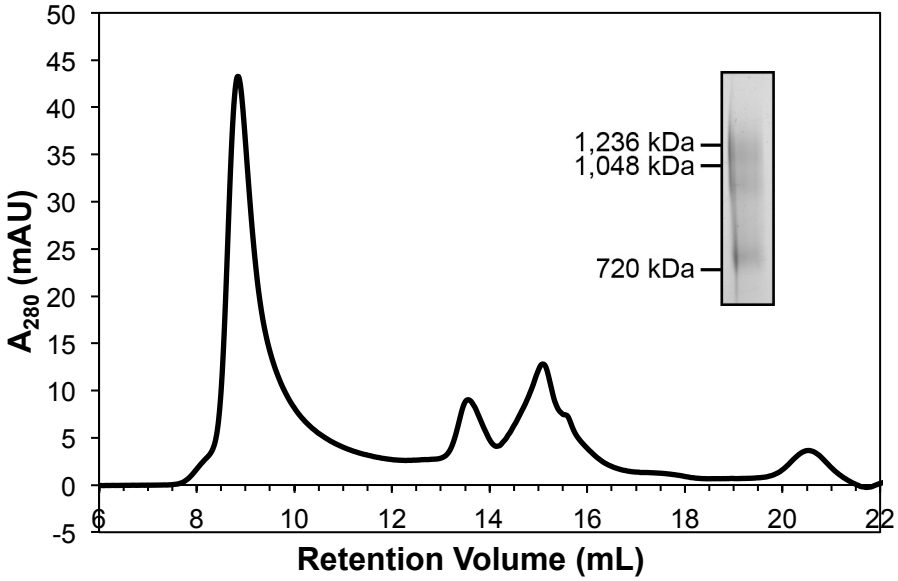


gp160 prepared as described in III.B was purified by gel filtration before use in binding assays, resulting in the above chromatogram. The majority of the gp160 eluted in the void volume, demonstrating the inability of this particular column to resolve high molecular weight species. Material eluting in the void volume was shown to contain a mixture of species when visualized by BN-PAGE (inset). Further details provided in the text.

When examined by Superdex S200 gel filtration (Figure 4), the majority of the material elutes in the column void volume (8.7 mL, MW >200,000 Da). This material appears to comprise multiple oligomeric species, as evidenced by BN-PAGE (figure 4, inset), due to the inability of this column to resolve high molecular weight species. I did not pursue fractionating this material further, as self-association is somewhat apparent in the detergent solubilized samples; this will be discussed further below. The doublet of material eluting around 15 mL may correspond to lower molecular weight cleavage products of gp160, but are difficult to visualize by SDS-PAGE.

**III.C.2 Assembly of gp160 ND**

When ND reconstitution takes place the absence of gp160, empty discs assemble and elute as a reasonably homogeneous species at ~16 mL when purified by gel filtration on a Superose 6 column (Fig 5A, dashed line). This column is preferable to the Superdex S200, as its exclusion limit is considerably higher (5 MDa). When gp160 is added to the assembly reaction, the distribution of material changes considerably, with a small amount of very large material eluting at ~7.5 mL- corresponding to $V_0$- followed by one broad peak which likely comprises multiple species (Figure 5A, solid line). The doublet that elutes at ~16-17 mL is composed of free MSP1D1 monomers and dimers, which cannot be resolved from empty ND on this column[*]. When the his-tagged MSP1D1 is excluded from the reaction mixture, no absorbance is seen in the chromatogram (dotted line), demonstrating the ability of the IMAC step (figure 3) to purify away species not containing His-tags, such as aggregated gp160.

[*] Empty NDs formed under these conditions are separable from free MSP1D1 monomer and dimer on gel filtration columns capable of resolving lower molecular weight species, such as the S200 used for detergent-solubilized gp160 (not shown). They also appear comparable to empty ND formed under more extensively characterized conditions (Ritchie, 2009).

*Figure 5. SEC purification and identification of gp160 ND containing fractions*

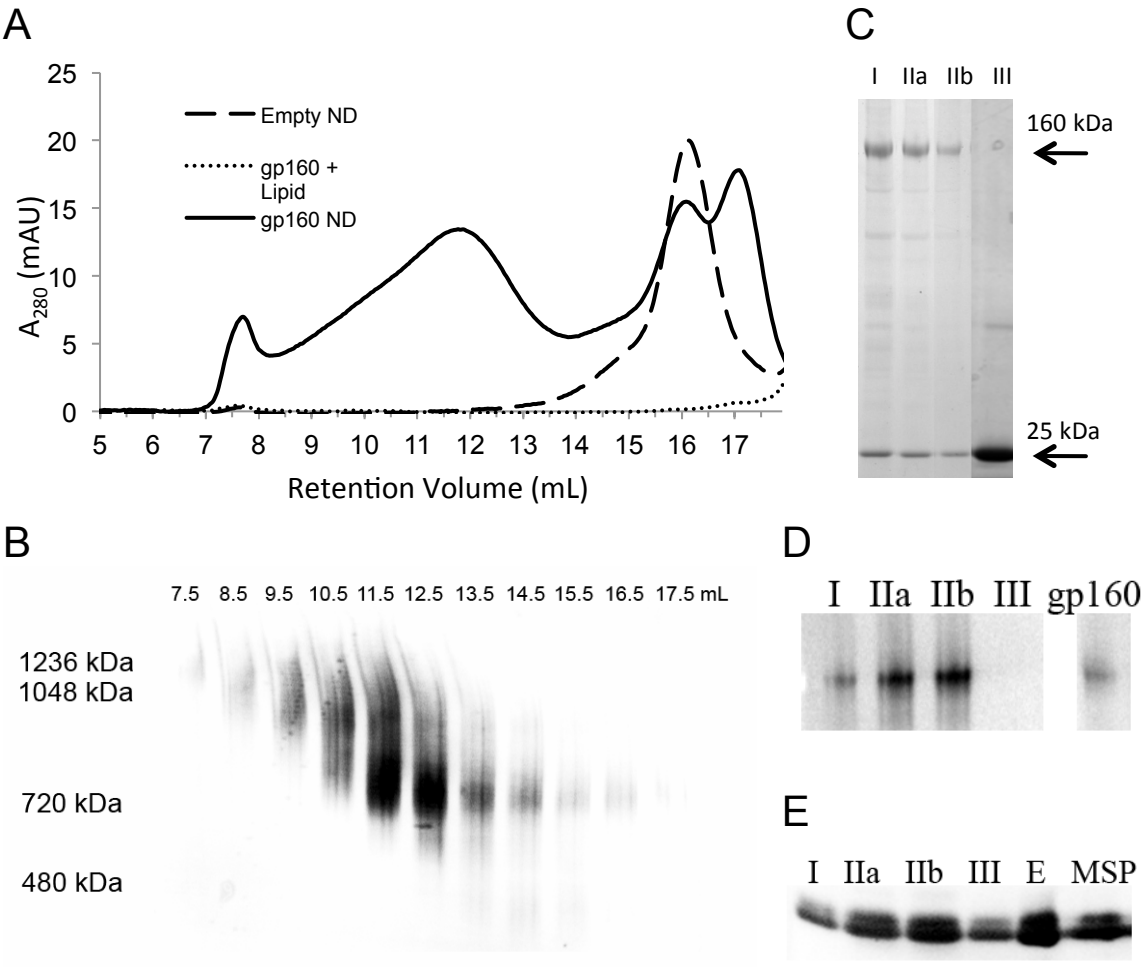


*Panel A. Size Exclusion Chromatography of gp160 ND*. In the absence of gp160, empty ND are formed (dashed line). In the presence of gp160, material is shifted to lower retention volumes and the peak distribution changes significantly. None of the material binds to the IMAC media when MSP1D1 is excluded from the reaction mixture (dotted line). Further details provided in the text. *Panel B. BN-PAGE and Western Blot of gp160 ND Gel Filtration Fractions*. Selected fractions from the SEC purification were separated by BN-PAGE and blotted using HIV-IG to visualize Env content; four highly diffuse bands are apparent, with the most immunoreactive occurring at ~720 kDa. *Panel C. SDS-PAGE of Pooled gp160 ND Fractions*. Fractions analyzed by SDS-PAGE were visualized with Coomassie. Peaks I-IIb contain both gp160 (160 kDa) and MSP1D1 (25 kDa), while peak III contains only MSP1D1. *Panels D, E. SDS-PAGE and Western Blot of Pooled gp160 ND Fractions*. Samples were treated in the same manner as in panel *C* and blotted either with HIV-IG (*panel D*) or anti-$His_6$ IgG to visualize MSP1D1 (*panel E*). As expected, peaks I-IIb contained gp160 and MSP1D1 while peak III only contained MSP1D1. As positive controls either gp160 in detergent or empty NDs (E) and MSP1D1 were run.

### III.C.3 Examination of reaction products by electrophoresis

Selected 0.5 mL fractions from the gp160 ND SEC purification step (Figure 5A) were analyzed by 3-12% BN-PAGE and blotted using HIV-IG as the primary antibody in order to visualize gp160 content of each fraction (Figure 5, panel B). Approximately four species, all of which run as highly diffuse bands, are apparent with the largest at ~1100 kDa, two at ~ 1000 and ~720 kDa, followed by one weakly immunoreactive band at ~400 kDa. Based upon the Western blot and the chromatographic data, fractions were pooled as follows: fractions eluting at 7-8 mL are referred to as "peak I"; 8.5-10 mL are referred to as "peak IIa"; 11-13 mL are referred to as "peak IIb"; 15.5-17.5 mL are referred to as "peak III". Note that trace amounts of immunoreactive material are detectable in peak III, which I had believed to contain free MSP1D1. This material is only visible by WB; it is not apparent by SDS- or BN-PAGE with standard Coomassie or silver staining, nor do these fractions possess appreciable sCD4 binding activity.

*Figure 6: ND incorporation excludes aggregated gp160*

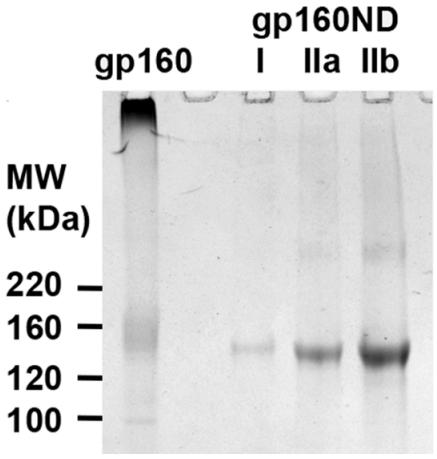


gp160 and nanodisc samples were TCA precipitated, separated by SDS-PAGE, and visualized using Coomassie; note the presence of large deposits of material near the gel well in the case of the detergent-solubilized protein. The same aggregation of gp160 is observed without TCA precipitation as well. This accumulation of large material is not seen with any of the species purified from the ND reaction.

When TCA precipitated to remove lipid and examined by SDS-PAGE, it is clear that peaks I-IIb contain both gp160 (~160 kDa) and MSP1D1 (~25 kDa), while peak III contains only MSP1D1 (Figure 5C). It is interesting to note that extremely large aggregates are observed upon SDS-PAGE analysis of gp160 solubilized in 1% octyl glucoside plus 1% deoxycholate, in the form of a smear that does not migrate past the gel well. This material is highly resistant to dissociation even after prolonged boiling, addition of detergent and denaturants, and TCA precipitation. Nonetheless, it appears to consist of aggregated gp160 as it is recognized by HIV-IG in Western blots. This material is effectively excluded in the gp160ND (Figure 6), and does not appear even upon prolonged storage.

**III.C.4 Estimation of number of gp160 subunits per nanodisc**

Video densitometry of the SDS-PAGE gels (Figure 5C) was used to estimate the number of gp160 subunits per ND in each set of pooled fractions (Figure 7, panel A). Although the gp160:MSP ratio in peak I is too variable to comment on oligomeric state, it is clear that peak IIa contains larger ratios of gp160 : MSP than IIb ($p < 0.05$). I thus interpret these to be NDs containing trimers and dimers of gp160, respectively. Caution must be exercised in the interpretation of these data, however, as resolution was not sufficient to rule out IIb as the trimeric species. This derives from the fact that detergent solublized gp160 was used to construct the standard curve for quantitation, and a considerable amount of the protein remains at or near the gel wells (Figure 6). This feature complicates accurate quantitation of gp160 at the well edges and it is expected that these artifacts add considerable error to the calculations performed here.

*Figure 7. Composition of gp160 ND pooled fractions*

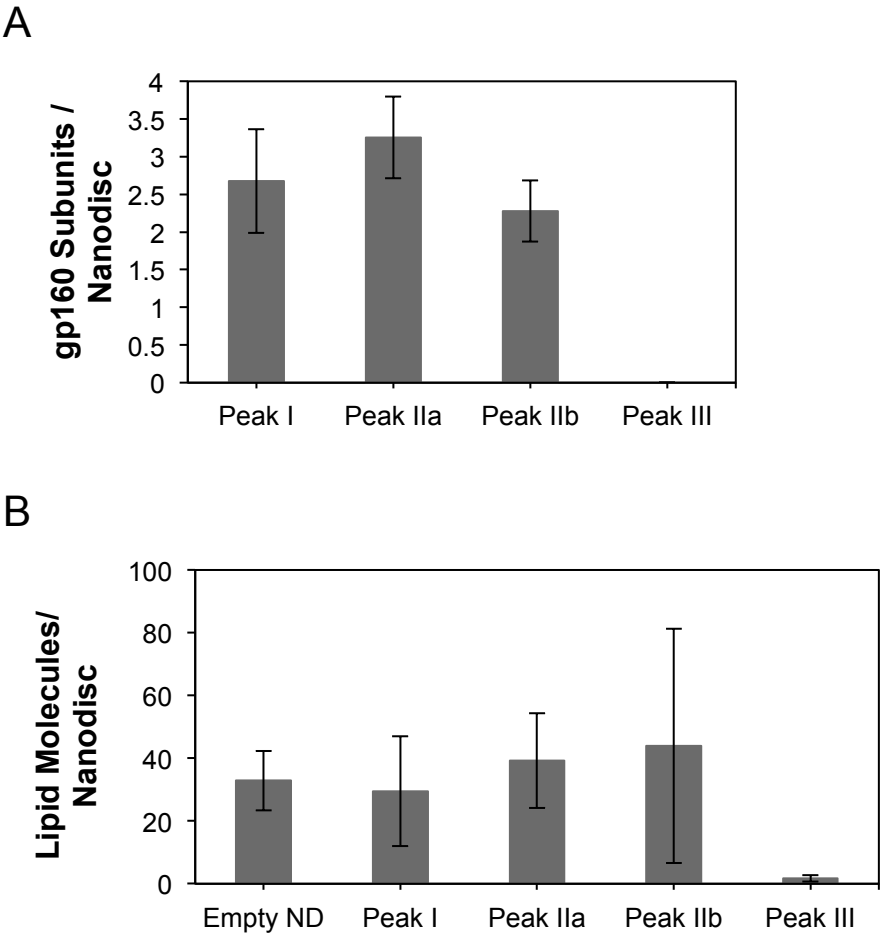


*Panel A. Approximate Number of gp160 Subunits per ND*. The number of gp160 subunits per ND in each set of pooled fractions was determined by video densitometry. Although the oligomeric state of the material in peak I is unclear, it appears as though peaks IIa and IIb are comprised of NDs containing trimers and dimers of gp160, respectively ($p < 0.05$). Peak III contains no gp160 detectable by Coomassie staining. *Panel B. Estimated Number of Lipid Molecules per ND*. Phospholipid content of each set of pooled fractions was determined by phosphomolybdate assay. Although the numbers of lipid per ND determined by this assay were relatively low in all cases, it appears that the material in peaks I-IIb contains amounts of lipid similar to those found in empty NDs formed under the same conditions. The material in peak III appears to contain little to no lipid and likely corresponds to free MSP1D1 monomer and dimer. These results are summarized in Table 1.

### III.C.5 Western blot analysis of TCA precipitated material

Blotting with either HIV-IG (Figure 5D) or rabbit anti-$His_6$ IgG to visualize MSP1D1 (Figure 5E) reveals that only peaks I-IIb contained gp160 and MSP1D1 while peak III exclusively contains MSP1D1, as expected. As positive controls either gp160 in detergent or

MSP1D1 were run alongside the ND samples. To check for full disassembly of NDs upon TCA precipitation, empty ND were also run as a control.

*Table 1. Composition of products purified from gp160ND reaction mixture*

| Fraction | gp160 (mole) | Lipid (mole) | MSP[a] (mole) |
|---|---|---|---|
| Empty ND | 0 | 33 ± 10 | 2 |
| gp160-ND I | 2.7 ± 0.7 | 30 ± 18 | 2 |
| gp160-ND IIa | 3.3 ± 0.5 | 39 ± 15 | 2 |
| gp160-ND IIb | 2.3 ± 0.4 | 44 ± 37 | 2 |
| gp160-ND III | 0 | 1.7 ± 1.1 | 2 |

[a]gp160 and lipid content were normalized to MSP

**III.C.6 Estimation of number of lipid molecules per nanodisc**

The phospholipid content of each set of pooled fractions was then determined by phosphomolybdate assay. Although the numbers of lipid per ND determined by this assay are considerably lower than the anticipated ~130 molecules per disc (Ritchie, 2009), it appears that the material in peaks I-IIb contains amounts of lipid similar to those found in empty ND formed under the same conditions (Figure 7B). It is likely that as performed here, the technique is only semi-quantitative as variability was quite high between experiments, even within the same preparation of discs. The material in peak III, however, repeatably contained little to no lipid and thus was concluded to comprise free MSP1D1 monomer and dimer. The estimated compositions of the peaks purified in the gp160 ND reaction mixture are listed in Table 1.

**III.C.7 Electron microscopy of purified fractions**

The structural features of the material eluting in peaks I-IIa and empty ND were

examined by transmission electron microscopy (Figure 8, panel A). As expected, the material eluting in peak I appears to be aggregated, and seems likely too large to constitute functional gp160 ND. This fraction is hypothesized to contain either soluble aggregates of gp160, MSP, and lipid or highly stable higher-order gp160 ND complexes. As structures this large are not observed in the context of the native virion, this material was not investigated further. The particles that elute in peaks IIa and IIb are more similar in size and morphology to trimeric Env spikes captured by EM in the past, close to what is expected for gp160 trimer and possibly dimer incorporated in to ND. Detergent-solubilized gp160 (not shown) contains an apparent mixture of species similar to those observed in peaks I-IIb, which was unsurprising as it had not been fractionated as thoroughly as the ND samples.

An approximate 2-D spatial model was constructed for gp160 ND assuming trimer dimensions identical to those observed by electron tomography (Liu, 2008), a ND about 10 nM in diameter (Denisov, 2004) and 5 nm thick, and a protruding gp160 cytoplasmic domain that resembles a 4 nm long by 4 nm thick stalk (a molecular weight-based approximation, as the true dimensions of this portion of the protein are unknown). This model fits quite convincingly into many of the densities observed in EM images of both peaks IIa and IIb. The images of gp160 ND are also quite similar in appearance to some of those obtained for uncleaved gp140s examined by EM in a recent study (Ringe, 2013). A spectrum of gp160 conformations is apparent (Figure 8, panel B) from extended, “open” particles resembling a CD4 bound state, to those appearing to adopt the “closed”, or unliganded form (Liu, 2008). If peaks IIa and IIb do, in fact, comprise trimer and dimer it is unsurprising that this model would fit equally well into some of the densities observed for both peaks, as full chromatographic separation of the gp160 ND species could not be achieved.

*Figure 8. Electron microscopy of gp160 ND pooled fractions*

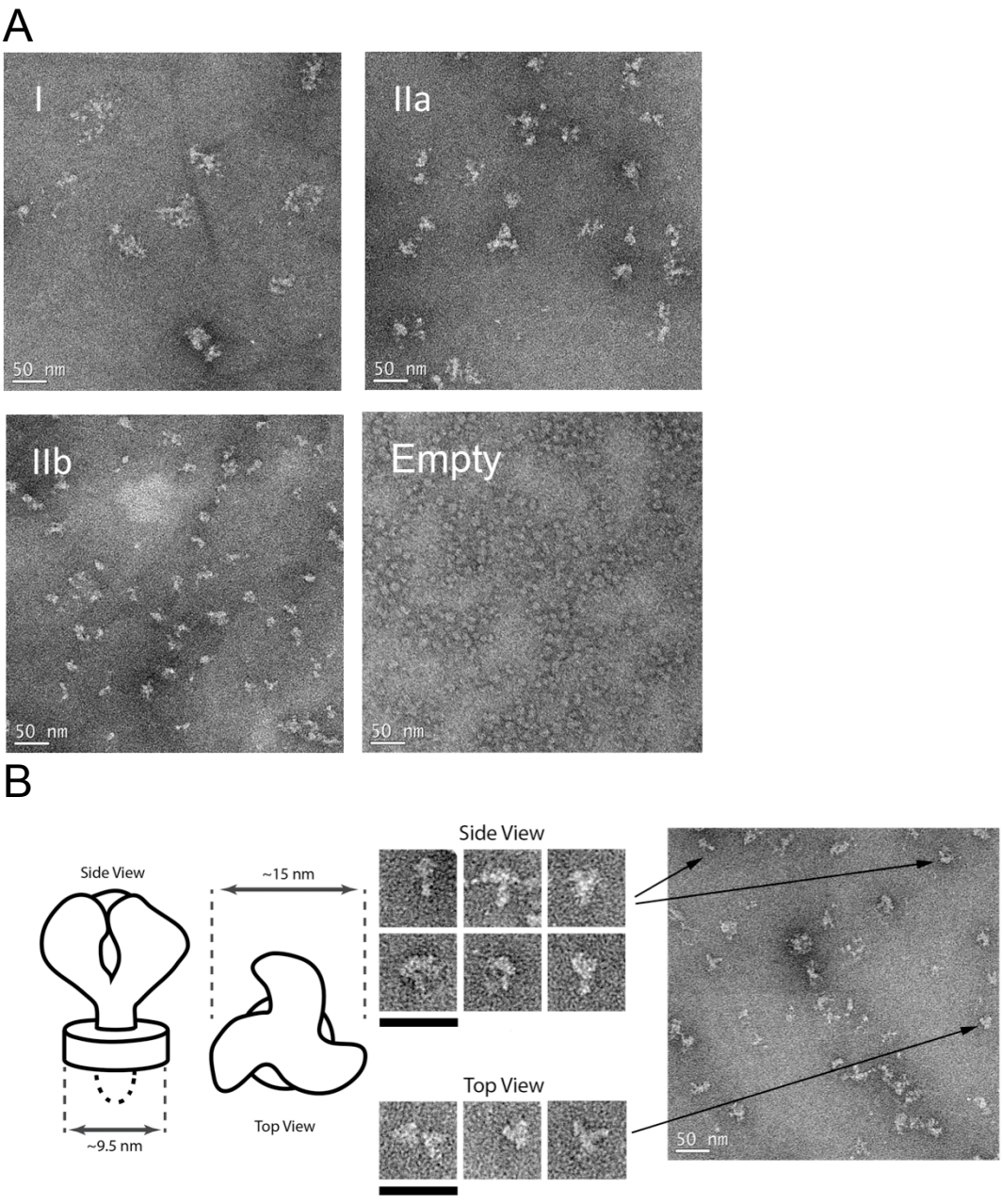


*Panel A.* Pooled SEC fractions were stained with Nano-W and imaged by transmission electron microscopy. As expected, the material eluting in peak I was largest, likely too large to constitute functional gp160 ND and is hypothesized to contain soluble aggregates of gp160 and MSP or multi-gp160 ND complexes. The material eluting in peaks IIa and IIb is more similar in size and morphology to what is expected for gp160 trimer and possibly dimer incorporated in to ND. Empty ND are also shown for reference. *Panel B.* Comparison of gp160 ND model based upon cryo-electron tomography data (Liu, 2008), with particles seen in IIa. Note the presence of both species that appear compact, as well as splayed. Size bars indicate 50 nm in all cases.

*Figure 9: Binding of sCD4 to gp160 and gp160ND*

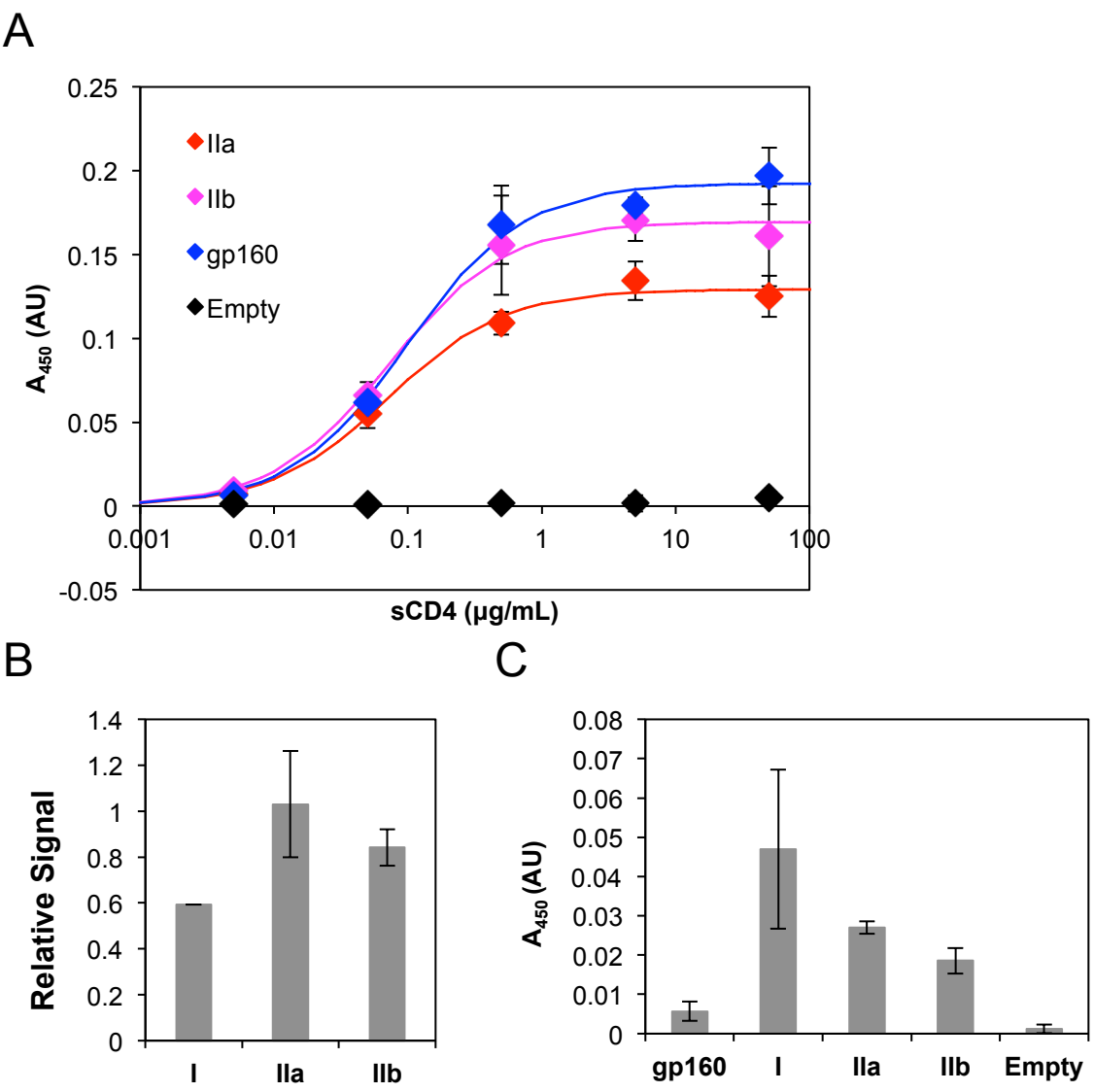


*Panel A*. Measurement of sCD4 binding to detergent-solubilized gp160 and gp160 ND. $K_{d,app}$ are all comparable and are listed in Table 2. *Panel B.* Saturation binding of sCD4 to gp160 ND using the usual Env-capture method. Signal is shown normalized to that obtained from detergent-solubilized gp160. Note differences in total binding levels seen here (with fresh sample) and *panel A* (after one freeze-thaw cycle). *C: sCD4 Binding by $His_6$ Capture ELISA*. The sCD4 binding ELISA from *Panel B* was repeated, except with the use of a rabbit anti-$His_6$ capture antibody in place of the anti-gp120 capture antibody. In this case, signals are absolute and have not been normalized to detergent-solubilized protein. Peak I shows relatively high but inconsistent sCD4 binding, which may again indicate the presence of soluble aggregates composed of variable ratios of gp160 to MSP1D1. Note that gp160 and empty NDs exhibit minimal levels of sCD4 binding in this assay, demonstrating the need for both gp160 and MSP1D1 to be present for samples to show signal.

### III.C.8 sCD4 binding of gp160 ND

The ability of material in gp160 ND SEC peaks to bind 4-domain, human sCD4 was examined by ELISA (fig 9A). The $K_{d,app}$ obtained for each peak and for detergent-solubilized gp160 are listed in Table 2, and are similar (~0.07-0.1 μg/mL) . Peak IIb and the detergent-solubilized protein bind sCD4 to comparable levels, while Peak IIa exhibits modestly reduced overall binding. This is possibly due to differences in sample sensitivity to freeze-thaw cycles (all had gone through one), as saturation binding experiments performed on fresh sample show comparable overall sCD4 binding between peaks IIa, IIb, and gp160 (fig 9B). The effect of freeze-thaw cycles on apparent affinity was not investigated further, as material yield was extremely limiting. Nonetheless, these results together suggest that the structural integrity of the gp160 is preserved for the most part through the ND incorporation process, particularly in the case of the peak IIb material. This also indicates no observable difference in apparent sCD4 binding affinity between the gp160 oligomeric states captured in the ND.

To confirm the presence of both MSP and gp160 in the particles, the sCD4 binding ELISA was repeated, except with the use of a rabbit anti-$His_6$ capture antibody in place of the anti-gp120 capture antibody, and using saturating concentrations of sCD4 in order to measure overall binding levels (fig 9C). Peak I was also examined in this case, and shows overall high but inconsistent sCD4 binding. This may again indicate the presence of soluble aggregates of variable gp160:MSP1D1 ratio, which would complicate estimates of gp160 concentration in the assay. The binding in peaks IIa and IIb is low, possibly due in part to weak affinity of the ND $His_6$ tag to the capture antibody as it becomes partially buried upon ND assembly. However, the binding signal obtained for these peaks is highly reproducible between experiments and ND preparations, suggesting that the gp160:MSP stoichiometry is more controlled in these fractions.

The fact that IIa binds sCD4 at slightly higher levels than IIb in all of the saturating binding studies on fresh protein further substantiates the hypothesis that IIa contains gp160 ND of a higher oligomeric state than IIb. Note that Peak III, gp160, and empty NDs all exhibit minimal levels of sCD4 binding in this assay, demonstrating the need for both gp160 and MSP1D1 to be present in a single particle for samples to show appreciable signal.

*Table 2. $K_{d,app}$ for sCD4 and bNAbs, measured by ELISA*

| **Fraction** | **sCD4 (μg/mL)** | **b12 (μg/mL)** | **4E10 (μg/mL)** | **pg9 (μg/mL)** |
|---|---|---|---|---|
| Detergent-solubilized gp160 | 0.1 ± 0.04[a] | 0.042 ± 0.002[a]<br>0.06 ± 0.04[b] | 8.1 ± 1[a]<br>0.29 ± 0.26[b] | 20 ± 6.9[a] |
| gp160 ND IIa | 0.07 ± 0.03[a] | 0.06 ± 0.02[a]<br>0.05 ± 0.04[b] | 6.2 ± 2.1[a]<br>1.3 ± 1.4[b] | 29 ± 46[a] |
| gp160 ND IIb | 0.07 ± 0.03[a] | 0.034 ± 0.006[a]<br>0.06 ± 0.056[b] | 4.7 ± 1.7[a]<br>0.33 ± 0.26[b] | 30 ± 12[a] |
| gp160 ND + Cholesterol IIa | --- | --- | 13.7 ± 5.4[a] | 22 ± 59[a] |
| gp160 ND + Cholesterol IIb | --- | --- | 11.1 ± 3.4[a] | 14.6 ± 3.7[a] |

[a]Direct immobilization
[b]Env capture

**III.C.9 Competition of sCD4 binding by VRC01, VRC03**

In order to evaluate the ability of two very broadly neutralizing, CD4 binding site specific Abs to compete with sCD4 binding, I used the same gp120 capture ELISA as in figure 10A, except that the indicated amounts of VRC01 or VRC03 were included in the incubation along

with sCD4 (Figure 10, panels A & B). Extent of inhibition was examined by setting the signal at $[VRC01]_0 = 0$. $IC_{50}$s determined for VRC01 are listed in Table 3.

*Figure 10. Inhibition of sCD4 binding to gp160 and gp160ND by VRC01 and VRC03*

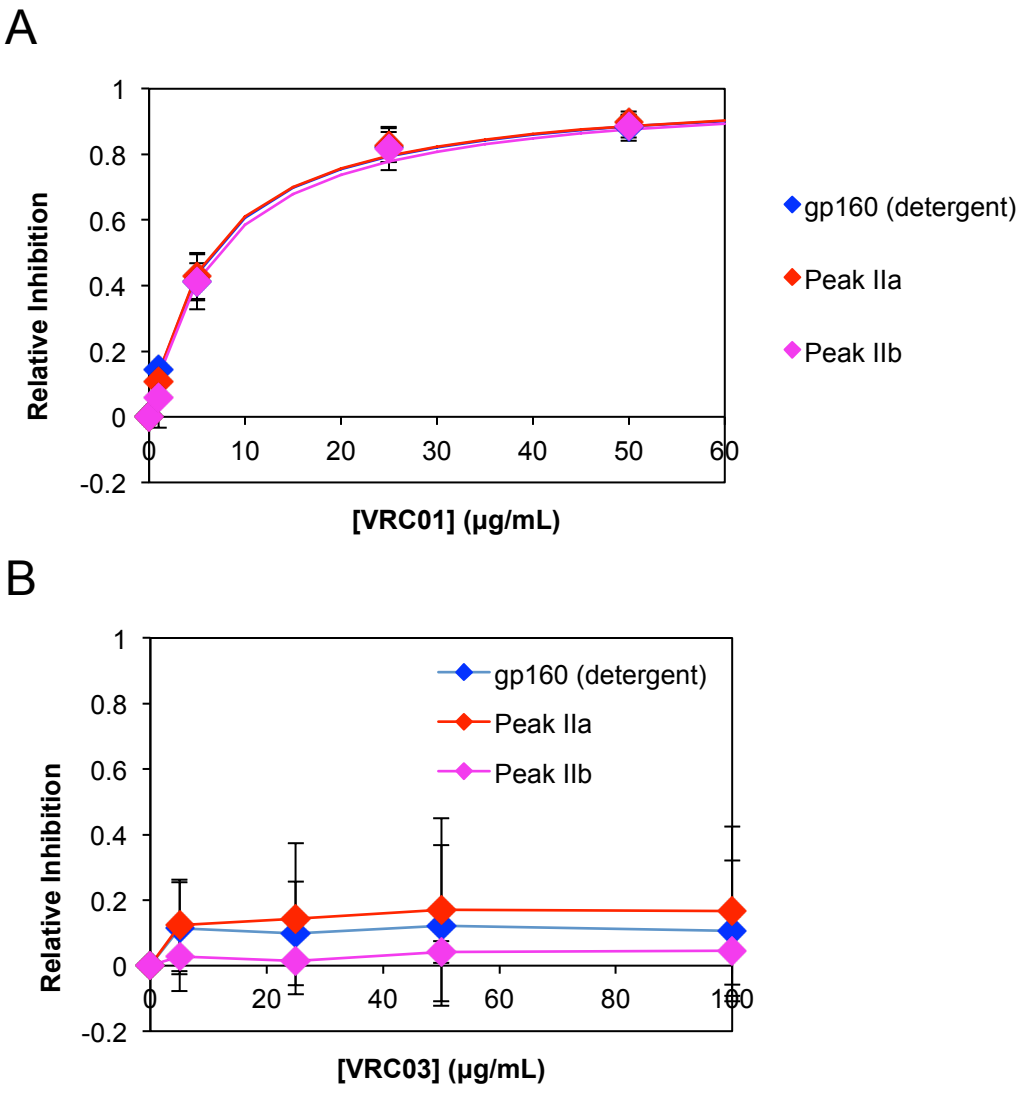


*Panel A: Inhibition of sCD4 Binding by VRC01*. Inhibition of sCD4 binding by VRC01 was examined for ND and detergent solubilized gp160. $IC_{50}$s for VRC01 for each peak were determined using a hyperbolic fit and are listed in Table 2. They are highly similar, further indicating that the CD4 binding site has been preserved in the gp160 ND samples. *Panel B: Inhibition of sCD4 Binding by VRC03*. Inhibition of sCD4 by VRC03 was examined, as for VRC01 above. Lines here are not fits, and are meant only to aid the eye. It is apparent that VRC03 does not effectively prevent sCD4 binding in this isolate of gp160.

They are all similar to one another, further indicating that the CD4 binding site has been preserved in the gp160 ND samples, and that a specific oligomeric state is not required for effective competition by this antibody. It is apparent that VRC03 does not effectively prevent sCD4 binding to this isolate of gp160 at the concentrations examined, which is somewhat unsurprising in light of past studies indicating more limited breadth in neutralization of clade C pseudoviruses by VRC03 than VRC01 (Wu, 2010).

*Table 3. $IC_{50}$ Values measured for VRC01 at 5 µg/mL sCD4*

| **Fraction** | **VRC01 (µg/mL)** |
|---|---|
| Detergent-solubilized gp160 | 6.8 ± 2.2 |
| gp160 ND IIa | 7.2 ± 2.1 |
| gp160 ND IIb | 8.3 ± 5.2 |

**III.C.10 Binding of broadly neutralizing antibodies to gp160 ND**

ELISA using direct immobilization of gp160 in detergent and gp160ND was employed to measure their apparent affinity for three bNAbs of interest, b12, 4E10, and pg9. These antibodies bind to conformation-dependent epitopes on the envelope protein, and are used here as probes of the structural integrity of gp160 incorporated into ND.

*Binding by b12.* Binding of peaks IIa, IIb, and detergent solubilized gp160 to b12 (Burton, 1991; Barbas, 1992; Roben, 1994; Burton, 1994), a bNAb that recognizes an epitope overlapping the CD4 binding site (Burton, 1994; Pantophlet, 2003), was examined first. No

significant change in $K_{d,app}$ is observed between samples (Figure 11A, Table 2). However, levels of binding overall are reduced in the ND incorporated material, surprising given the relative lack of change in sCD4 and VRC01 binding.

*Figure 11. Binding of b12 using various immobilization strategies*

A

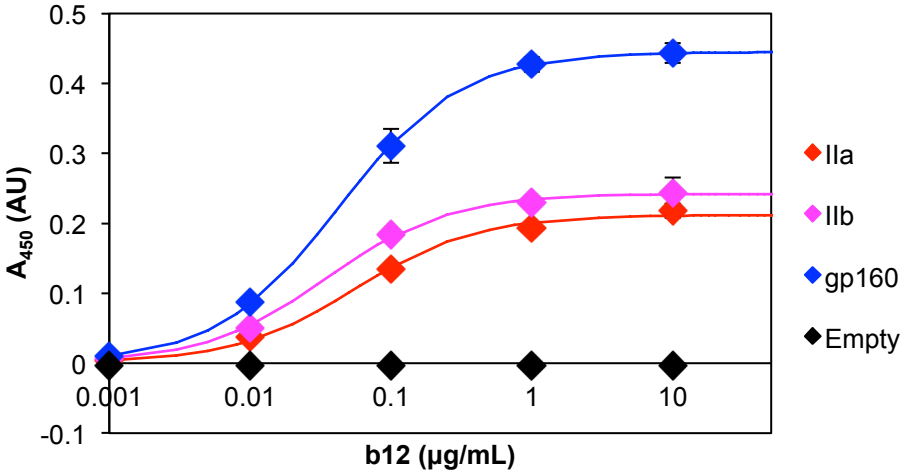


B

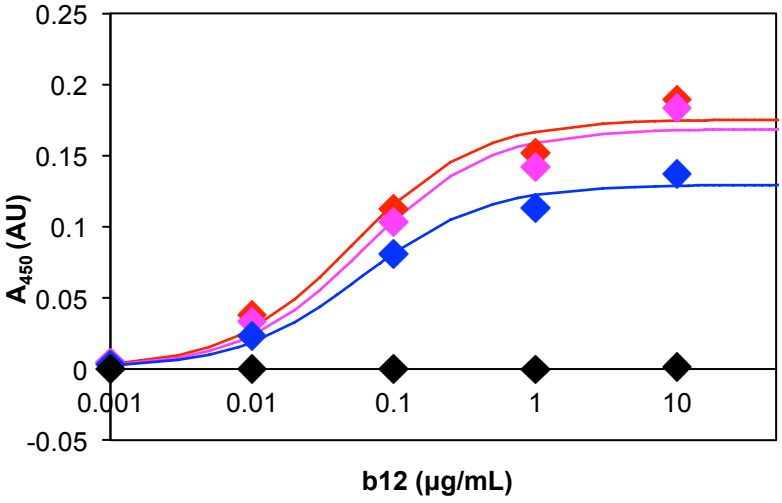


Measurement of b12 binding using direct immobilization (*Panel A*) and Env-capture methods (*Panel B*). $K_{d,app}$ values measured were all similar for both methods, and are listed in Table 2. Note that the use of a capture antibody causes saturation binding levels to converge, suggesting a tendency for gp160 ND to orient themselves differently than gp160 alone when immobilized. Error bars from duplicate wells are shown, but are not visible in some cases.

This could reflect a number of phenomena, including propensity for ND to capture a form of gp160 less sensitive to b12 recognition, or a greater tendency for immobilized gp160 ND to orient in a manner that precludes b12 attachment. It is thought that b12 may encounter more steric hindrance than VRC01 upon binding to its epitope, and possibly requires a greater degree of structural reorganization in order to bind (Li, 2011). Thus, I thought it possible that the restricted area of the ND may not be sufficient to allow gp160 the full range of motion required to bind to b12, or that b12 may have more difficulty accessing the CD4 binding site of gp160 ND due to changes in protein packing upon ND incorporation. To determine whether this steric hindrance or a simple particle orientation effect was the cause of the inconsistency, the ELISA was repeated using immobilization with D7324 (as in the sCD4 binding assay). Though the fits were not nearly as clean, $K_{d,app}$ measured for the samples were nearly identical (Table 2), and overall levels of binding for detergent solubilized gp160 and gp160ND converged somewhat. This implies that some type of orientation effect, and not a true difference in material activity, was the cause of the disparity (fig 11B).

*Binding of 4E10.* I next wished to probe the interaction of gp160 in detergent and in ND with an MPER-directed bNAb. 4E10 (Stiegler, 2001) is a very broadly neutralizing antibody that was able to neutralize all of the 90 viral isolates tested in one 2004 study, albeit with moderate potency (Binley, 2004). It was also of particular interest in my studies, as it has been shown that lipid plays an important role in the 4E10 epitope (Franquelim, 2011). Additionally, the presence of uncleaved gp160 on the surface of viral particles was shown to be required for 4E10 recognition in a virus capture assay (Leaman, 2010). In light of this, I hoped to evaluate the effect of lipid from the surrounding ND on binding of this antibody to uncleaved gp160. ELISAs using both modes of immobilization discussed earlier were carried out (fig 12A,B), and the

measured $K_{d,app}$ are listed in Table 2.

*Figure 12. Binding of 4E10 using various immobilization strategies*

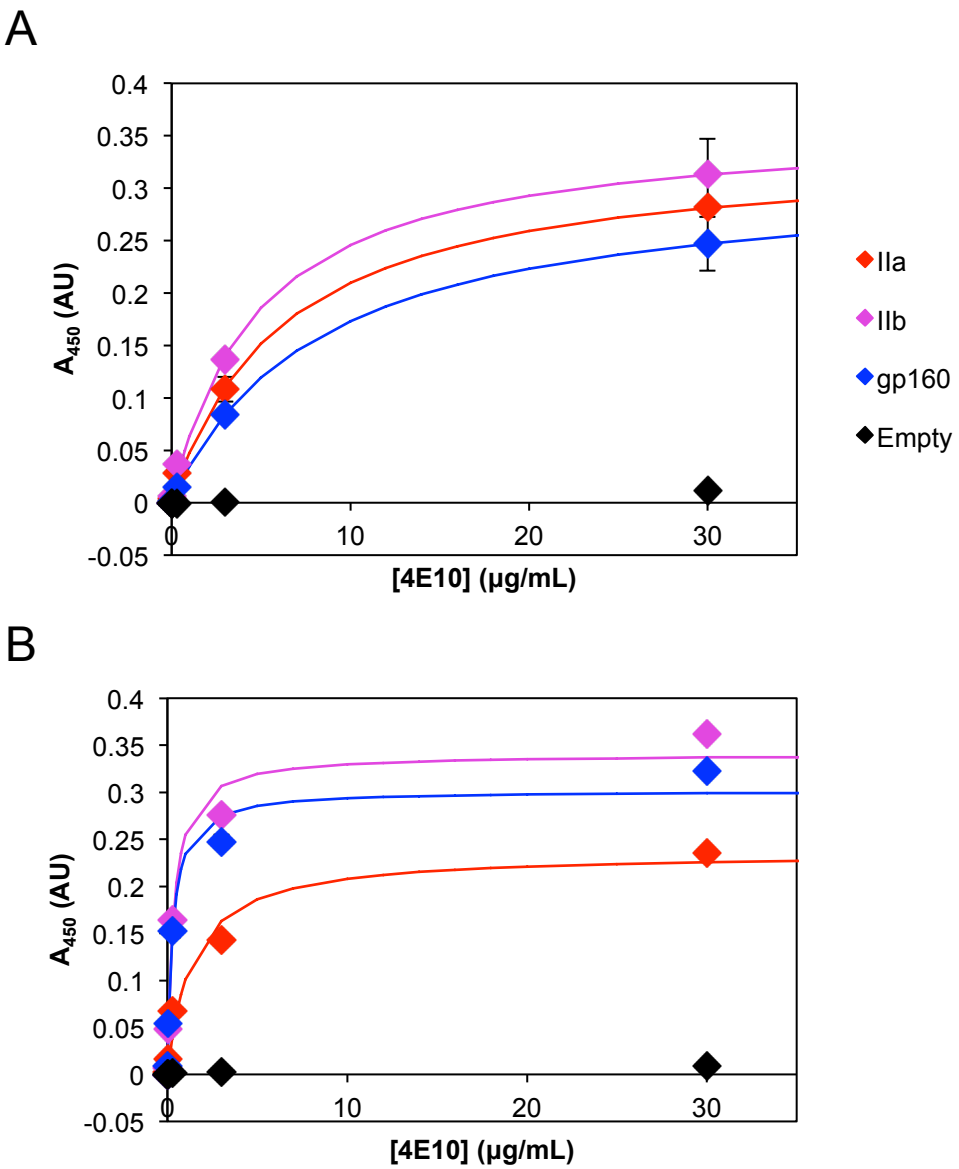


Measurement of 4E10 binding using direct immobilization (*Panel A*) and Env-capture methods (*Panel B*). $K_{d,app}$ values measured were similar for the direct immobilization method, with a modest improvement in $K_{d,app}$ for peak IIb. Measurement using Env capture yielded extremely poor fits with variable $K_{d,app}$. Apparent affinities measured using both methods are listed in Table 2. Error bars from duplicate wells are shown, but are not visible in some cases.

It is interesting to note that in this case, the use of immobilizing antibody actually decreases overall levels of peak IIa, but not IIb, binding. Additionally, there is over an order of magnitude of difference in the $K_{d,app}$ values measured for both peaks IIb and free gp160; this is attributed to poorer hyperbolic fit of data generated by the antibody capture technique and underscores the fact that these data should be examined in conjunction with those obtained from direct immobilization in this case. Better fits were achieved using the direct method, with ND incorporation appearing to impart a very modest (approximately 2-fold) increase in apparent affinity of 4E10 for the material in peak IIb.

*Binding of pg9.* Several bNAbs have been described which were suggested to be specific to certain quaternary epitopes present on oligomeric Env, notably pg9 which has shown reasonable breadth and potency in the neutralization of a panel of clade C isolates (Walker, 2009). The role of a quaternary epitope in pg9 binding remains unclear in light of studies demonstrating its preferential recognition of monomeric forms of Env in ELISA and immunoprecipitation experiments (Davenport, 2011). It is possible either that the affinity for the monomeric species is truly higher, or that the fraction of protein present in a truly "native" conformation tends to be higher in preparations of monomer than in those of trimer.

Env from a clade B isolate is shown to bind pg9 equally well when present on transfected cells in cleaved, WT trimers and in uncleaved mutants; this was recapitulated in cleaved and uncleaved, soluble gp140s retaining the native furin maturation site (Davenport, 2011). Because the ND platform appeared to allow for separation of oligomeric states of gp160, I hoped to take advantage of the system to examine pg9 binding to both the apparent trimer (peak IIa) and dimer (peak IIb) forms of wild-type, uncleaved Env. Direct immobilization ELISA was carried out as for 4E10 and b12 (Figure 13), and $K_{d,app}$ measured are listed in Table 2. Signals are quite weak in

comparison with the other antibodies, requiring longer incubation periods and higher concentrations of secondary antibody to develop appreciable absorbance. Binding of pg9 to both peaks IIa and IIb appears similar, though relatively large errors in the data for peak IIa preclude the determination of a $K_{d,app}$ with any confidence. Overall it appears that the detergent-solubilized form shows higher levels of binding, but as was the case with b12, it is unclear whether this reflects an orientation effect or a tendency for ND to exclude the forms of gp160 more sensitive to recognition by pg9. Unfortunately, limiting yield prevented the further investigation of pg9 binding.

*Figure 13. Binding of pg9 using direct immobilization*

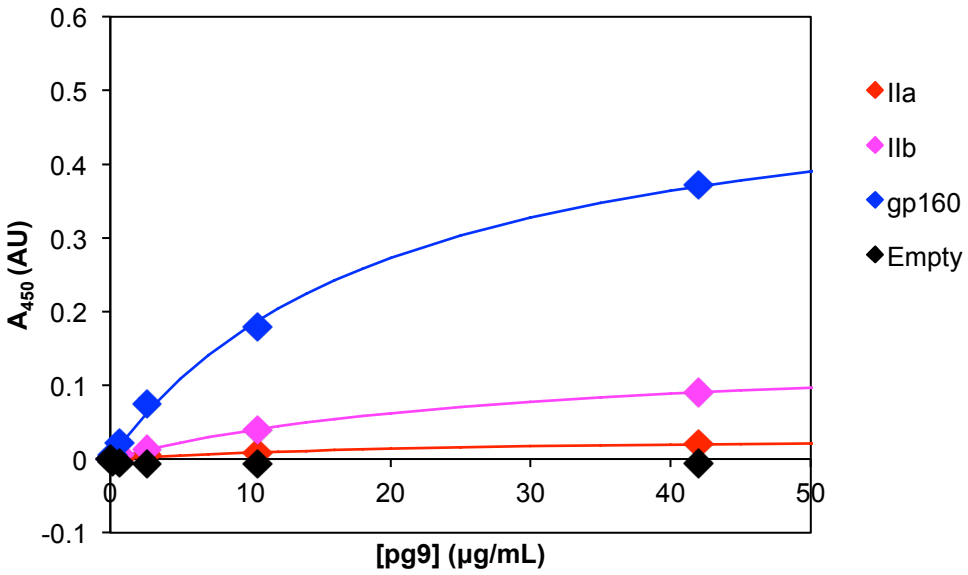


Measurement of pg9 binding was carried out using direct immobilization. $K_{d,app}$ values measured appeared similar for all peaks, though weak signal in the case of IIa obfuscates accurate determination of apparent binding affinity (all are listed in Table 2). the direct immobilization method, with a modest improvement in $K_{d,app}$ for peak IIb. The reason for differences in saturation binding levels was not investigated, but likely either reflect and orientation effect as in b12 binding, or binding exclusively to a sub-population of particles that tend to be excluded from ND or are damaged during incorporation. Error bars from duplicate wells are shown, but are not visible in some cases.

### III.C.11 Attempted incorporation of cholesterol into gp160 ND

As was mentioned numerous times above, the inability to obtain sufficient material (and to concentrate it once purified) presents a significant hindrance the full characterization of gp160 ND. Overall particle yield varies considerably between preparations, and is at best around 6% based upon total gp160 input. In a number (~20-25%) of cases, yield was so low that no usable material could be recovered after gel filtration. In a final attempt to address the considerable obstacles experienced in the ND incorporation process, ND were formed with the substitution of 40% of the POPC with cholesterol.

Palmitoylation of membrane proteins has been shown to cause partitioning out of the "raft" phase in model cell membranes, and Env requires this PTM to impart infectivity to viral particles (Rousso, 2000). I theorized that this might cause preferential partitioning of the biologically relevant species out of the POPC membranes under the assembly conditions. To test this hypothesis, ND were assembled in an identical fashion to those containing only POPC, except that a 4 : 6 molar ratio of cholesterol : POPC was used.

Empty ND formed in this manner were more heterogeneous, as evidenced by a less symmetric peak upon purification by gel filtration (Figure 14, panel A). The gp160 ND elution profile appeared largely unchanged, and with little apparent effect on yield (Figure 14, Panel A). Due to the extremely low concentration of the particles, the cholesterol content of the resulting particles could not be determined. However, 4E10 and pg9 binding to these ND were examined (Figure 14, Panels B and C), and appeared largely similar to those for particles formed in the absence of cholesterol (Table 2). Though the addition of cholesterol to mimic a "raft" phase failed to improve particle yield, further investigation into the use of other lipids, ideally native HIV lipid, in the nanodiscs may be warranted.

*Figure 14: Effect of cholesterol on ND incorporation, binding of bNAbs*

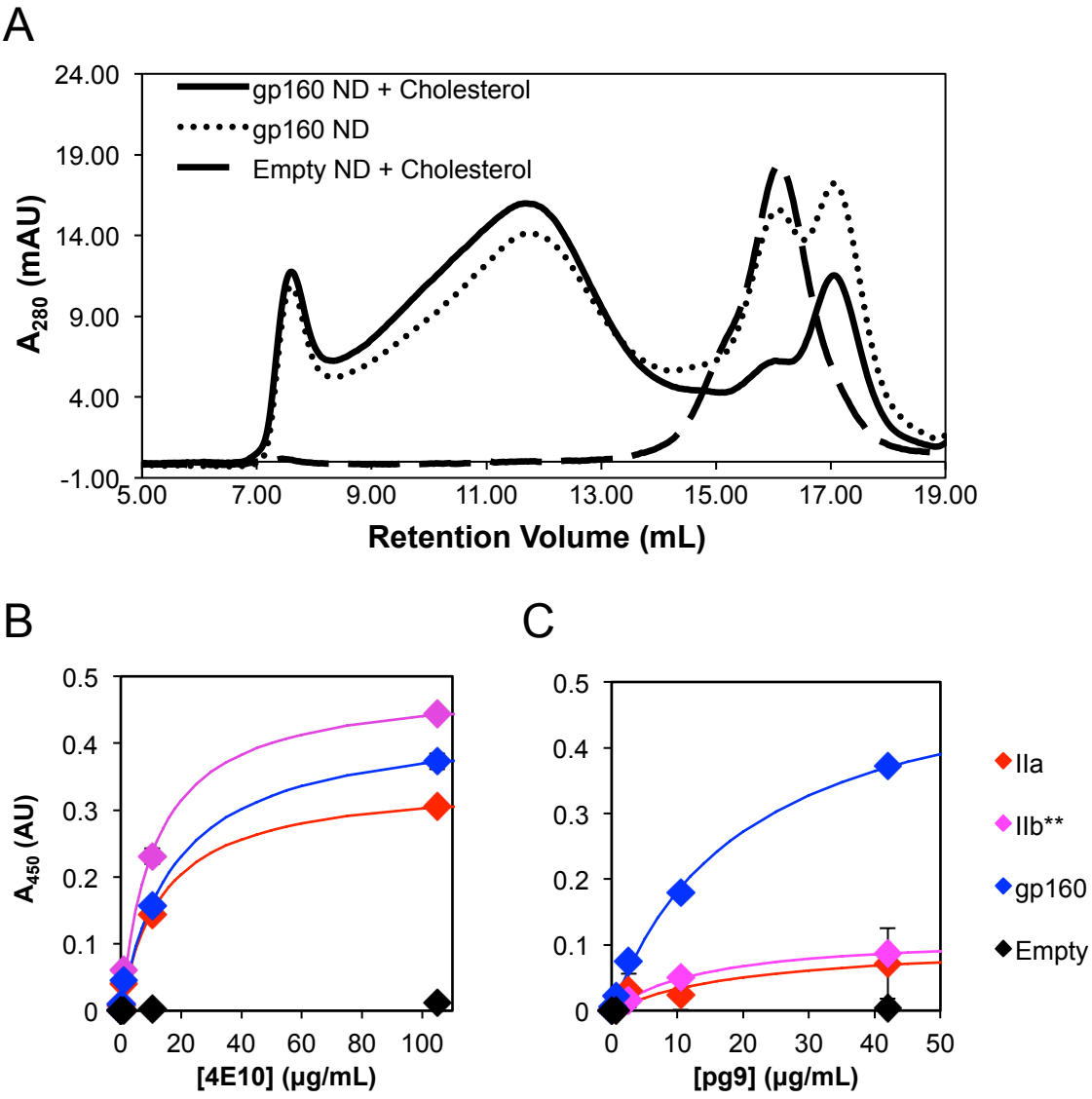


*Panel A*. Inclusion of 40% cholesterol in the ND assembly mixture (as outlined in III.B) did not seem to result in appreciable change to particle yield, as indicated by 280 nm absorbance when purified by SEC (yield is highly variable, so it is unlikely the modest increase is significant). The reason for the decrease in free scaffold protein is unclear. Limiting yields prevented the quantitation of cholesterol in ND fractions. *Panel B*. Binding of 4E10 to detergent-solubilized gp160 and gp160 ND + cholesterol was examined by ELISA using direct immobilization. $K_{d,app}$ values were similar to those measured for gp160 ND and are reported in Table 2. *Panel C*. Binding of pg9 to detergent-solubilized gp160 and gp160 ND + cholesterol was examined by ELISA using direct immobilization. $K_{d,app}$ values were similar to those measured for gp160 ND and are reported in Table 2. Unless otherwise indicated, error bars from duplicate wells are displayed but are not visible in all cases.

**Due to limited material, pg9 titration of IIb is a result of measurements made from single wells.

In summary, the studies outlined here indicate that the incorporation of full-length,

uncleaved Env into lipid nanodiscs can be achieved, albeit at regrettably low yield. gp160 ND appear to be separable by oligomeric state, with apparent trimer and dimer species present. ELISA did not show any appreciable difference in sCD4 or bNAb binding between these and the detergent solubilized protein, demonstrating that the ND incorporation process did not in any way perturb major structural features critical for antibody or receptor binding. When examined by EM, the particles were highly heterogeneous and similar to micrographs of solubilized gp140s (Ringe, 2013).

The EM data shown here adds to the evidence that both mutant and wild-type uncleaved Env exist in an array of "open" and "closed" conformations, and presumably only a limited number of these would be fusion-competent if cleaved. This may, in fact, be reflective of the heterogeneity of envelope protein as it exists on native viral particles (Zhu, 2003; Leaman, 2010) and highlights a unique difficulty in HIV vaccine design. The density of Env spikes on the surface of each virion is so low in the case of HIV, that it is unlikely that antibody cross-linking plays a role in neutralization. It is more probable that fusion competent Env spikes are inactivated directly by antibody binding. All of the configurations that both cleaved and uncleaved Env assume on the surface of an infectious viral particle are arguably "native", but only a small fraction of these are capable of supporting infection.

It is evident from the work done here and elsewhere, that a number of bNAbs readily recognize epitopes displayed by non-functional forms of Env. However, increased affinity for a fusion-incompetent form does not necessarily preclude neutralization by binding to the active form. Regardless of the mechanism, it is clear that rational HIV vaccine design from this point forward should be driven by a detailed analysis of structural differences between inactive and fusion-competent forms of Env.

# IV. Conclusion

In the body of work outlined in the previous chapters, I aimed to harness the surface proteins of viral particles from two very distinct systems for the purpose of nanoparticle design. By doing so, I also hoped to shed light on assembly processes as they occur *in vivo*, using the nanoparticle assembly systems as simple models for much more intricate events that occur within infected cells.

In the case of bacteriophage λ, I was able to lay the foundation for the development of targeted, multifunctional λ capsid-based nanoparticles assembled entirely *in vitro* from constituent proteins. Using a combination of these *in vitro* techniques to model events in the λ development pathway, I also elucidated a number of features of viral assembly and maturation that likely apply in the context of the cell. I demonstrated a balance between viral capsid yield and fidelity mediated by the scaffold protein, with optimal particle formation occuring at a ratio of 0.3:1 scaffold : major capsid protein. This corresponds to a concentration of scaffold that is likely in monomer-dimer equilibrium, with monomer more heavily favored but both species required for appropriate shell formation.

Expansion, at least in the case of full λ procapsids, only appears to show strict reversibility to an intermediate state at $Mg^{2+}$ concentrations of approximately 3-10 mM, though this has not been directly demonstrated. Removal of the urea in the presence of lower concentrations of $Mg^{2+}$ causes the formation of a discrete, more fully mature species that had not previously been distinguished from the species in urea. It is undetermined whether this fully mature form can revert back to the intermediate if urea is reintroduced at low $Mg^{2+}$, but

discovery of these two distinct, expanded species has opened the door for even further investigation of the urea-triggered maturation event.

Modeling of the decoration protein binding site implicated a ring of aspartate residues which could potentially uncover the mechanism of λ capsid expansion *in vivo*. In the model I constructed, these negatively charged residues point radially toward each other and face the interior of the procapsid, where they may be involved in binding of $Mg^{2+}$. Packaging of negatively charged DNA could effectively strip the $Mg^{2+}$ from these sites, which in combination with pressure exerted by the packaged genome may serve to destabilize the procapsid form, resulting in expansion. It is notable that the chelating agent ethylenediaminetetraacetic acid (EDTA) destroys λ infectivity (Smith and Feiss, 1993; Sternberg and Hoess, 1995). Chelation of capsid-associated $Mg^{2+}$ using EDTA was shown to be ineffective at promoting expansion (Medina, unpublished), It is possible, however, that removal of the divalent metal alone is not sufficient to trigger this event, or that EDTA does not effectively remove $Mg^{2+}$ bound to the capsid. Upon expansion, the ring of Asp residues is expected to rise to face the exterior of the capsid, where it would become available to form salt bridges with a ring of His residues at the base of the decoration protein trimer.

In sum, these results have significantly improved our understanding of λ capsid assembly and maturation, particularly on a structural basis, and may also be applicable to related dsDNA viruses as these pathways are highly conserved. These studies also serve as the foundation for future experiments both in λ nanoparticle design and in the study of λ assembly, maturation, and decoration protein binding. In regard to the former, studies in our lab are currently being carried out on encapsidation of functionalized scaffold proteins within λ VLP. In regard to the latter, a number of experiments are currently underway including demonstration of strict reversibility

between procapsid and intermediate states under a variety of conditions, as well as mutagenesis analyses which will attempt to address the true role of residues implicated in the model in capsid expansion and decoration protein binding.

In the case of HIV-1, I demonstrated the incorporation of low levels of full length, uncleaved envelope protein into lipid nanodiscs and constructed a rough antigenic profile of the protein in the different oligomeric states that appeared to be captured. While low and exceedingly variable yield limit the practical use of this approach, the somewhat incomplete analyses conducted here suggest it is an effective method of preventing formation of large aggregates of Env, and segregating it in various oligomeric states.

The protein appears to maintain its overall structure and activity throughout the incorporation process, though no significant improvement to antibody or sCD4 binding affinity is observed. The failure of the ND assembly reaction to reproducibly capture large amounts of gp160 may to some extent reflect some level of partitioning and preferential lipid association on the part of Env, or aggregation and misfolding of a large fraction of the detergent-solubilized preparation, which cannot be captured in ND. Further structural studies on the state of the detergent solubilized protein are warranted before full conclusions about the true efficiency of ND incorporation can be drawn.

The morphology of purified gp160ND particles and gp160 solubilized in detergent is extremely varied, though this apparent structural heterogeneity does not discourage recognition by sCD4 or bNAbs VRC01, 4E10, or b12. The antibody pg9 also binds both to detergent solubilized gp160 and gp160ND, though it appears that in this case only a small subpopulation of each species is capable of being recognized. It is unclear whether this population represents a species with a fold similar to the active, cleaved protein or contaminating monomer, as monomer

has been shown to bind IgG pg9 with enhanced affinity in some gp140s (Davenport, 2011). In any case, it is clear that particle heterogeneity in the case of the material purified here, and apparently in the context of the whole virus, is an extremely large obstacle that must be surmounted for rational vaccine design to prove successful in the future.

It is my sincere hope that the work summarized here has made a mark, however small, in the burgeoning field of therapeutic nanoparticle design. Attempts to apply my understanding of *in vitro* assembly to the construction of nanoparticle therapeutics met with varying degrees of success. However, the experiments conducted here have helped to uncover potential structural and biophysical features also present in the *in vivo* assembly pathways of these viruses, demonstrating the utility of such simple model systems in shedding light on multifaceted *in vivo* processes.

# References


Alexis, F., Pridgen, E., Molnar, L. K., & Farokhzad, O. C. (2008). Factors affecting the clearance and biodistribution of polymeric nanoparticles. *Molecular pharmaceutics*, *5*(4), 505-515.

Alkhatib, G. (2009). The biology of CCR5 and CXCR4. *Current Opinion in HIV and AIDS*, *4*(2), 96-103.

Amgen. (2008). Enbrel® (etanercept) for Subcutaneous Injection: Full Prescribing Information. Retrieved from http://pi.amgen.com/united_states/enbrel/derm/enbrel_pi.pdf.

Aniagyei, S. E., DuFort, C., Kao C. C., Dragnea B. (2008) Self-assembly approaches to nanomaterial encapsulation in viral protein cages. *J Mater Chem, 18*, 3763-3774.

Baas, B. J., Denisov, I. G., Sligar, S. G. (2004). Homotropic cooperativity of monomeric cytochrome P450 3A4 in a nanoscale native bilayer environment. *Arch Biochem Biophys, 430*, 218-228.

Bachmann, M. F., & Jennings, G. T. (2010). Vaccine delivery: a matter of size, geometry, kinetics and molecular patterns. *Nature Reviews Immunology*, *10*(11), 787-796.

Baines, J. D. (2011). Herpes simplex virus capsid assembly and DNA packaging: a present and future antiviral drug target. *Trends in microbiology*, *19*(12), 606-613.

Bancroft, J. B., Hiebert, E., & Bracker, C. E. (1969). The effects of various polyanions on shell formation of some spherical viruses. *Virology*, *39*(4), 924-930.

Barbas, C. F., Björling, E., Chiodi, F., Dunlop, N., Cababa, D., Jones, T. M., ... & Norrby, E. (1992). Recombinant human Fab fragments neutralize human type 1 immunodeficiency virus *in vitro*. *Proceedings of the National Academy of Sciences*, *89*(19), 9339-9343.

Barenholz, Y. C. (2012). Doxil®—The first FDA-approved nano-drug: Lessons learned. *Journal of controlled release*, *160*(2), 117-134.

Bayburt, T. H., Grinkova, Y.V., Sligar, S.G. (2006). Assembly of single bacteriorhodopsin trimers in bilayer nanodiscs. *Arch Biochem Biophys, 450*, 215–222.

Bayburt, T. H., Sligar, S. G. (2003). Self-assembly of single integral membrane proteins into soluble nanoscale phospholipid bilayers. *Protein Sci, 12*, 2476–2481.

Bayburt, T. H., Sligar, S. G. (2010). Membrane protein assembly into nanodiscs. *FEBS Lett, 584*, 1721-1727.

Beddows, S., Franti, M., Dey, A. K., Kirschner, M., Iyer, S. P. N., Fisch, D. C., ... & Moore, J. P. (2007). A comparative immunogenicity study in rabbits of disulfide-stabilized, proteolytically cleaved, soluble trimeric human immunodeficiency virus type 1 gp140, trimeric cleavage-defective gp140 and monomeric gp120. *Virology*, *360*(2), 329-340.

Bhattacharya, P., Grimme, S., Ganesh, B., Gopisetty, A., Sheng, J. R., Martinez, O., Jayarama, S., Artinger, M., Meriggioli, M., Prabhakar, B. S. (2010). Nanodisc-incorporated hemagglutinin provides protective immunity against influenza virus infection. *J Virol, 84*, 361-371.

Binley, J. M., Sanders, R. W., Master, A., Cayanan, C. S., Wiley, C. L., Schiffner, L., Travis, B., Kuhmann, S., Burton, D. R., Hu, S-L., Olson, W. C., Moore, J. P. (2002). Enhancing the proteolytic maturation of Human Immunodeficiency Virus Type 1 envelope glycoproteins. *J Virol, 76*, 2606-2616.

Binley, J. M., Wrin, T., Korber, B., Zwick, M. B., Wang, M., Chappey, C., ... & Burton, D. R. (2004). Comprehensive cross-clade neutralization analysis of a panel of anti-human immunodeficiency virus type 1 monoclonal antibodies. *Journal of virology*, *78*(23), 13232-13252.

Boldog, T., Grimme, S., Li, M., Sligar, S. G., Hazelbauer, G. L. (2006). Nanodiscs separate chemoreceptor oligomeric states and reveal their signaling properties. *Proc Natl Acad Sci*, *103*, 11509–11514.

Bourne, C., Lee, S., Venkataiah, B., Lee, A., Korba, B., Finn, M. G., & Zlotnick, A. (2008). Small-molecule effectors of hepatitis B virus capsid assembly give insight into virus life cycle. *Journal of virology*, *82*(20), 10262-10270.

Bower, J. F., Li, Y., Wyatt, R., Ross, T. M. (2006). HIV-1 Env gp140 trimers elicit neutralizing antibodies without efficient induction of conformational antibodies. *Vaccine, 24*, 5442 5545.

Bravo, D. A., Gleason, J. B., Sanchez, R. I., Roth, R. A., Fuller, R. S. (1994). Accurate and efficient cleavage of the Human Insulin Receptor by the human proprotein-processing protease furin. *J Biol Chem, 269*, 25830-25837.

Bron, R., Ortiz, A., Dijkstra, J., Stegmann, T., Wilschut, J. (1993). Preparation, properties, and applications of reconstituted influenza virus envelopes (virosomes). *Methods Enzymol, 220*, 313–31.

Brügger, B., Glass, B., Haberkant, P., Leibrecht, I., Wieland, F. T., Krausslich, H-G. (2006). The HIV lipidome: a raft with an unusual composition. *Proc Nat Acad Sci, 103*, 2641-2646.

Brunel, F. M., Zwick, M. B., Cardoso, R. M. F., Nelson, J. D., Wilson, I. A., Burton, D. R., Dawson, P. E. (2006). Structure-function analysis of the epitope for 4E10, a broadly neutralizing human immunodeficiency virus type 1 antibody. *J Virol, 80*, 1680–1687.

Burton, D. R., Barbas, C. F., Persson, M. A., Koenig, S., Chanock, R. M., & Lerner, R. A. (1991). A large array of human monoclonal antibodies to type 1 human immunodeficiency virus from combinatorial libraries of asymptomatic seropositive individuals. *Proceedings of the National Academy of Sciences*, *88*(22), 10134-10137.

Burton, D. R., Pyati, J., Koduri, R., Sharp, S. J., Thornton, G. B., Parren, P. W., ... & Nara, P. L. (1994). Efficient neutralization of primary isolates of HIV-1 by a recombinant human monoclonal antibody. *Science*, *266*(5187), 1024-1027.

Casjens, S. R. (2011). The DNA-packaging nanomotor of tailed bacteriophages. *Nature Reviews Microbiology*, *9*(9), 647-657.

Catalano, C. E., Cue, D., & Feiss, M. (1995). Virus DNA packaging: the strategy used by phage λ. *Molecular microbiology*, *16*(6), 1075-1086.

Center, R. J., Leapman, R. D., Lebowitz, J., Arthur, L. O., Earl, P. L., Moss, B. (2002). Oligomeric structure of the human immunodeficiency virus type 1 envelope protein on the virion surface. *J Virol, 76*, 7863-7867.

Ceres, P., Stray, S. J., & Zlotnick, A. (2004). Hepatitis B virus capsid assembly is enhanced by naturally occurring mutation F97L. *Journal of virology*, *78*(17), 9538-9543.

Champion, J. A., Katare, Y. K., Mitragotri, S. (2007). Particle shape: a new design parameter for micro-and nanoscale drug delivery carriers. *Journal of Controlled Release*, *121*(1), 3-9.

Chang, J. R., Andrews, B. T., & Catalano, C. E. (2011). Energy-independent helicase activity of a viral genome packaging motor. *Biochemistry*, *51*(1), 391-400.

Chen Jr, P. S., Toribara, T. T., & Warner, H. (1956). Microdetermination of phosphorus. *Analytical chemistry*, *28*(11), 1756-1758.

Chidambaram, M., Manavalan, R., & Kathiresan, K. (2011). Nanotherapeutics to overcome conventional cancer chemotherapy limitations. *Journal of Pharmacy & Pharmaceutical Sciences*, *14*(1), 67-77.

Congress of the United States- Congressional Budget Office. (2006). A CBO Study: Research and development in the pharmaceutical industry. Retrieved from http://www.cbo.gov/sites/default/files/cbofiles/ftpdocs/76xx/doc7615/10-02-drugr-d.pdf

Cornet, B., Decroly, E., Thines-Sempoux, D., Ruysschaert, J. M., Vandenbranden, M. (1992). Properties of HIV membrane reconstituted from its recombinant gp160 envelope glycoprotein. *AIDS Res Hum Retrovir, 8*, 1823-1831.

Cornuz, J., Zwahlen, S., Jungi, W. F., Osterwalder, J., Klingler, K., Van Melle, G., ... & Cerny, T. (2008). A vaccine against nicotine for smoking cessation: a randomized controlled trial. *PLoS One*, *3*(6), e2547.

Davenport, T. M., Friend, D., Ellingson, K., Xu, H., Caldwell, Z., Sellhorn, G., ... & Stamatatos, L. (2011). Binding interactions between soluble HIV envelope glycoproteins and quaternary-structure-specific monoclonal antibodies PG9 and PG16. *Journal of virology*, *85*(14), 7095-7107.

Davis, M. E. Chen, Z; Shin, D.M. (2008). Nanoparticle therapeutics: an emerging treatment modality for cancer. *Nature Reviews Drug Discovery*, *7*(9), 771-782.

de Beer, T., Fang, J., Ortega, M., Yang, Q., Maes, L., Duffy, C., ... & Catalano, C. E. (2002). Insights into specific DNA recognition during the assembly of a viral genome packaging machine. *Molecular cell*, *9*(5), 981-991.

Denisov, I. G., Grinkova, Y. V., Lazarides, A. A., Sligar, S. G. (2004). Directed self-assembly of monodisperse phospholipid bilayer nanodiscs with controlled size. *J Am Chem Soc, 126*, 3477-3487.

Dey, A. K., David, K. B., Lu, M., & Moore, J. P. (2009). Biochemical and biophysical comparison of cleaved and uncleaved soluble, trimeric HIV-1 envelope glycoproteins. *Virology*, *385*(1), 275-281.

Doan, L. X., Li, M., Chen, C., & Yao, Q. (2005). Virus-like particles as HIV-1 vaccines. *Reviews in medical virology*, *15*(2), 75-88.

Dokland, T., & Murialdo, H. (1993). Structural transitions during maturation of bacteriophage lambda capsids. *Journal of molecular biology*, *233*(4), 682-694.

Dokland, T. (1999). Scaffolding proteins and their role in viral assembly. *Cellular and Molecular Life Sciences CMLS*, *56*(7-8), 580-603.

Duda, R. L., Hempel, J., Michel, H., Shabanowitz, J., Hunt, D., Hendrix, R. W. (1995). Structural transitions during bacteriophage HK97 head assembly. *J Mol Biol, 247*, 618-635.

Fane, B. A., & Prevelige Jr, P. E. (2003). Mechanism of scaffolding-assisted viral assembly. *Advances in protein chemistry*, *64*, 259-299.

Fauci, A. S. (2008). 25 years of HIV. *Nature, 453*, 289-290.

Forshey, B. M., von Schwedler, U., Sundquist, W. I., & Aiken, C. (2002). Formation of a human immunodeficiency virus type 1 core of optimal stability is crucial for viral replication. *Journal of virology*, *76*(11), 5667-5677.

Frank, P. G., & Marcel, Y. L. (2000). Apolipoprotein AI: structure–function relationships. *Journal of lipid research*, *41*(6), 853-872.

Franquelim, H. G., Chiantia, S., Veiga, A. S., Santos, N. C., Schwille, P., & Castanho, M. A. (2011). Anti-HIV-1 antibodies 2F5 and 4E10 interact differently with lipids to bind their epitopes. *AIDS*, *25*(4), 419-428.

Fu, C-Y., Morais, M. C., Battisti, A. J., Rossmann, M. G., Prevelige, P. E. (2007). Molecular dissection of φ29 scaffolding protein function in an *in vitro* assembly system. *J Mol Biol, 366*, 1161-1173.

Fuller, D. N., Raymer, D. M., Rickgauer, J. P., Robertson, R. M., Catalano, C. E., Anderson, D. L., ... & Smith, D. E. (2007). Measurements of single DNA molecule packaging dynamics in bacteriophage λ reveal high forces, high motor processivity, and capsid transformations. *Journal of molecular biology*, *373*(5), 1113-1122.

Furlan, R., Bergami, A., Brambilla, E., Butti, E., De Simoni, M. G., Campagnoli, M., ... & Martino, G. (2006). HSV-1-mediated IL-1 receptor antagonist gene therapy ameliorates MOG35–55-induced experimental autoimmune encephalomyelitis in C57BL/6 mice. *Gene therapy*, *14*(1), 93-98.

Galisteo, M. L., & King, J. (1993). Conformational transformations in the protein lattice of phage P22 procapsids. *Biophysical journal*, *65*(1), 227-235.

Gamage, L. N., Ellis, J., Hayes, S. (2009). Immunogenicity of bacteriophage lambda particles displaying porcine Circovirus 2 (PCV2) capsid protein epitopes. *Vaccine, 27*, 6595-6604.

Garber, E. A., Seidman, M. M., & Levink, A. J. (1980). Intracellular SV40 nucleoprotein complexes: synthesis to encapsidation. *Virology*, *107*(2), 389-401.

Garland, S. M., Hernandez-Avila, M., Wheeler, C. M., Perez, G., Harper, D. M., Leodolter, S., Tang, G. W., Ferris, D. G., Steben, M., Bryan, J., et al. (2007). Quadrivalent vaccine against human papillomavirus to prevent anogenital diseases. *N Engl J Med, 356*, 1928-1943.

Garnett, M. C., Kallinteri, P. (2006). Nanomedicines and nanotoxicology: some physiological principles. *Occ Med, 56*, 307-311.

Gaussier, H., Yang, Q., & Catalano, C. E. (2006). Building a virus from scratch: assembly of an infectious virus using purified components in a rigorously defined biochemical assay system. *Journal of molecular biology*, *357*(4), 1154-1166.

Gertsman, I., Gan, L., Guttman, M., Lee, K., Speir, J. A., Duda, R. L., ... & Johnson, J. E. (2009). An unexpected twist in viral capsid maturation. *Nature*, *458*(7238), 646-650.

Georgopoulos, C., Tilly, K., and al, e. (1983). Lambdoid Phage Head Assembly. *In* "Lambda II" (R. W. Hendrix, J. W. Roberts, F. W. Stahl, and R. A.Weisberg, Eds.), pp. 279-304. Cold Spring Harbor Laboratory, Cold Spring Harbor, NY

Gill, S. C., von Hippel, P. H. (1989) Calculation of protein extinction coefficients from amino acid sequence data. *Analytical Biochemistry, 182*, 319-326.

Govan, V. A. (2008). A novel vaccine for cervical cancer: quadrivalent human papillomavirus (types 6, 11, 16 and 18) recombinant vaccine (Gardasil®). *Therapeutics and clinical risk management*, *4*(1), 65.

Gu, M. L., Rappaport, J., Leppla, S. H. (1995). Furin is an important but not essential protease for maturation on gp160 of HIV-1. *FEBS Lett, 365*, 95-97.

Guo, X., Huang, L. (2012). Recent advances in nonviral vectors for gene delivery. *Acc Chem Res, 45*(7)*, 971–979.*

Guttman, M., & Lee, K. K. (2013). A Functional Interaction between gp41 and gp120 Is Observed for Monomeric but Not Oligomeric, Uncleaved HIV-1 Env gp140. *Journal of virology*, *87*(21), 11462-11475.

Haynes, B. F., Fleming, J., St. Clair, E. W., Katinger, H., Steigler, G., Kunert, R., Robinson, J., Scearce, R. M., Plonk, K., Staats, H. F., Ortel, T. L., Liao, H-X., Alam, S. M. (2005). Cardiolipin polyspecific autoreactivity in two broadly neutralizing HIV-1 antibodies. *Science, 308*, 1906-1908.

Hedestam, G. B. K., Fouchier, R. A., Phogat, S., Burton, D. R., Sodroski, J., & Wyatt, R. T. (2008). The challenges of eliciting neutralizing antibodies to HIV-1 and to influenza virus. *Nature Reviews Microbiology*, *6*(2), 143-155.

Heymann, J. B., Cheng, N., Newcomb, W. W., Trus, B. L., Brown, J. C., & Steven, A. C. (2003). Dynamics of herpes simplex virus capsid maturation visualized by time-lapse cryo electron microscopy. *Nature Structural & Molecular Biology*, *10*(5), 334-341.

Hill, S. A., & McQueen, M. J. (1997). Reverse cholesterol transport-a review of the process and its clinical implications. *Clinical biochemistry*, *30*(7), 517-525.

Hohn, T., Wurtz, M., Hohn, B. (1976). Capsid transformation during packaging of bacteriophage lambda DNA. *Phil Trans R Soc Lond, 276*, 51-61.

Hong, C. S., Goins, W. F., Goss, J. R., Burton, E. A., & Glorioso, J. C. (2006). Herpes simplex virus RNAi and neprilysin gene transfer vectors reduce accumulation of Alzheimer's disease-related amyloid-β peptide *in vivo*. *Gene therapy*, *13*(14), 1068-1079.

Hoxie, J. A. (2010). Toward an antibody-based HIV-1 vaccine. *Annu Rev Med, 61*, 135-152.

Hu, S-L., Kosowski, S. G., Dalrymple, J. M. (1986) Expression of AIDS virus envelope gene in recombinant vaccinia viruses. *Nature, 320*, 537-540.

Hu, S-L., Stamatatos, L. (2007). Prospects of HIV Env modification as an approach to HIV vaccine design. *Curr HIV Res, 5*, 507-513.

Huang, R. K., Khayat, R., Lee, K. K., Gertsman, I., Duda, R. L., Hendrix, R. W., & Johnson, J. E. (2011). The Prohead-I structure of bacteriophage HK97: implications for scaffold mediated control of particle assembly and maturation. *Journal of molecular biology*, *408*(3), 541-554.

Huang, X., Bronstein, L. M., Retrum, J., Dufort, C., Tsvetkova, I., Aniagyei, S., ... & Dragnea, B. (2007). Self-assembled virus-like particles with magnetic cores. *Nano letters*, *7*(8), 2407-2416.

Iwai, H., Forrer, P., Plückthun, A., & Güntert, P. (2005). NMR solution structure of the monomeric form of the bacteriophage λ capsid stabilizing protein gpD. *Journal of biomolecular NMR*, *31*(4), 351-356.

Iyer, S. P. N., Franti, M., Krauchuk, A. A., Fisch, D. N., Ouattara, A. A., Roux, K. H., ... & Olson, W. C. (2007). Purified, proteolytically mature HIV type 1 SOSIP gp140 envelope trimers. *AIDS research and human retroviruses*, *23*(6), 817-828.

Jardine, P. J., and Anderson, D. L. (2006). DNA Packaging in double-stranded DNA phages. 2nd ed. *In* "In The Bacteriophages" (R. Calendar, and S. T. Abedon, Eds.), pp. 49-65. Oxford University Press, New York, NY.

Jarvis, B; Faulds, D. (1999). Etanercept: a review of its use in rheumatoid arthritis. *Drugs*, 57(6), 945-966.

Johannsen, M., Gneveckow, U., Eckelt, L., Feussner, A., Waldöfner, N., Scholz, R., ... & Jordan, A. (2005). Clinical hyperthermia of prostate cancer using magnetic nanoparticles: presentation of a new interstitial technique. *International Journal of Hyperthermia*, *21*(7), 637-647.

Katen, S., & Zlotnick, A. (2009). The thermodynamics of virus capsid assembly. *Methods in enzymology*, *455*, 395-417.

Kelley, L. A., & Sternberg, M. J. (2009). Protein structure prediction on the Web: a case study using the Phyre server. *Nature protocols*, *4*(3), 363-371.

Klug, A. (1999). The tobacco mosaic virus particle: structure and assembly. *Philosophical Transactions of the Royal Society of London. Series B: Biological Sciences*, *354*(1383), 531-535.

Konarev, P. V., Volkov, V. V., Sokolova, A. V., Koch, M. H., & Svergun, D. I. (2003). PRIMUS: a Windows PC-based system for small-angle scattering data analysis. *Journal of Applied Crystallography*, *36*(5), 1277-1282.

Kunzler, P., Hohn, T. (1978). Stages of bacteriophage lambda head morphogenesis: physical analysis of particles in solution. *J Mol Biol, 122*, 191-211.

Lander, G. C., Evilevitch, A., Jeembaeva, M., Potter, C. S., Carragher, B., Johnson, J. E. (2008). Bacteriophage lambda stabilization by auxiliary protein gpD: timing, location, and mechanism of attachment determined by cryo-EM. *Structure, 16,* 1399-1406.

Lata, R., Conway, J. F., Cheng, N., Duda, R. L., Hendrix, R. W., Wikoff, W. R., Johnson, J. E., Tsuruta, H., Steven, A. C. (2000). Maturation dynamics of a viral capsid: visualization of transitional intermediate states. *Cell, 100*, 253-263.

Leaman, D. P., Kinkead, H., & Zwick, M. B. (2010). In-solution virus capture assay helps deconstruct heterogeneous antibody recognition of human immunodeficiency virus type 1. *Journal of virology*, *84*(7), 3382-3395.

Lederberg, E. M., & Lederberg, J. (1953). Genetic studies of lysogenicity in Escherichia coli. *Genetics*, *38*(1), 51.

Lee, K. K., Gan, L., Tsuruta, H., Hendrix, R. W., Duda, R. L., Johnson, J. E. (2004). Evidence that a local refolding event triggers maturation of HK97 bacteriophage capsid. *J Mol Biol, 340*, 419-433.

Lee, K. K., Tsuruta, H., Hendrix, R. W., Duda, R. L., Johnson, J. E. (2005). Cooperative reorganization of a 420 subunit virus capsid. *J Mol Biol, 352*, 723-735.

Levental, I., Lingwood, D., Grzybek, M., Coskun, Ü., & Simons, K. (2010). Palmitoylation regulates raft affinity for the majority of integral raft proteins. *Proceedings of the National Academy of Sciences*, *107*(51), 22050-22054.

Li, Y., O'Dell, S., Walker, L. M., Wu, X., Guenaga, J., Feng, Y., ... & Mascola, J. R. (2011). Mechanism of neutralization by the broadly neutralizing HIV-1 monoclonal antibody VRC01. *Journal of virology*, *85*(17), 8954-8967.

Li-Blatter, X., Nervi, P., Seelig, A. (2009). Detergents as intrinsic P-glycoprotein substrates and inhibitors. *Biochim. Biophys. Acta, 1788*, 2335–2344.

Liu, J., Bartesaghi, A., Borgnia, M. J., Sapiro, G., & Subramaniam, S. (2008). Molecular architecture of native HIV-1 gp120 trimers. *Nature*, *455*(7209), 109-113.

Lotem, M., Hubert, A., Lyass, O., Goldenhersh, M. A., Ingber, A., Peretz, T., & Gabizon, A. (2000). Skin toxic effects of polyethylene glycol-coated liposomal doxorubicin. *Archives of dermatology*, *136*(12), 1475-1480.

Maeda, H., Wu, J., Sawa, T., Matsumura, Y., & Hori, K. (2000). Tumor vascular permeability and the EPR effect in macromolecular therapeutics: a review. *Journal of Controlled Release*, *65*(1), 271-284.

Manservigi, R., Argnani, R., & Marconi, P. (2010). HSV recombinant vectors for gene therapy. *The open virology journal*, *4*, 123-156.

Matsumura, Y., Gotoh, M., Muro, K., Yamada, Y., Shirao, K., Shimada, Y., ... & Takahashi, K. (2004). Phase I and pharmacokinetic study of MCC-465, a doxorubicin (DXR) encapsulated in PEG immunoliposome, in patients with metastatic stomach cancer. *Annals of Oncology*, *15*(3), 517-525.

Maurer, P., Jennings, G. T., Willers, J., Rohner, F., Lindman, Y., Roubicek, K., Renner, W. A., Muller, P., Bachmann, M. F. (2005). A therapeutic vaccine for nicotine dependence: preclinical efficacy, and phase I safety and immunogenicity. *Eur J Immunol, 35*, 2031-2040.

McNew, J. A., Weber, T., Parlati, F., Johnston, R. J., Melia, T. J., Söllner, T. H., & Rothman, J. E. (2000). Close Is Not Enough: SNARE-Dependent Membrane Fusion Requires an Active Mechanism That Transduces Force to Membrane Anchors. *The Journal of cell biology*, *150*(1), 105-118.

Medina, E., Wieczorek, D., Medina, E. M., Yang, Q., Feiss, M., Catalano, C. E. (2010). Assembly and maturation of the bacteriophage lambda procapsid: gpC is the viral protease. *J Mol Biol, 401*, 813-830.

Medina, E., Nakatani, E., Kruse, S., & Catalano, C. E. (2012). Thermodynamic Characterization of Viral Procapsid Expansion into a Functional Capsid Shell. *Journal of Molecular Biology*, *418*(3), 167-180.

Medina, E. M., Andrews, B. T., Nakatani, E., & Catalano, C. E. (2011). The bacteriophage lambda gpNu3 scaffolding protein is an intrinsically disordered and biologically functional procapsid assembly catalyst. *J Mol Biol, 412*, 723-736.

Mikawa, Y. G., Maruyama, I. N., Brenner, S. (1996). Surface display of proteins of bacteriophage λ heads. *J Mol Bio, 1*, 21-30.

Moore, J. P., McKeating, J. A., Weiss, R. A., & Sattentau, Q. J. (1990). Dissociation of gp120 from HIV-1 virions induced by soluble CD4. *Science*, *250*(4984), 1139-1142.

Moore, P. L., Crooks, E. T., Porter, L., Zhu, P., Cayanan, C. S., Grise, H., ... & Binley, J. M. (2006). Nature of nonfunctional envelope proteins on the surface of human immunodeficiency virus type 1. *Journal of virology*, *80*(5), 2515-2528.

Mornet, S., Vasseur, S., Grasset, F., & Duguet, E. (2004). Magnetic nanoparticle design for medical diagnosis and therapy. *Journal of Materials Chemistry*, *14*(14), 2161-2175.

Moulard, M., Decroly, E. (2000). Maturation of HIV envelope glycoprotein precursors by cellular endoproteases. *Bioch Biophys Acta, 1469*, 121-132.

Newcomb, W. W., Juhas, R. M., Thomsen, D. R., Homa, F. L., Burch, A. D., Weller, S. K., & Brown, J. C. (2001). The UL6 gene product forms the portal for entry of DNA into the herpes simplex virus capsid. *Journal of virology*, *75*(22), 10923-10932.

Olfson, M., & Marcus, S. C. (2013). Decline In Placebo-Controlled Trial Results Suggests New Directions For Comparative Effectiveness Research. *Health Affairs*, *32*(6), 1116-1125.

Oppenheim, A. B., Kobiler, O., Stavans, J., Court, D. L., & Adhya, S. (2005). Switches in bacteriophage lambda development. *Annu. Rev. Genet.*, *39*, 409-429.

Owens III, D. E., & Peppas, N. A. (2006). Opsonization, biodistribution, and pharmacokinetics of polymeric nanoparticles. *International journal of pharmaceutics*, *307*(1), 93-102.

Pace, C. N., Shaw, K. L. (2000). Linear extrapolation method of analyzing solvent denaturation curves. *PROTEINS Struct Funct Genet Suppl, 4*, 1-7.

Pantophlet, R., Burton, D. R. (2006). GP120: target for neutralizing HIV-1 antibodies. *Ann Rev Immunol, 24*, 739-769.

Paradiso, B., Marconi, P., Zucchini, S., Berto, E., Binaschi, A., Bozac, A., ... & Simonato, M. (2009). Localized delivery of fibroblast growth factor–2 and brain-derived neurotrophic factor reduces spontaneous seizures in an epilepsy model. *Proceedings of the National Academy of Sciences*, *106*(17), 7191-7196.

Parent, K. N., Doyle, S. M., Anderson, E., & Teschke, C. M. (2005). Electrostatic interactions govern both nucleation and elongation during phage P22 procapsid assembly. *Virology*, *340*(1), 33-45.

Parent, K. N., Zlotnick, A., & Teschke, C. M. (2006). Quantitative analysis of multi-component spherical virus assembly: scaffolding protein contributes to the global stability of phage P22 procapsids. *Journal of molecular biology*, *359*(4), 1097-1106.

Peppel, K., Crawford, D., & Beutler, B. (1991). A tumor necrosis factor (TNF) receptor-IgG heavy chain chimeric protein as a bivalent antagonist of TNF activity. *The Journal of experimental medicine*, *174*(6), 1483-1489.

Petros, R. A., DeSimone, J. M. (2010). Strategies in the design of nanoparticles for therapeutic applications. *Nat Rev Drug Discov, 9*, 615-627.

Pettersen, E. F., Goddard, T. D., Huang, C. C., Couch, G. S., Greenblatt, D. M., Meng, E. C., Ferrin, T. E. (2004). UCSF Chimera--a visualization system for exploratory research and analysis. *J Comput Chem, 25*, 1605-1612.

Phogat, S., Wyatt, R. (2007). Rational modifications of HIV-1 envelope glycoproteins for immunogen design. *Curr Pharmaceut Des, 13*, 213-227.

Poignard, P., Moulard, M., Golez, E., Vivona, V., Franti, M., Venturini, S., ... & Burton, D. R. (2003). Heterogeneity of envelope molecules expressed on primary human immunodeficiency virus type 1 particles as probed by the binding of neutralizing and nonneutralizing antibodies. *Journal of virology*, *77*(1), 353-365.

Preston, B. D., Poiesz, B. J., & Loeb, L. A. (1988). Fidelity of HIV-1 reverse transcriptase. *Science*, *242*(4882), 1168-1171.

Rao, V. B., & Feiss, M. (2008). The bacteriophage DNA packaging motor. *Annual review of genetics*, *42*, 647-681.

Rasmussen, R. A., Ong, H., Kittel, C., Ruprecht, C. R., Ferrantelli, F., Hu, S. L., ... & Ruprecht, R. M. (2006). DNA prime/protein boost immunization against HIV clade C: safety and immunogenicity in mice. *Vaccine*, *24*(13), 2324-2332.

Ringe, R. P., Sanders, R. W., Yasmeen, A., Kim, H. J., Lee, J. H., Cupo, A., ... & Moore, J. P. (2013). Cleavage strongly influences whether soluble HIV-1 envelope glycoprotein trimers adopt a native-like conformation. *Proceedings of the National Academy of Sciences*, *110*(45), 18256-18261.

Ritchie, T. K., Kwon, H., Atkins, W. M. (2011). Conformational analysis of human ATP Binding Cassette transporter ABCB1 in lipid nanodiscs and inhibition by the antibodies MRK16 and UIC2. *J Biol Chem*, *286*(45), 39489-39496.

Ritchie, T. K., Grinkova, Y. V., Bayburt, T. H., Denisov, I. G., Zolnerciks, J. K., Atkins, W. M., Sligar, S. G. (2009). Reconstitution of membrane proteins in phospholipid bilayer nanodiscs. *Methods Enzymol, 464*, 211-231.

Roben, P., Moore, J. P., Thali, M., Sodroski, J., Barbas, C. 3., & Burton, D. R. (1994). Recognition properties of a panel of human recombinant Fab fragments to the CD4 binding site of gp120 that show differing abilities to neutralize human immunodeficiency virus type 1. *Journal of virology*, *68*(8), 4821-4828.

Rockwell, N. C., Thorner, J. W. (2004). The kindest cuts of all: crystal structures of Kex2 and furin reveal secrets of precursor processing. *Trends Biochem Sci, 29*, 80-87.

Rousso, I., Mixon, M. B., Chen, B. K., & Kim, P. S. (2000). Palmitoylation of the HIV-1 envelope glycoprotein is critical for viral infectivity. *Proceedings of the National Academy of Sciences*, *97*(25), 13523-13525

Roy, A., Kucukural, A., Zhang, Y. (2010). I-TASSER: a unified platform for automated protein structure and function prediction. *Nat Protocols, 5*, 725-738.

Ryan, R. O. (2010). Nanobiotechnology applications of reconstituted high density lipoprotein. *J Nanobiotech, 8*, 28.

Sanders, R. W., Vesanen, M., Schuelke, N., Master, A., Schiffner, L., Kalyanaraman, R., ... & Moore, J. P. (2002). Stabilization of the soluble, cleaved, trimeric form of the envelope glycoprotein complex of human immunodeficiency virus type 1. *Journal of virology*, *76*(17), 8875-8889.

Santini, C., Brennan, D., Mennuni, C., Hoess, R. H., Nicosia, A., Cortese, R., & Luzzago, A. (1998). Efficient display of an HCV cDNA expression library as C-terminal fusion to the capsid protein D of bacteriophage lambda. *Journal of molecular biology*, *282*(1), 125-135.

Santoro, M. M., Bolen, D. W. (1988). Unfolding free energy changes determined by the linear extrapolation method. 1. Unfolding of phenylmethanesulfonyl a-chymotrypsin using different denaturants. *Biochemistry, 27*, 8063– 8068.

Scanu, A. M., & Edelstein, C. (2008). HDL: bridging past and present with a look at the future. *The FASEB Journal*, *22*(12), 4044-4054.

Schief, W. R., Ban, Y. E. A., & Stamatatos, L. (2009). Challenges for structure-based HIV vaccine design. *Current Opinion in HIV and AIDS*, *4*(5), 431-440.

Sessa, G., & Weissmann, G. (1968). Phospholipid spherules (liposomes) as a model for biological membranes. *Journal of lipid research*, *9*(3), 310-318.

Shubayev, V. I., Pisanic II, T. R., & Jin, S. (2009). Magnetic nanoparticles for theragnostics. *Advanced drug delivery reviews*, *61*(6), 467-477.

Singal, P. K., & Iliskovic, N. (1998). Doxorubicin-induced cardiomyopathy. *New England Journal of Medicine*, *339*(13), 900-905.

Singh, P., Shaffer, S. A., Scherl, A., Holman, C., Pfuetzner, R. A., Freeman, T. J. L., Miller, S. I., Hernandez, P., Appel, R. D., Goodlett, D. R. (2008). Characterization of Protein Cross Links via Mass Spectrometry and an Open-Modification Search Strategy. *Anal Chem, 80*, 8799-8806.

Singh, P., Nakatani, E., Goodlett, D. R., & Catalano, C. E. (2013). A Pseudo-Atomic Model for the Capsid Shell of Bacteriophage Lambda Using Chemical Cross-Linking/Mass Spectrometry and Molecular Modeling. *Journal of molecular biology*, *425*(18), 3378-3388.

Smith, A. M., Duan, H., Mohs, A. M., & Nie, S. (2008). Bioconjugated quantum dots for *in vivo* molecular and cellular imaging. *Advanced drug delivery reviews*, *60*(11), 1226-1240.

Smith, M. P., & Feiss, M. (1993). Sites and gene products involved in lambdoid phage DNA packaging. *Journal of bacteriology*, *175*(8), 2393-2399.

Sternberg, N., Hoess, R. (1995). Display of peptides and proteins on the surface of bacteriophage λ. *Proc Nat Acad Sci, 92*, 1609-1613.

Steven, A. C., Heymann, J. B., Cheng, N., Trus, B. L., & Conway, J. F. (2005). Virus maturation: dynamics and mechanism of a stabilizing structural transition that leads to infectivity. *Current opinion in structural biology*, *15*(2), 227-236.

Stiegler, G., Kunert, R., Purtscher, M., Wolbank, S., Voglauer, R., Steindl, F., & Katinger, H. (2001). A potent cross-clade neutralizing human monoclonal antibody against a novel epitope on gp41 of human immunodeficiency virus type 1. *AIDS research and human retroviruses*, *17*(18), 1757-1765.

Sulakvelidze, A., Alavidze, Z., & Morris, J. G. (2001). Bacteriophage therapy. *Antimicrobial agents and chemotherapy*, *45*(3), 649-659.

Tomka, M. A., & Catalano, C. E. (1993). Physical and kinetic characterization of the DNA packaging enzyme from bacteriophage lambda. *Journal of Biological Chemistry*, *268*(5), 3056-3065.

Tuma, R., Tsuruta, H., French, K. H., & Prevelige, P. E. (2008). Detection of intermediates and kinetic control during assembly of bacteriophage P22 procapsid. *Journal of molecular biology*, *381*(5), 1395-1406.

UNAIDS. (2013). Global report: UNAIDS report on the global AIDS epidemic 2013. Retrieved from http://www.unaids.org/en/media/unaids/contentassets/documents/epidemiology/2013/gr2013/UNAIDS_Global_Report_2013_en.pdf

Veesler, D., Quispe, J., Grigorieff, N., Potter, C. S., Carragher, B., & Johnson, J. E. (2012). Maturation in action: CryoEM study of a viral capsid caught during expansion. *Structure*.

Vennema, H., Godeke, G. J., Rossen, J. W., Voorhout, W. F., Horzinek, M. C., Opstelten, D. J., Rottier, P. J. (1996). Nucleocapsid-independent assembly of coronavirus-like particles by co-expression of viral envelope protein genes. *EMBO J, 15*, 2020–2028.

Villa, Luisa L.; Perez, Gonzalo; Kjaer, Susanne K.; et al (2007). Quadrivalent vaccine against human papillomavirus to prevent high-grade cervical lesions. *The New England journal of medicine, 356*(19),1915-1927.

Volcy, K., Dewhurst, S. (2009). Proteasome inhibitors enhance bacteriophage lambda mediated gene transfer in mammalian cells. *Virology, 384*, 77-87.

Walker, B. D., Burton, D. R. (2008). Towards an AIDS vaccine. *Science, 320*, 760-764.

Walker, L. M., Phogat, S. K., Chan-Hui, P. Y., Wagner, D., Phung, P., Goss, J. L., ... & Burton, D. R. (2009). Broad and potent neutralizing antibodies from an African donor reveal a new HIV-1 vaccine target. *Science*, *326*(5950), 285-289.

Walker, L. M., Burton, D. R. (2010). Rational antibody-based HIV-1 vaccine design: current approaches and future directions. *Curr Opin Immunol, 22*, 358-366.

Wang, S., Chandramouli, P., Butcher, S., Dokland, T. (2003). Cleavage leads to expansion of bacteriophage P4 procapsids *in vitro*. *Virology, 314*, 1-8.

Weber, T., Zemelman, B. V., McNew, J. A., Westermann, B., Gmachl, M., Parlati, F., ... & Rothman, J. E. (1998). SNAREpins: minimal machinery for membrane fusion. *Cell*, *92*(6), 759-772.

Wu, X., Yang, Z. Y., Li, Y., Hogerkorp, C. M., Schief, W. R., Seaman, M. S., ... & Mascola, J. R. (2010). Rational design of envelope identifies broadly neutralizing human monoclonal antibodies to HIV-1. *Science*, *329*(5993), 856-861.

Yang, F., Forrer, P., Dauter, Z., Conway, J. F., Cheng, N., Cerritelli, M. E., ... & Wlodawer, A. (2000). Novel fold and capsid-binding properties of the λ-phage display platform protein gpD. *Nature Structural & Molecular Biology*, *7*(3), 230-237.

Yang, Q., Catalano, C. E. (2003). Biochemical characterization of bacteriophage lambda genome packaging *in vitro*. *Virology, 305*, 276-287.

Yang, Q., Maluf, N. K., & Catalano, C. E. (2008). Packaging of a Unit-Length Viral Genome: The Role of Nucleotides and the gpD Decoration Protein in Stable Nucleocapsid Assembly in Bacteriophage λ. *Journal of molecular biology*, *383*(5), 1037-1048.

Yang, Q-E., Stephen, A. G., Adelsberger, J. W., Roberts, P. E., Zhu, W., Currens, M. J., Feng, Y., Crise, B. J., Gorelick, R. J., Rein, A. R., Fisher, R. J., Shoemaker, R. H., Sei, S. (2005). Discovery of small-molecule Human Immunodeficiency Virus Type 1 entry inhibitors that target the gp120-binding domain of CD4. *J Virol, 79*, 6122-6133.

Zhang, L., Gu, F. X., Chan, J. M., Wang, A. Z., Langer, R. S., Farokhzad, O. C. (2008). Nanoparticles in medicine: therapeutic applications and developments. *Clin Pharmacol Ther, 83*, 761-769.

Zhang, Y. (2007). Template-based modeling and free modeling by I-TASSER in CASP7. *Proteins, 69*(Suppl 8), 108-117.

Zhang, Y. (2008). I-TASSER server for protein 3D structure prediction. *BMC Bioinformatics, 9*, 40.

Zhu, P., Chertova, E., Bess, J., Lifson, J. D., Arthur, L. O., Liu, J., Taylor, K. A., Roux, K. H. (2003). Electron tomography analysis of envelope glycoprotein trimers on HIV and simian immunodeficiency virus virions. *Proc. Nat. Acad. Sci*., *100*, 15812-15817.

Zhu, P., Winkler, H., Chertova, E., Taylor, K. A., & Roux, K. H. (2008). Cryoelectron tomography of HIV-1 envelope spikes: further evidence for tripod-like legs. *PLoS pathogens*, *4*(11), e1000203.

Ziegelhoffer, T., Yau, P., Chandrasekhar, G. N., Kochan, J., Georgopoulos, C., & Murialdo, H. (1992). The purification and properties of the scaffolding protein of bacteriophage lambda. *Journal of Biological Chemistry*, *267*(1), 455-461.

# Curriculum Vitae

**ERI NAKATANI-WEBSTER**
University of Washington
Department of Medicinal Chemistry
Box 357610
Health Sciences Building Room H-172
Seattle, WA 98195-7610
Tel: (520) 820-1625
E-mail: nakae@u.washington.edu
(United States Citizen)

## EDUCATION

**University of Arizona, Tucson, AZ** **2003-2008**
B.S., Biochemistry & Molecular Biophysics, Magna Cum Laude, with honors
Minor in Japanese Language
**University of Washington, Seattle, WA** **2008-2013**
Ph. D., Medicinal Chemistry

## PUBLICATIONS

Zhou, M.; **Nakatani, E.;** Gronenberg, L. S.; Tokimoto, T; Lynch, R.; Wirth, M; Ghosh, I. Peptide Labeled Quantum Dots for Imaging GPCRs in Whole Cells and as Single Molecules. *Bioconjugate Chemistry.* 2007, **18** (2), 323-332.

Medina, E. M.; Andrews, B. T.; **Nakatani, E.;** Catalano, C. E. The Bacteriophage Lambda gpNu3 Scaffolding Protein is an Intrinsically Disordered and Biologically Functional Procapsid Assembly Catalyst. *JMB*. 2011, 412 (4), 723-736.

Medina, E.[1]; **Nakatani, E.[1];** Kruse, S.; Catalano, C. E. Thermodynamic Characterization of Viral Procapsid Expansion into a Functional Capsid Shell. *JMB.* 2012, 418(3-4), 167-180.
***[1]Co-First Author.***

Singh, P.[1]; **Nakatani, E.[1];** Goodlett, D. R.; Catalano, C. E. A Pseudo Atomic Model for the Capsid Shell of Bacteriophage Lambda Using Chemical Cross-Linking/Mass Spectrometry and Molecular Modeling. *JMB.* 2013, 425(18), 3378-3388.
***[1]Co-First Author.***

Chang, J. R.; Song, E-H.; **Nakatani-Webster, E.;** Monkkonen, L.; Ratner, D. M.; Catalano, C. E. Phage Lambda Capsids as Tunable Display Nanoparticles. *Manuscript in preparation.*

**Nakatani-Webster, E.;** Hu, S-L.; Catalano, C.E. Incorporation of Uncleaved HIV-1 Envelope Glycoprotein into Phospholipid Bilayer Nanodiscs. *Manuscript in preparation.*

## AWARDS & HONORS

2006 University of Arizona Chemistry Dept. Alumni Award for Excellence in Undergraduate Research

2006 University of Arizona Student Showcase President's Award, Best Exhibit by an Undergraduate Student

2007 University of Arizona Chemistry Department Undergraduate Poster Competition, 2nd place
2007 Galileo Circle Scholarship
2008 University of Washington Graduate School Top Scholar Award
2012-2013 Warren G. Magnuson Scholarship
2012-2013 Hope Barnes Graduate Fellowship

**MEMBERSHIPS**
Phi Eta Sigma Freshman Honor Society, inducted fall 2004
Alpha Chi Sigma Chemistry Fraternity, Beta Tau Chapter, inducted fall 2005
Phi Beta Kappa Honor Society, inducted spring 2007

**RESEARCH EXPERIENCE**
**University of Arizona, Tucson, AZ** **Jan. 2005-May 2008**
Undergraduate Researcher, Indraneel Ghosh Laboratory, Department of Chemistry
Conjugation of synthetic peptides to Quantum Dots for imaging of G-protein coupled receptors
Synthesis of multivalent peptide inhibitors of HIV-1 attachment
**University of Washington, Seattle, WA** **Sept. 2008-Dec 2013**
Graduate Student, Carlos E. Catalano Laboratory, Department of Medicinal Chemistry
Thermodynamic and structural characterization of bacteriophage lambda capsid assembly/ maturation
Assembly of native HIV-1 envelope glycoprotein into phospholipid bilayer nanodiscs

**TEACHING EXPERIENCE**
**Catalina Foothills Alternative High School, Tucson, AZ** Aug. 2006- Nov. 2007
Volunteer Chemistry Tutor
**University of Washington, Seattle, WA**
Teaching Assistant, MedCH 400 (Fundamental Concepts in Medicinal Chemistry) Fall 2009
Teaching Assistant, MedCH 570 (Medicinal Biochemistry) Winter 2010, Winter 2011
Student Mentor, Pharmacological Sciences Summer Diversity Program Summer 2011

**RESEARCH PRESENTATIONS/ ABSTRACTS**
University of Arizona Chemistry Department Undergraduate Poster Competition Spring 2006
ACS Rocky Mountain Regional Meeting Undergraduate Research Symposium October 2006
University of Arizona Student Showcase Poster Presentation Fall 2006
UA Chemistry Department Undergraduate Poster Competition Spring 2007
**Nakatani, E**.; Zhou, M.; Ghosh, I. "Targeting HIV-1 Envelope Proteins Utilizing a Multivalent Approach"
57th Annual ASMS Conference on Mass Spectrometry May 31-June 4 2009
Singh, P.; Pfuetzner, R. A.; Shaffer, S. A.; Panchaud, A.; **Nakatani, E**.; Catalano, C. E.; Miller, S. I.; Goodlett, D. R. "Structural characterization of macromolecular protein complexes using chemical cross-linking and mass spectrometry"

FASEB Summer Research Conference on Virus Structure & Assembly June 27-July 2 2010

Medina, E.M., Andrews, B.T., **Nakatani, E**., and Catalano, C.E. "Characterization of Bacteriophage Lambda Scaffolding Protein and its Role in Proper Capsid Assembly"

58th Annual ASMS Conference on Mass Spectrometry May 23-27 2010

Monkkonen, L.; Singh, P.; Panchaud, A.; Medina, E.; **Nakatani, E**.; Catalano, C. E.; Goodlett, D. R. **"**Comparison of Two Orthogonal Informatic Pipelines for Detection of Tandem Mass Spectra of Cross-Link Peptides"

Pacific Northwest Biacore User Group Meeting Mar 2 2011

**Nakatani, E.**; Medina, E.; Sumida, J. P.; Lee, K. K.; Catalano, C. E. "Thermodynamic Characterization of the Reversible Expansion of Bacteriophage Lambda Procapsids"

XXII Biennial Conference on Phage/ Virus Assembly Oct 9-14 2011

**Nakatani, E**.; Nyamweya-Simmons, C.; Kahn, M.; Hu, S-L.; Catalano, C. E. "Incorporation of HIV-1 Envelope Glycoprotein Precursor gp160 into Phospholipid Bilayer Nanodiscs"

Kruse, S.; **Nakatani, E**.; Catalano, C. E. "Thermodynamic Characterization of Reversible Capsid Expansion"

Physical Virology Gordon Research Conference Jan 20-25 2013

Chang, J.R.; Song, E-H.; **Nakatani, E.**; Monkkonen, L. M.; Ratner, D. M; Catalano, C. E. "Phage Lambda Nanoparticles as Vehicles for Targeted-Drug Therapy"